Development of a method for the quantification of volumetric wear on incongruent articulating surfaces of Total Joint Replacement prostheses through the use of coordinate metrology and mathematical fitting techniques

Matthew James Holland

A thesis submitted to the University of Huddersfield in partial fulfilment of the requirements for the degree of Doctor of Philosophy.

May 2021

Statement of Copyright

i. The author of this thesis (including any appendices and/or schedules to this thesis) owns any copyright in it (the "Copyright") and s/he has given The University of Huddersfield the right to use such copyright for any administrative, promotional, educational and/or teaching purposes.

ii. Copies of this thesis, either in full or in extracts, may be made only in accordance with the regulations of the University Library. Details of these regulations may be obtained from the Librarian. This page must form part of any such copies made.

iii. The ownership of any patents, designs, trademarks and any and all other intellectual property rights except for the Copyright (the "Intellectual Property Rights") and any reproductions of copyright works, for example graphs and tables ("Reproductions"), which may be described in this thesis, may not be owned by the author, and may be owned by third parties. Such Intellectual Property Rights and Reproductions cannot and must not be made available for use without the prior written permission of the owner(s) of the relevant Intellectual Property Rights and/or Reproductions.

Acknowledgements

The research presented in this thesis has been carried out as part of the bio-metrology group within the EPSRC Future Metrology Hub at the University of Huddersfield. Collaborative work was conducted with the Institute of Medical and Biological Engineering (iMBE) at the University of Leeds and the London Implant Retrieval Centre (LIRC). The author would like to express his appreciation to researchers and students from both of these institutions who have assisted in the completion of this work.

I would also like to express my thanks to Shapemaster Global Limited and Manchester Metropolitan University for allowing me to continue with my PhD rewrite over the last year.

I wish to express my gratitude to my supervisory team of Dr Paul Bills and Dr Radu Racasan, as well as my former supervisor Dr Leigh Fleming for their direction and encouragement throughout this project.

Special thanks go to the remainder of the bio-metrology group for their support and advice as the project progressed, as well as from the wider metrology hub group. Other members of the CPT, far too numerous to mention individually are also gratefully appreciated for their help and guidance.

I would like to thank my family, especially my parents Kevin and Anita for their encouragement, unwavering support and understanding. Finally, I would like to show my deepest appreciation to my fiancée Josh for his encouragement, never-ending optimism, and ability to keep my silly mind sensible, thank you for always believing in me.

Abstract

Volumetric wear measurement of orthopaedic components is an essential tool for the evaluation of implant success. Subsequent generations of implants should generate a lower wear volume than their predecessors, as a lower wear rate can lead to a longer implant service life before failure. Wear measurements methods have been widely developed and standardised for components used in Total Hip Replacement (THR), but as is the case with most areas of research, there is a severe lag in development related to Total Knee Replacement (TKR) Prostheses, in particular in the area of standardisation. This lag is even more pronounced when considering Total Ankle Replacement (TAR) components, where very little research has been conducted due to a general lack in the number of prostheses.

This thesis presents the development of a method for the measurement of volumetric wear on UHMWPE orthopaedic components of TKR and TAR through the use of coordinate measurement machines. Currently, the only standardised method of volumetric wear measurement on TKR components is the use of Gravimetric Measurement, the assessment of small mass changes that can be divided by component density to give wear volumes. Gravimetric Measurement is widely used and considered as the “gold standard” of orthopaedic wear measurement for components worn in simulator trials. Unfortunately, gravimetric measurement is impeded by issues with fluid absorption affecting wear value calculation. However, the greatest flaw of Gravimetric Measurement is the lack of applicability to clinically relevant retrieval studies, where no pre-wear data is available.

The method developed in this study reconstructs a worn component's unworn geometry to use as reference geometry, with comparison used to calculate the volume of wear on a component. This comparison is conducted through the use of both manual and automatic wear edge definition techniques, combined with curve fitting techniques in a two-dimensional setting, followed by a three-dimensional calculation of volumetric wear on the surface.

Numerous studies have been conducted to evaluate the efficacy of the CMM measurement method developed and to refine aspects of the post-measurement data analysis method. These studies have considered both wear-simulated and retrieved TKR components, as well as an artificially created TKR component. Volumetric wear analysis has also been performed on wear-simulated TAR components.

These studies found that the method developed provided accurate and repeatable results for volumetric wear on all cohorts of components across a wide range in terms of the severity of wear, with the effectiveness and accuracy of the method developed analysed.

Contents

List of Tables

List of Figures

Table of Abbreviations

ACL – Anterior Cruciate Ligament

AP – Antero-posterior

ASCII – American Standard Code for Information Interchange

CAD – Computer-Aided Design

CATIA – Computer-Aided Three-Dimensional Program

CMM – Coordinate Measurement Machine

CR – Cruciate Retaining

CT – Computed Tomography

FB – Fixed Bearing

FVM – Focus Variation Microscopy

IGES – International Graphic Exchange Specification

ISO – International Standard Organisation

LCS – Low Contact Stress

MATLAB – Matrix Laboratory

MB – Mobile Bearing

MoP – Metal-on-Polyethylene

ML – Medial/Lateral

OA – Osteoarthritis

PCL – Posterior Cruciate Ligament

PS – Posterior Stabilised

STEP – Standard for the Exchange of Product Data

STL – Standard Tessellation Language

TAR – Total Ankle Replacement

THR – Total Hip Replacement

TJR – Total Joint Replacement

TKR – Total Knee Replacement

UHMWPE – Ultra-High Molecular Weight Polyethylene

List of Symbols

Paired t-tests:

M - Mean

SD – Standard Deviation

df – Degrees of Freedom

t – t-statistic

p – significance value

Product-moment correlation coefficient

df – Degrees of Freedom

r – r statistic

p – significance value

One-Way ANOVA

F – F-Value – variation between sample means/variation within the samples

Co-ordinate Measurement Machine Related Parameters

E0 – Length Measurement

L – Length

MPE_p – Maximum Permissible Probing Error

MATLAB ischange function

C – Cost Function

A_n – Data Segment

τ – Threshold Value

N – Number of elements

Surface Topographical Parameters

Sq – RMS Surface Roughness

Ssk – Surface Skewness

Sku – Surface Kurtosis

Sp – Maximum Peak Height

Sv – Maximum Valley Depth

Sz – Maximum Peak-Valley Amplitude

Sdq – RMS Surface Slope

Sa – Surface Roughness

Sds – Summit Density

Miscellaneous

R^2 – Coefficient of Determination

d – Profile Spacing Distance

Publications and Conference Contributions

The content of sections of this thesis has been presented at conferences and published in academic journals. Where content from these publications has been used within the thesis this has been indicated at the beginning of the appropriate chapter.

1. Matthew Holland, Leigh Fleming, Karl Walton, Arianna Cerquiglini, Harry Hothi, Alister Hart, John Skinner, Paul Bills (2018): Characterisation of wear areas on UHMWPE total knee replacement prostheses through the study of their areal surface topographical parameters. Surface Topography: Metrology and Properties: Volume 6, Number 3 "Selected Papers from Met & Props 2017".
    a. **Statement of Contribution:** Author developed the rationale and methodology, performed measurements and conducted data analysis to draw conclusions. The paper was written in its entirety by the author.
2. Paul Bills, Radu Racasan, Matthew Holland, Harry S. Hothi, John A. Skinner, Alice Hirschmann, Arianna Cerquiglini, Johann Henckel, Niccolo Rotigliano (2017): Understand Why Knee Implants Fail, American Academy of Orthopaedic Surgeons Annual Meeting
    a. **Statement of Contribution:** The author contributed technical data results to the paper. The paper was written by AC at the London Implant Retrieval Centre.
3. Matthew Holland, Radu Racasan, Paul Bills (2018): Measurement of two-dimensional linear wear on total knee replacement prostheses using coordinate metrology and fitting techniques, The 18th Nordic Symposium on Tribology
    a. **Statement of Contribution:** The author produced all content of this publication which was presented at NORDTRIB 2018 including the collection, analysis and presentation of all data.
4. Matthew Holland, Radu Racasan, Paul Bills (2018) Creation of a methodology for three-dimensional characterisation of volumetric wear on total knee replacement components, 4th International Conference on BioTribology
    a. **Statement of Contribution:** The author produced all content of this publication which was presented at ICoBT 2018 including the collection, analysis and presentation of all data.

Chapter 1 – Introduction

This chapter will introduce the research project that is detailed in the next 11 chapters of this thesis. The project will be introduced with a discussion of the motivation leading the project and background information relevant to the components studied. This will then be followed by an overview of the structure of the remainder of the thesis.

1.1 Problem Statement

It was once proclaimed by Dr H.James Harrington that "Measurement is the first step that leads to control and eventually to improvement. If you can't measure something, you can't understand it. If you can't understand it, you can't control it. If you can't control it, you can't improve it".

Millions of people worldwide undergo Total Joint Replacement (TJR) every year, with this primarily being of the hip (THR) or the knee (TKR). At either implant failure or patient failure, many of these components are collected by retrieval centres. Whilst in service, the articulation of two or more parts causes wear to occur on these TJR prostheses. This wear is sometimes the primary reason, but nearly always contributes to the failure of such components (S. M. Kurtz, 2004).

Consequently, orthopaedic prostheses are designed to minimise component wear and therefore prolong the lifespan of a component. It is now common for a THR or a TKR to last more than 25 years, and although a morbid perspective, it is hoped that eventually, TJR components will routinely outlast the body in which the components have been installed.

Historical development has shown huge improvement of TJR components throughout the 20th and into the 21st century, with components now being considered incredibly successful for both THR and TKR. Components designed for use in other joints, such as the shoulder (TSR) or ankle (TAR) are showing increasing success and will likely mirror the success of their more popular counterparts in the future.

However, despite the millions of orthopaedic prostheses that are in service across the world, there remains limited knowledge or standardisation for post-service wear analysis of such components. Currently, there are no standardised methods for the measurement of volumetric wear on a retrieved orthopaedic component. However, first steps have been made towards the standardisation of methods for the measurement of volumetric wear in retrieved total hip replacement components. Current methods for the assessment of

retrieval components centres around the visual and subjective analysis of damage of components, with no consideration given to the actual magnitude of wear that has occurred on the component.

This relates to the opening quote from Dr Harrington. Currently, the volumetric wear of retrieved orthopaedic components cannot be measured. It follows from this that a full understanding of the component performance cannot be achieved and this limits improvement and successful development in orthopaedic design.

Since 2003 there have been 963,846 Total Knee Replacement procedures performed in the UK, the most of any type of Total Joint Replacement, equating to approximately 65,000 per year (NJR, 2018). This compares to just 5,330 TAR procedures since recording started in 2010, equating to approximately 600 per year. A meteoric rise in the demand for TJR is projected in the next 15 years, therefore methods for the measurement of volumetric wear on retrieved orthopaedic components must be developed and standardised. It is projected that by 2032, the number of annual TKR procedures in the UK could increase to approximately 100,000 (Culliford et al., 2015). In the USA it has been predicted that the increase in TKR demand could grow by as much as 673% by the year 2030 when compared to 2005 (S. Kurtz, Ong, Lau, Mowat, & Halpern, 2007).

Clinical success in modern arthroplasty is largely attributed to the excellent work of Sir John Charnley during the 1960s. Charnley pioneered the use of metal-on-polyethylene (MoP) bearings in THR, showing great improvement in clinical performance when compared to previous designs. This design methodology was then transferred to TKR by Frank Gunston, working alongside Charnley at the Wrightington Hospital. Gunston's MoP bearings also showed a great performance in clinical performance against previous designs of TKR.

It can be no coincidence then, that in modern-day TKR procedures, more than 80% of components implanted in the UK are of this metal articulating with ultra-high molecular weight polyethylene composition. As previously mentioned, it is now very common for a TKR component to last 25 or more years in service, this success is largely due to the evolution started by Charnley and Gunston.

Total Ankle Replacement is a relatively new and fast-developing area of orthopaedics, with the adoption of the MoP bearing type in the 1970s. Low implantation rates and generally poor, verging on unacceptable, clinical results have contributed to a severe lag in development in comparison to THR and TKR. As a result, third-generation TAR components, with a significant level of bespoke development rather than a replication of TKR technology, are still in a short-term clinical implantation time frame, with long term outcomes unknown. This

development lag and relative lack of success has subsequently led to a dearth of research in the general area of TAR.

There are methods of volumetric wear measurement on orthopaedic components that have been well developed and standardised for laboratory wear-testing of implants. The gravimetric measurement method for example, which assesses small changes in the mass of a component pre and post wear and correlates this to a wear volume using the density of the component, is a method that is widely considered as a "gold standard" in volumetric wear measurement and is generally used for wear assessment in wear-simulator studies. Despite this, gravimetric measurement cannot be applied in the case of retrieved components due to a necessity for pre-wear mass to be analysed, reducing the clinical applications of the method.

Components that are collected by retrieval centres often travel with little or no information on either the manufacturer, design, size, tolerance or any engineering-related specifics on the component. Generally, retrieved components are defined in terms of their implantation time and general information regarding the particulars of the patient in which the component completed its service. As a result, volumetric wear assessment that is performed on these types of components is limited in data to what can be attained from the component post-wear.

1.2 The Anatomical Knee Joint

The human knee joint is a synovial joint that is formed by two major interactions between bones. These are the femorotibial joint, which is the articulation between the inferior tibial and superior femoral bones, and the patellofemoral joint which is the interface between the patella (kneecap) and the trochlear groove of the femur. While the patellofemoral joint is a relatively non-load bearing joint that is essentially present to aid in ease of extension (straightening) of the leg, the femorotibial joint is the main load-bearing joint of the knee and the joint that is replaced during TKR.

Figure 1 shows the alignment of a typical knee joint with the convex bicondylar femoral portion of the joint above the tibial plateau. The two condyles of the femoral knee are often referred to in terms of anatomical location, being described as the medial and lateral condyles. Due to the incongruent engagement between the femoral and tibial surfaces, the two femoral condyles are covered with thicker layers of cartilage known as the knee's menisci, which act as shock-absorbers within the knee joint.

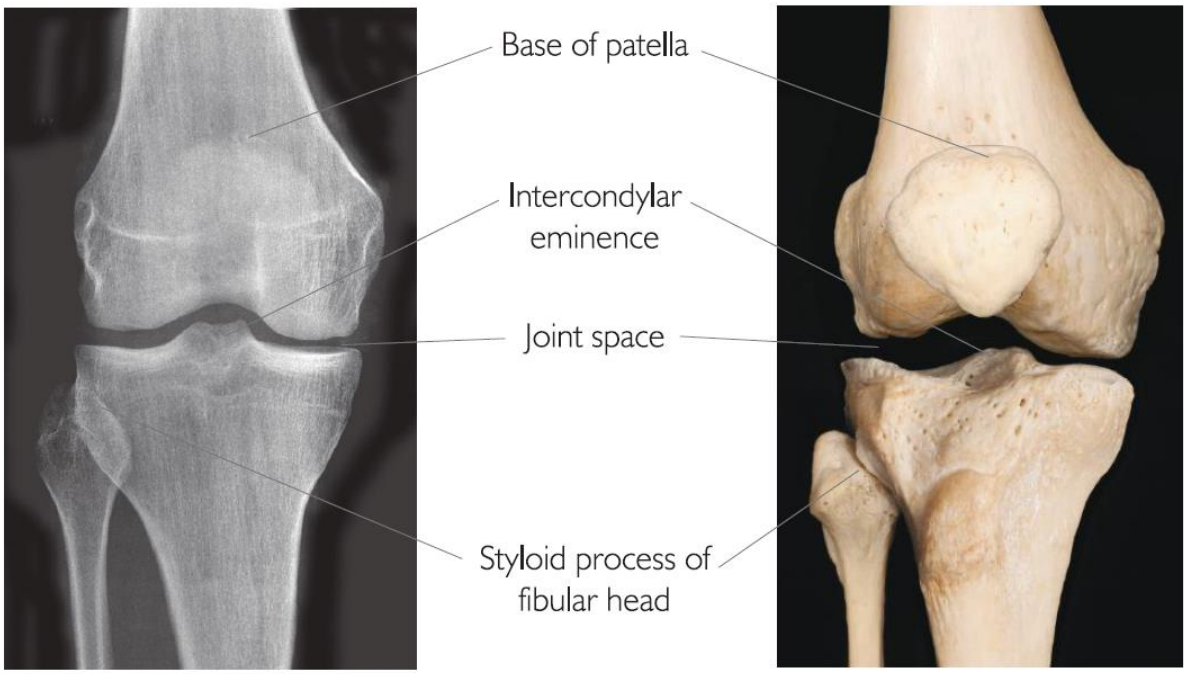

Figure 1 - Diagram of Anatomical Knee showing the orientation of bones. (Harris, Ranson, & Robertson, 2014)

This incongruence between the articulating bones makes the knee joint inherently unstable and therefore stability within the joint is provided by a network of ligaments that surround the joint. 4 main ligaments surround the joint, known as the Anterior Cruciate Ligament (ACL), Lateral Collateral Ligament (LCL), Posterior Cruciate Ligament (PCL) and the Medial Collateral Ligament (MCL). The ACL is the most critical of these 4 ligaments, and a tear of this ligament is one of the most common injuries found in competitive sport (Harris et al., 2014). The cruciate ligaments are so named from the fact that the two ligaments form a cross shape across the knee joint. It is well accepted that these two ligaments are critical to the stability and function of a knee joint (Goldblatt & Richmond, 2003). A healthy knee would be expected to have an average inter-bone spacing of approximately 5mm, this can be affected by disease and injury (Anas et al., 2013).

1.3 Total Knee Replacement

1.3.1 History and Origins of Total Knee Replacement (Pre-1950's)

Total Knee Arthroplasty as a concept began in the mid-19th century, with Jules P'Eau suggesting that artificial joints could be created to help restore motion within a human joint. Before the notion of using external materials to restore motion the generally accepted practice was arthrodesis, the fusion of the joint. Another solution that was oft used at this time was either gap arthroplasty or interposition arthroplasty, first suggested in 1860 (Verneuil, 1860), and further explored through the early 20th century by numerous authors. Both of these procedures involved the interposition of soft tissue, either from a human or animal between the articulating surfaces, to reduce the risk of bone-on-bone contact, or ankylosis.

One of the main issues resulting from such an operation into the joint at this time involved a shortening of the involved limb. The evolution of this technique led to the advent of a new technique known as hemiarthroplasty.

In the 1890s Themistocles Gluck began the development of two distinct technologies that could potentially be used as a solution in Total Knee Replacement. The first of these is the aforementioned hemiarthroplasty. This essentially involved the "resurfacing" of the articular surface of the tibia with an ivory prosthesis to aid in the restoration of motion in the knee joint. Although this approach was novel and widely acclaimed, hemiarthroplasty did not develop as a common concept until the middle of the following century. The second of Gluck's well-renowned inventions in the 1890s was the hinged prosthesis. This was of a simplification of the bicondylar joint that is formed by the knee, however at the time was seen as a novel and "genius" solution in TKR (Shetty, Tindall, Ting, & Heatley, 2003a, 2003b).

Figure 2 shows the success rates of many different attempts at performing arthroplasty, or replacement, of the knee joint in the early 20th century. As can be seen, the results are somewhat mixed, with most of the larger cohort studies showing an alarmingly low success rate. There was also a lack of standardisation at this time for what may constitute a "good" outcome. This necessitated the creation of more successful prostheses which could reliably be used in TKR. This development began in the 1950s and onwards towards the modern age of components.

Year of Publication	Author	No. of Cases	No. of Good Results
1914	Payr	23	17
1917	Lange	9	1
1918	Baer	28	15
1918	Henderson	117	18
1919	Lexer	34	7
1921	Hohlbaum	85	48
1921	Ryersson	10	1
1923	Groves	18	4
1926	Putti	63	52
1928	Albee	10	9
1928	Campbell	87	43
1937	Courvoisier	23	17
1939	Steindler	51	13
1944	Hass	9	7
1948	Platou	16	10
1949	Samson	47	26
1949	Speed & Trout	65	29
1950	de la Camp	67	36
1950	Kuhns & Potter	12	0
1950	Kuhns & Potter	25	22
1952	Lange	20	6
1952	Miller & Friedman	36	11
1953	Roasenda	26	14
1953	Lacheretz	15	6
		896	412 (46 %)

Figure 2 - Historical Perspective of TKR Success (Walldius, 1957)

1.3.2 Modern Development of Total Knee Replacement Prostheses (1950's onwards)

Building on the concept of a hinged prosthesis as suggested by Gluck in the late 19th century, Walldius created a very simple hinged prosthesis, shown in Figure 3 that could be used as a basis for TKR in 1957. This prosthesis was very technically simple, allowing the surgeon to remove all load-bearing and stability components of the anatomical knee, including ligaments, leaving the joint reliant purely on the significant mechanical strength of the hinged prosthesis.

However, despite relative long-term success in patients over the following decades, a high early failure rate combined with the fact that the prostheses could not accurately replicate the complex motion of the human knee meant that there was a drive to move away from simple hinge prostheses towards a more complex component design.

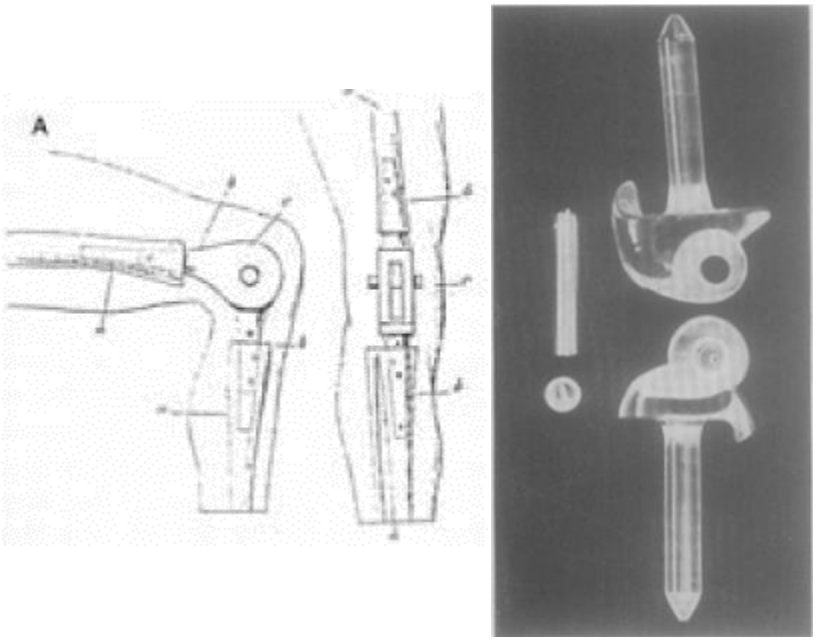

Figure 3 - Comparison between Gluck's ivory TKR hinge (Gluck, 1902) and Walldius' more modern design of hinge (Walldius, 1957).

In the 1960s Frank Gunston devised a design for a “polycentric” TKR, based on Charnley’s low friction principles that had proven so successful in arthroplasty of the hip. Unlike Walldius’ hinge prosthesis and other designs of the time, Gunston’s design retained many of the anatomical structures of the knee, aiding in more accurately replicating the natural movements the human knee can achieve, with the two condyles of the knee requiring separate components.

This design consisted of two components that formed the basis that has led to nearly all TKR prostheses since, a metallic femoral component articulating with a polyethylene tibial component. Gunston’s prosthesis proved very successful in terms of patient mobility, but issues with weak fixation caused some issues (E. K. Song et al., 2013). 1972 saw the introduction of the Geomedic knee arthroplasty. This design was similar to Gunstons in that it was designed with the idea of maintaining as many anatomical structures as possible. Unfortunately, extreme loosening proved to be an issue for this design (Coventry, Finerman, Riley, Turner, & Upshaw, 1972).

Building from the two-component designs from Gunston and Coventry, among others, tri-compartmental designs began to appear. In 1976 the first “total” knee arthroplasty was created (Walker, Ranawat, & Insall, 1976). This design consisted of a single metallic femoral component, with a long stem into the femur, articulating with an also stemmed UHMWPE tibial component.

These designs developed in the 1970s are still the basis of the majority of TKR components that are used today. Figure 4 shows an example of some of the different design types that are available for TKR. As can be seen, all the designs still rely on the formula of a single metallic femoral part interfacing with a UHMWPE tibial part. However, a modern alteration to these components is the use of a metallic tibial tray in which the UHMWPE insert is situated. Studies have often debated whether this is a necessary design decision, with often no difference noted between using an all-UHMWPE or metal-backed design (Norgren, Dalén, & Nilsson, 2004; Ranawat et al., 2005; Rodriguez, Baez, Rasquinha, & Ranawat, 2001).

Figure 4 - Examples of Modern TKR Designs from several different manufacturers (E. K. Song, Moon, Seon, & Hyoun, 2013)

1.4 The Anatomical Ankle Joint

The ankle joint is far more complex than the knee joint comprising of three major articulations known as the talocrural, subtalar and distal tibiofibular joints (Galhoum, Wiewiorski, & Valderrabano, 2017). The major joint of these, and the one which relates specifically to total ankle replacement is the talocrural joint. This is the interface of the superior portion of the talus, commonly known as the ankle bone, and the inferior portion of the tibia.

Figure 5 shows a cross-section of the talocrural joint. As can be seen, there is much better congruency between the bones in this joint when compared to those in the knee joint. Despite this, there is still a need for a system of ligamentous structures to help provide stability within the joint. The major ligaments that support the talocrural joint are the anterior talofibular ligament (ATFL), posterior talofibular ligament (PTFL), the calcaneofibular ligament (CFL) and the deltoid ligament, with the deltoid being the strongest of these. The joint spacing within a healthy ankle would be approximately 2mm (Imai et al., 2015). A joint spacing smaller than this would indicate potential osteoarthritis.

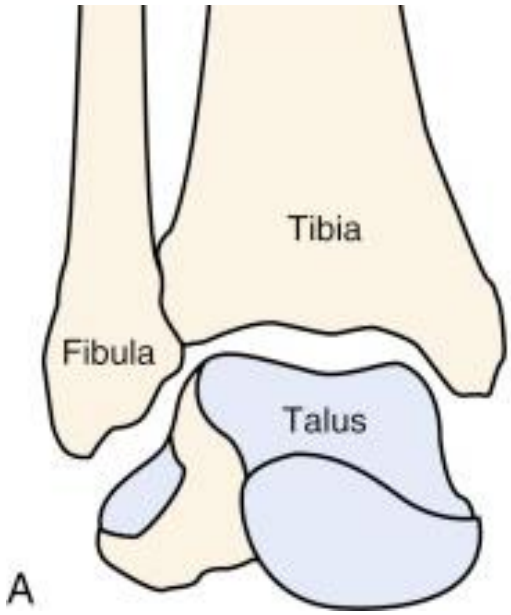

Figure 5 - Cross Section Showing Talocrural joint (Mansfield & Neumann, 2019)

1.5 Total Ankle Replacement

1.5.1 History and Origins of Total Ankle Replacement

Ankle arthroplasty as a concept was first pioneered in 1913 by Eloesser. Similarly to original development steps within TKR, TAR was initiated through the development of interposition arthroplasty, involving the implantation of a bearing material between two articulating surfaces. (Eloesser, 1913). Before Eloesser's attempts at arthroplasty, the range of options in ankle surgery was very limited. The generally accepted approach was arthrodesis, or fusion, of the joint.

1.5.2 Modern Development of Total Ankle Replacement Prostheses

TAR as a practical concept began to gain interest in the 1970s when the successful MoP principles suggested by Charnley and Gunston for hip and knee replacement began to be used to design prostheses for use in TAR. The first design building on these principles was suggested in 1973, although this attempt essentially involved the repurposing of THR prostheses for use in the ankle (Lord & Marotte, 1973). This attempt although novel was highly unsuccessful with just 28% of the 25 components implant being considered a success. One useful outcome from the study was the statement that the anatomical ankle cannot be considered a simple hinge, and therefore TAR components should not be designed as such (Lord & Marotte, 1980).

Concurrently with the work performed by Lord and Marotte, other authors used similar techniques and designs. One study reported outcomes related to the ICLH ankle arthroplasty during the 1970s. This again found that the success rate of these components was similar with only a 21% success rate. Interestingly alongside this success rate, it was found that a further 21% required conversion to arthrodesis. The rather unsuccessful nature of this paper and the ultimate recommendation from the authors that arthrodesis was a preferable option to the ICLH meant that this design on TAR was withdrawn (Bolton-Maggs, Sudlow, & Freeman, 1985).

As previously mentioned, these designs of components found their foundations in the successful work that had been performed in TKR and THR. This success meant that a huge number of TAR designs appeared based on this principle.

From the huge range of components available there are a few designs that have had standout success and popularity. Many of the early designs (pre-1980) showed relatively low success and therefore were generally

discontinued. These designs are often considered as the first generation of TAR prostheses, and as always with the first generation of a design concept, success is expected to be limited.

Figure 6 shows an example of some of the TAR designs that were created during the first generation of development. The implants shown are (clockwise from top left); Mayo (1976), Oregon (1977), TPR (1976), Newton (1973) and Smith (1972). All designs consist of a MoP type articulation, with variation as to whether the metallic part is inserted in the tibia or the talus. Some of these designs did display reasonable survivorship but were ultimately succeeded by the next generation of implants.

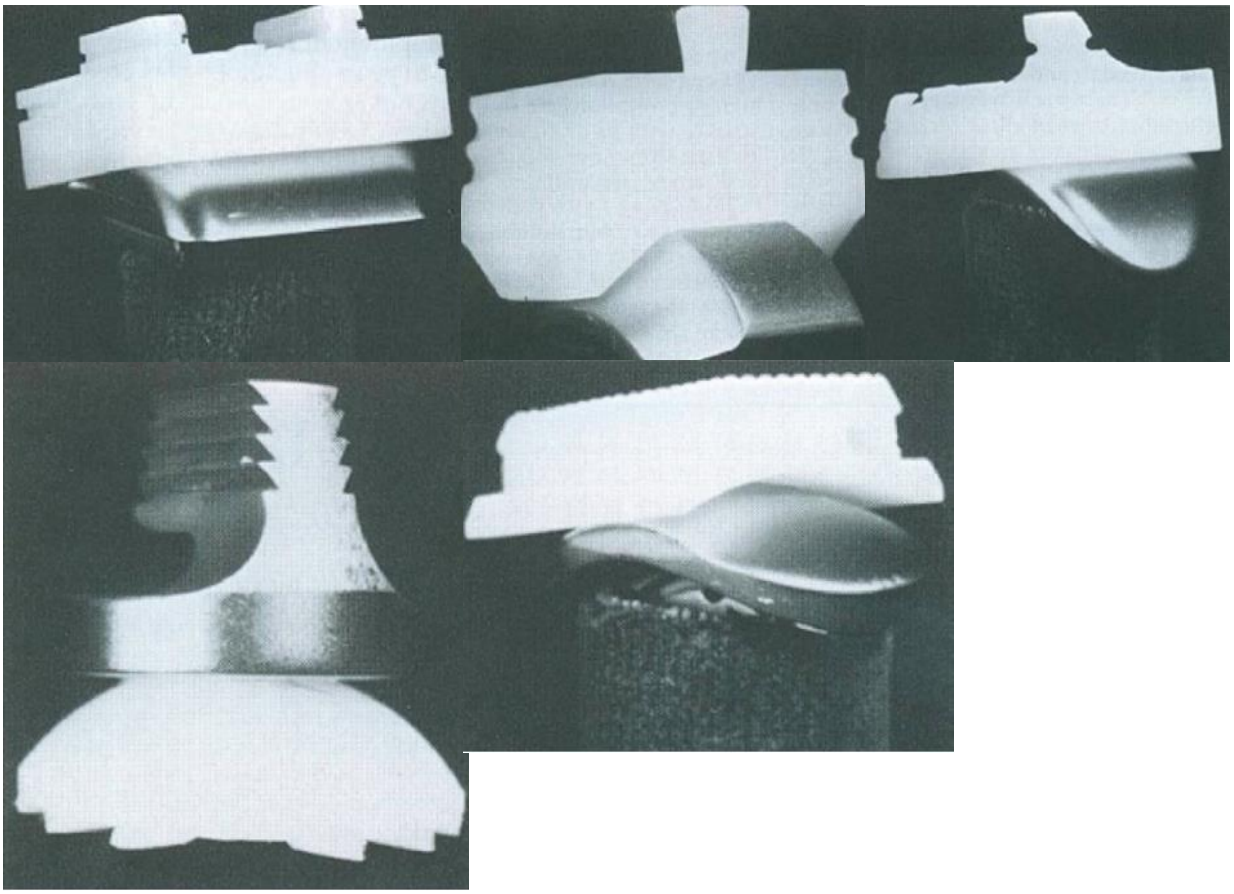

Figure 6 - Examples of First-Generation TAR Designs of multiple types. Adapted. (Vickerstaff, Miles, & Cunningham, 2007)

The second generation of TAR components has generally shown far greater success than the original designs. The main designs that showed great success and popularity are the Agility (1984), STAR (Scandinavian Total Ankle Replacement, 1986) and the Buechel-Pappas (1989).

As shown in Figure 7 these components far more closely resemble more modern orthopaedic components, with a three-component design similar to typical TKR designs. Although these components represented a

considerable improvement in survivorship when compared to the first generation of components, there were still considerable issues in the long-term success of such components.

Figure 7 – Agility (top left), STAR (bottom left) and Buechel-Pappas (right) design 2nd generation TAR components (Vickerstaff et al., 2007)

Considering the Agility TAR prostheses, studies found failure rates ranging between 5% and 32%. This often depended on the length of implantation with a noticeable spike in the survivorship after a decade or more of implantation (Hurowitz, Gould, Fleisig, & Fowler, 2007; Knecht, Estin, Callaghan, Zimmerman, & KJ;, 2004; Kopp, Patel, Deland, & O'Malley, 2006). The STAR TAR also found similar results, with survivorship at 12 years of 70% (Kofoed, 1995). Numerous other studies considering mixed-term results of STAR TAR components found the failure rate to be between 4% and 24% (Anderson, Montgomery, & Carlsson, 2003; Brunner et al., 2013). Similarly, the Buechel-Pappas design showed failure rates as high as 8% in some studies, although

another study found that 100% of the components were successful at up to 7 years post-op (Buechel, Buechel, & Pappas, 2004; Gougoulias, Khanna, & Maffulli, 2010; San Giovanni, Keblish, Thomas, & Wilson, 2006). These alarmingly high long-term failure rates led to the 3rd and current generation of implants that exist today.

The third generation of TAR designs is unfortunately still in a relatively early stage of analysis, with long-term survivorship is not yet known. Mid-term implantation has shown encouraging results which it is hoped will extend to long term studies. Since 2000, there are at least another 8 popular designs that have come to market, these are:

- Salto; Tornier SA
- HINTEGRA; Newdeal SA
- Mobility; DePuy
- Ramses; France MBA
- TNK (Takura Nara Kyocera); Kyocera
- OSG (Oberes Sprunggelenk); Corin
- AES (Ankle Evolutive System); Biomet
- BOX (Bologna-Oxford); Finsbury Orthopaedics

Aside from the TNK design components, all of these new designs are relatively similar to the Buechel-Pappas design of the 1980s. As previously mentioned, there is very little literature relating to clinical performance of these designs, due to the lack of data on long-term survivorship. However, some short-term studies have been conducted. A study was performed analysing 98 Salto prostheses. Survivorship was found at 5.7 years to be 98% (Bonnin et al., 2004). Another study considered the survivorship of the HINTEGRA design of component and found the failure rate to be 8.2%, although the short implantation times of this study suggest that it cannot be accurately compared to long term results of second-generation components (Hintermann, Valderrabano, Dereymaeker, & Dick, 2004). Other designs of implant, notably the BOX design currently undergoing long term surgical trials, but have been extensively described in the literature in their formative phase (Vickerstaff et al., 2007). Numerous other studies have evaluated modern TAR designs. A consensus between studies is that until long term results are published very little will be known about the efficacy of third-generation TAR component designs (Barg, Knupp, Henninger, Zwicky, & Hintermann, 2012; Jung, Shin, Lee, Eom, & Lee, 2015; Popelka et al., 2016; Popelka et al., 2010).

1.6 Ultra High Molecular Weight Polyethylene (UHMWPE)

Polymeric materials were relatively unexplored in TJR until the 1950s when designers began to attempt to integrate polymeric materials into orthopaedic components. The use of operational polymeric materials is not a new area and has been used across a wide variety of industries. However, due to the nature of the environment that TJR components are used within, numerous polymeric compounds are simply unsuitable for use within such components. Many polymeric materials are not biocompatible and would cause adverse tissue reactions around the prosthesis upon implantation making them impossible to be used. Likewise, some polymers exhibit low wear resistance, another undesirable characteristic for a joint replacement component. For this reason, there is a very limited variety of polymer that is used within orthopaedics.

Generally, polyethylene compounds have been used for orthopaedic bearing surfaces, with high-density polyethylene (HDPE) being the material of choice for the original attempts at incorporating polymers into total joint replacement components. However, in modern orthopaedics Ultra-High Molecular Weight Polyethylene (UHMWPE) has become the gold standard of material. Figure 8 shows a comparison between the mechanical properties of the two materials, showing that UHMWPE displays far more desirable properties for most factors.

Property	HDPE	UHMWPE
Molecular weight (10^6 g/mol)	0.05–0.25	3.5–7.5
Melting temperature (°C)	130–137	132–138
Poisson's ratio	0.40	0.46
Specific gravity	0.952–0.965	0.925–0.945
Tensile modulus of elasticity* (GPa)	0.4–4.0	0.5–0.8
Tensile yield strength* (MPa)	26–33	21–28
Tensile ultimate strength* (MPa)	22–31	39–48
Tensile ultimate elongation* (%)	10–1200	350–525
Impact strength, Izod* (J/m of notch; 3.175 mm thick specimen)	21–214	>1070 (No Break)
Degree of crystallinity (%)	60–80	39–75
*Testing conducted at 23°C.		

Figure 8 – Comparison of properties of HDPE and UHMWPE (Knowlton & Wimmer, 2012; S. M. Kurtz, 2004; Walldius, 1957)

UHMWPE orthopaedic components are generally machined from billets of pre-moulded material, although occasionally components are directly moulded before being finished using a machining process. The high wear resistance and excellent mechanical properties displayed by UHMWPE has led to it being almost the sole

polymeric material used for orthopaedic bearing surfaces and, as a result, most research focuses on optimising the properties of the existing material as opposed to developing new materials.

A major focus of research since the 1990s is related to highly cross-linked polyethylene (HXPE). This is where either ionic or covalent bonds have been created to bind the polyethylene chains within the material. HXPE has been shown to improve wear resistance, as well reducing the risk of the material delaminating, where a large thin sheet of material fractures from the surface of the polymer (Minoda et al., 2009). Despite this, there are still major drawbacks to the use of HXPE. It has been found that the wear debris resulting from HXPE can be more biologically dangerous than that of UHMWPE, increasing the risk of osteolysis, as well as reducing the fracture toughness of the material (McKellop, Shen, Lu, Campbell, & Salovey, 1999).

Another common modern modification to standard UHMWPE is the introduction of Vitamin E into the component. Vitamin E aims to stabilise the material to reduce oxidation and improve the wear resistance of the component. This is a relatively new development within orthopaedics and is still a controversial method of "improving" the component. Initial studies are showing that the addition of vitamin E to UHMWPE could produce desirable improvements in these characteristics (Chen et al., 2016; Salemyr et al., 2015; Takahashi et al., 2016).

1.7 Aims and Objectives of Project

This thesis details a project that has been conducted to develop a measurement and analysis methodology that can measure volumetric wear on ultra-high molecular weight polyethylene (UHMWPE) orthopaedic total joint replacements of the knee and ankle without the need for any pre-wear information. This is conducted through reconstruction of the unworn geometry of a TKR or TAR prosthesis using portions of the component that have not experienced wear. Comparison of this unworn geometry to measured worn geometry leads to the calculation of volumetric wear on a prosthesis.

The broad overall aims of the project can be summarised as follows:

I. To create an accurate, repeatable, and transferrable method for the measurement of volumetric wear on the articular surfaces of UHMWPE TKR and TAR components through the use of verified and repeatable metrology equipment.

II. To accurately quantify volumetric wear on any TKR or TAR component without the presence of any type of pre-wear information, using only information attained from the worn component.

This will be completed through the accomplishment of several smaller objectives, which include, but are not limited to:

a. Development of a repeatable method for the configuration, fixturing, alignment, strategy and acquisition of data using a combination of metrology apparatus. This may include the use of coordinate measurement machines (CMMs) and Industrial Computed Tomography (CT).
b. Creation of a robust methodology for the isolation of unworn data of components, to be used to create reference geometry with which to compare measured worn component data.
c. Evaluation and selection of accurate and repeatable approaches for the reconstruction of unworn component geometry using unworn portions of prostheses to use as reference geometry for volumetric wear quantification.
d. Development of accurate calculation methods to quantify volumetric wear on the articular surface of UHMWPE orthopaedic components.
e. Application of the developed method to cohort studies on a variety of component designs, wear application methods and wear severity to calculate the material loss.
f. Evaluation and appraisal of volumetric wear results gained in cohort studies. Where possible, comparisons can be drawn between the measured results and data gained using alternative methods, such as gravimetric measurement.
g. Comparison between measured volumetric wear results and published data found in literature in situations where other comparator data is not available.

1.8 Thesis Structure

The work carried out towards the accomplishment of the aims and objectives defined in 1.7 will be detailed throughout the following 11 chapters and associated appendices. For ease of navigation and clarity of information, this section will include a summary of the content of each chapter.

- Chapter 2 – Literature Review
    - This chapter evaluates the current position of wear measurement in orthopaedics. A consideration of simulation methods will be proposed, alongside an evaluation of the typical wear volumes found in TKR and TAR. As well as this, methods that have been developed to measure wear on such components will be critiqued and evaluated to establish the novelty of the method proposed in this thesis.
- Chapter 3 – Methodology
    - This chapter introduces the measurement that has been created for the quantification of volumetric wear on UHMWPE TKR and TAR components. The metrology apparatus used will be described along with how they are applied in the context of the method. Further to this, factors affecting the method that can be defined through experimentation are discussed along with the linear process for the calculation of volumetric wear.
- Chapter 4 – Comparison of Surface Topographical Parameters between Worn and Unworn areas of TKR components.
    - Chapter 4 presents the first of the studies performed as part of this project. This study attempts to distinguish between worn and unworn areas of the same TKR component through the analysis of surface topographical parameters.
- Chapter 5 – Measurement and Validation of Two-Dimensional Wear Methodology on Computational and 3D printed component
    - This chapter presents a study using a computationally worn TKR component that was then manufactured using 3D printing. The developed method was applied to the 3D printed component to both validate the two-dimensional wear measurement methodology and linearise the overall method of volumetric calculation.
- Chapter 6 – Measurement of Volumetric Wear on Wear Simulated TKR components
    - This chapter applies the method developed in Chapter 3 to a cohort of TKR components that had undergone wear simulation. The volumetric results gained in this study were compared with those found by gravimetric weighing and the study also helped to further refine the methodology of the overall method.
- Chapter 7 – Measurement of Volumetric Wear on Retrieved TKR components

- This chapter applies the developed method to a cohort of retrieved TKR components of varying designs. As these components were retrieved, gravimetric reference data was unavailable. However, measured results were compared to published data for volumetric wear on retrieved components.

- Chapter 8 – Measurement of Volumetric Wear on Wear Simulated TAR components
  - Chapter 8 focuses on the application of the method developed in Chapter 3 to a cohort of wear-simulated TAR prostheses. Linearisation of the overall method for TAR volumetric calculation was performed along with a comparison between measured results and published data on volumetric wear in TAR components.
- Chapter 9 – Discussion
  - This chapter will include a discussion of the findings of the studies detailed in Chapters 4-8 related to the aims and objectives described in this chapter. The novelty of the research will also be defined in Chapter 9.
- Chapter 10 – Conclusions
  - This chapter will summarise the major outcomes arising from the application of the developed method to all studies, considering the conclusions that can be drawn.
- Chapter 11 – Further Work
  - This chapter will discuss potential future applications of the method developed as well as further studies that could be performed to improve the accuracy and repeatability of the method.

1.9 Summary

This chapter has introduced the rationale behind the content of this thesis as well as describing the overall aim of the project. In addition to this, the objectives to be fulfilled to reach this aim have been detailed and will be referred back to in Chapter 10 during a discussion of the thesis outcomes. Finally, the overall layout of the thesis has been provided, with a brief introduction to the content of each chapter.

Chapter 2 – Literature Review

2.1 Introduction

This chapter will explore existing literature in the area of volumetric wear measurement for TKR and TAR components. Methods that are used to simulate components will be reviewed, considering how components are tested in a laboratory setting. It will also be considered whether these components truly represent clinically relevant wear volumes, and thus whether they can be used to validate a measurement method.

Following this, analysis of typical wear volume on a TKR component will be performed, covering studies using both standardised and novel methodologies. Both simulated and retrieved components were analysed to provide a full study of the wear volumes that would be expected from TKR components.

An evaluation of the limitations of the standardised gravimetric method will be completed, alongside an appraisal of CMM methods that have been developed to measure volumetric wear in TKR. Micro-CT was also used in this project, as a development method to create CAD geometry for use with CMM as opposed to a measurement method, and therefore only a brief consideration of the application of Micro-CT in wear volume calculation will be discussed.

Total Ankle Replacement research lags significantly behind TKR research. However, the typical wear volumes that would be found in TAR will be considered, alongside wear measurement methods that have been used for TAR components.

2.2 Total Joint Replacement Simulation Methods

The simulation of wear on the articular surfaces of total joint replacement components has always been a tool for assessing product performance before the components become commercially available, and are a requirement of numerous international standards (S. M. Kurtz, 2004). Although historically, testing studies have been completed through the use of pin-on-disc or pin-on-plate testing, components are now generally tested on multi-station simulators which aim to replicate the natural joint motion seen in normal service life. Such simulation has been shown to replicate wear patterns and rates comparable to those found in a clinical setting (Abdelgaied, Fisher, & Jennings, 2017; Brandt, Charron, Zhao, MacDonald, & Medley, 2011; Claire L Brockett, Jennings, Hardaker, & Fisher, 2012; Cranin, 1987). This would suggest that the simulation of TKR components wear is an effective way of replicating the in-service wear conditions that a component would undergo.

TKR wear simulation is far more advanced than simulation methods for TAR components. An initial study in 2007 found that a knee simulator test rig could be used to successfully simulate TAR components, it was however noted that although the simulation studies appear successful, further analysis would be required to determine if the wear rates found were clinically relevant (Carol J. Bell & Fisher, 2007). A subsequent study compared wear volumes between a cohort of wear simulated (using a knee simulation rig) and short-term retrieved (up to two years) TAR components. The study found that this method of wear simulation produced comparable wear rates, again suggesting that wear generated through simulation of TAR components using a knee simulator is clinically representative (S. Affatato et al., 2009).

2.3 Typical Total Knee Replacement Wear Volumes

As discussed in 2.2, it is agreed that the application of wear using a simulation rig is a clinically representative method of applying wear to both TKR and TAR components. Another important factor to consider is the volume of wear that would be expected to occur on such components. This section will consider published studies reporting volumetric wear rates measured using a variety of methods. These wear rates can form a basis to assess whether the wear rates acquired in the current research by the author can be considered clinically relevant.

Volumetric wear is typically measured in cubic millimetres of material removed (mm^3). There can be variation in the reporting of wear rates depending on the method in which wear was applied, whether the components have been simulated or retrieved. In the case of simulated components, wear rate is typically reported as cubic millimetres per million cycles ($mm^3/1 \times 10^6$ cycles), whilst retrieved components are generally reported as cubic millimetres per year of implantation (mm^3/year). This is due to a lack of definitive quantification for the number of cycles in a retrieved component.

When using a gravimetric method wear rate is typically reported as a mass in milligrams per million cycles (mg/1 x 10^6 cycles). This can be easily converted to $mm^3/1 \times 10^6$ cycles using the density of UHMWPE, estimated to 0.97g/cm^3 (Tam & Bhatnagar, 2016). For example, a wear rate of 10mg/1 x 10^6 cycles would be equivalent to 10.31$mm^3/1 \times 10^6$ cycles.

To be able to directly compare volumetric wear rates from studies reporting in different ways, this thesis will consider all published wear rates in cubic millimetres per million cycles. Previous literature considering the

activity of patients who have undergone joint replacement has estimated that the annual number of cycles a lower-body joint (hip, knee and ankle) experiences varies between 0.9 and 1.5 million cycles per year of implantation (Gioe, 2007; Huddleston, 2009; Naal, 2009; Schmalzried et al., 1998; Wallbridge & Dowson, 1982; M. Wimmer, 2002). To be able to fully appreciate the measured wear rates, studies that report in a unit other than cubic millimetres per million cycles will be converted using these bounds, to directly compare wear rates.

Another consideration in the measurement of volumetric wear rate is the effect of "running in" wear. Running in wear describes the phenomenon of wear rate not being constant across the life cycle of a component and is often higher in the initial phase of either simulation or implantation (Blunt, Bills, Jiang, & Chakrabarty, 2008). This can be seen in Figure 9 with the wear rates for both CMM and Gravimetric measurement tapering with an increase in cycles.

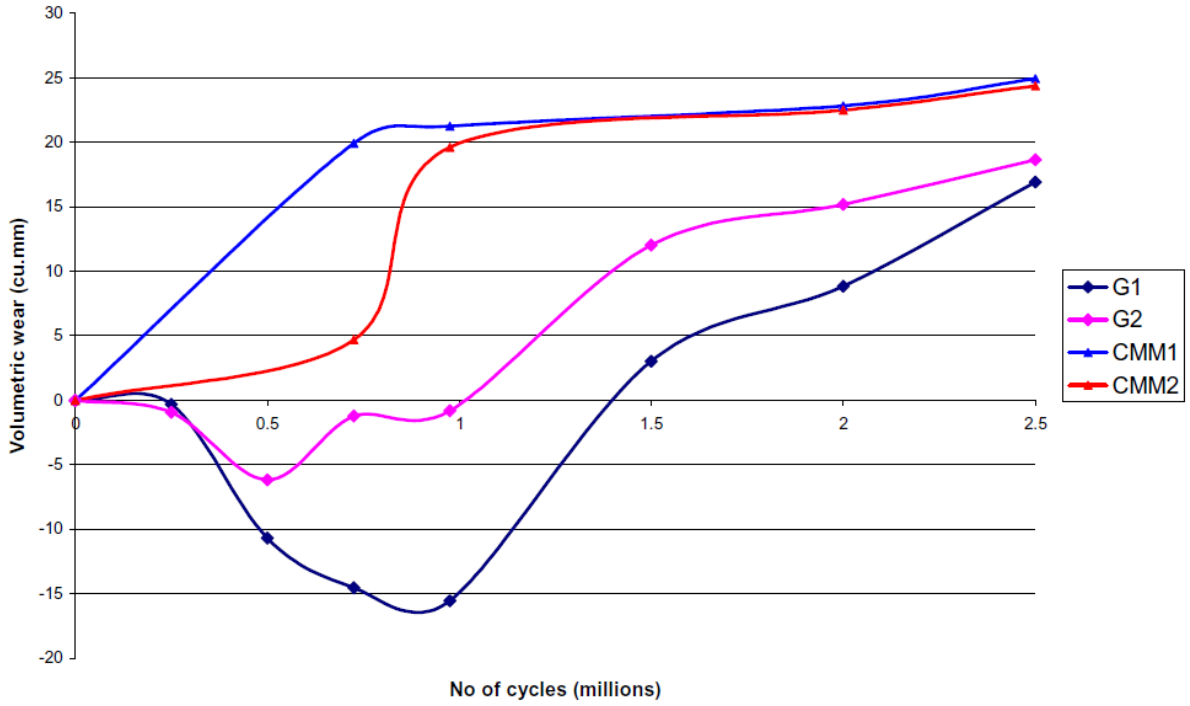

Figure 9 - Example of the effect of fluid uptake on the wear of simulated components (P. Bills, Brown, Jiang, &

2.3.1 Simulated TKR Components

Considering wear simulated components several studies have been performed to assess volumetric wear on TKR components. A study in 2015 performed 6.1 million cycles of simulator testing on a cohort of three fixed bearing type components. Gravimetric measurement was performed and found that the wear rate during the first 3 million cycles was between 26.3 $mm^3/1 \times 10^6$ cycles and $34.3mm^3/1 \times 10^6$ cycles, and then between $11.3mm^3/1 \times 10^6$ cycles and $23.3mm^3/1 \times 10^6$ cycles for the second 3 million cycles, suggesting a level of "running in" wear (M. G. Teeter, Parikh, Taylor, Sprague, & Naudie, 2015).

Flores-Hernandez et al found in 2015 considering volumetric wear on a cohort of crosslinked unicompartmental TKR components and found a wear rate of approximately $1.9mm^3/1 \times 10^6$ cycles. Unicompartmental TKR wear rates represent a single condyle, it could therefore be surmised that for a full component this wear rate could be estimated to be $3.8mm^3/1 \times 10^6$ cycles for a bicondylar design, although differing loading conditions across the condyles could affect this. It is also important to note that this study considers more modern highly crosslinked type UHMWPE components which typically display lower volumetric wear rates than traditional UHMWPE components.

As well as the type of component and material, the level of activity that components are subject to, can also affect the wear rate. Schwiesau (2013) studied the effect of highly demanding daily activities, such as stair climbing and rising from a chair, on the wear rate of a cohort of unicompartmental components. The highly demanding activities were simulated alongside an ISO 14243 standard gait cycle control cohort, with wear measured using the gravimetric method. The control cohort was found to have a volumetric wear rate of $3.1mm^3/1 \times 10^6$ cycles, with the highly demanding activities components having a volumetric wear rate of $12.1mm^3/1 \times 10^6$ cycles, showing the effect that different activities can have on measured wear rate.
A comparative study was performed in 2003 to evaluate differences in wear rate between traditional and crosslinked UHMWPE bicondylar TKR components. The study simulated components and then evaluated wear using the gravimetric method. It was found that there was no significant difference in wear rate between fixed and mobile-bearing components. Three different designs of non-crosslinked UHMWPE TKR components were found to have volumetric wear rates of $13.4\pm1.1mm^3/1 \times 10^6$ cycles, $14.8\pm1.2mm^3/1 \times 10^6$ cycles and $15.4\pm0.8mm^3/1 \times 10^6$ cycles. The crosslinked components displayed wear rates of $2.78\pm0.38mm^3/1 \times 10^6$ cycles,

again showing that crosslinked UHMWPE displays a significantly lower wear rate than non-crosslinked UHMWPE (Johnson et al., 2003).

The University of Leeds performed a study in 2018 to evaluate the effect of conformity on TKR wear rates. A cohort of highly-conforming components was compared to flat components to investigate this effect. It was found that highly conforming components displayed wear rates of 4±1mm^3/1 x 10^6 cycles compared to 2.3±0.3mm^3/1 x 10^6 cycles for non-conforming components. This suggests that a lower level of conformity may produce lower wear rates. All components used in this study were highly crosslinked UHMWPE (C. L. Brockett et al., 2018).

Blunt et al reported in 2008 on a series of simulated TKR components that were measured using both CMM and gravimetric methods. Volumetric wear rates measured using the gravimetric method were found to be between 5.3mm^3/1 x 10^6 cycles and 9.2mm^3/1 x 10^6 cycles, whilst the CMM method found a range of between 6.2mm^3/1 x 10^6 cycles and 9.7mm^3/1 x 10^6 cycles for the same components. The study did not discuss the type of UHMWPE used. (Blunt, Bills, Jiang, et al., 2008)

This section has shown that volumetric wear rates for simulated TKR components have been estimated to vary between 2.3mm^3/1 x 10^6 cycles and 34.3 mm^3/1 x 10^6 cycles. Such a wide range of values shows that many factors can affect volumetric wear rates, such as design, material, conformity, and simulation conditions.

2.3.2 Retrieved TKR Components

Retrieved components are quantified using different methods to simulated components. As previously discussed, the gravimetric method cannot be used for retrieved components due to the requirement for pre-wear data to be collected. This section describes several studies using alternatives to the gravimetric method to assess volumetric wear on TKR components.

Blunt et al reported wear volume from a single retrieved component, of similar visual appearance to two of the components used in the study in Chapter 7. This study used CMM as a measurement method, using an unworn manufacturer supplied CAD model as an unworn reference. It was found in this study that the magnitude of volumetric wear on the component equated to 93.6mm^3. It was discussed in the publication that the implantation time of the TKR was unknown, but not thought to exceed 5 years, equating to between

approximately 4.5 and 7.5 million cycles. Based on a 5-year implantation time this would lead to a volumetric wear rate of between 12.48mm^3/1 x 10^6 cycles and 20.8mm^3/1 x 10^6 cycles. (Blunt, Bills, Jiang, et al., 2008)

Knowlton et al twice reported wear volumes on retrieved TKR components. The first study in 2012 used a CMM based method to evaluate wear on a cohort of five TKR components. This study then used an autonomous mathematical reconstruction method to calculate volumetric wear, which did not require pre-wear geometry to be known. The study found volumetric wear of between 5mm^3 and 105mm^3 with the components undergoing 5 million cycles of testing, corresponding to volumetric wear rates of between 1mm^3/1 x 10^6 cycles and 21mm^3/1 x 10^6 cycles (Knowlton & Wimmer, 2012).

A subsequent study in 2016 applied the same methodology to a cohort of 64 retrieved components. The volumetric wear rate of the components was found to be 12.9±5.97mm^3/year which corresponds to a range of between 10.4mm^3/1 x 10^6 cycles and 17.0mm^3/1 x 10^6 cycles based on the upper and lower ranges of both the tolerances stated and the number of cycles per year (Knowlton et al., 2016).

A 2006 study considered volumetric wear on 2 cohorts of a total of 17 retrieved TKR components with varying implantation times. Again volumetric wear rate was assessed using a CMM based method with the wear rate calculated to be 77mm^3/year and 85mm^3/year for the two cohorts respectively, corresponding to volumetric wear rates of between 51.3mm^3/1 x 10^6 cycles and 85.6mm^3/1 x 10^6 cycles, or 56.7mm^3/1 x 10^6 cycles and 94mm^3/1 x 10^6 cycles for each cohort respectively depending on the number of cycles per year. (M Kop & Swarts, 2007).

A 2001 study evaluated volumetric wear on a cohort of 33 retrieved components, many of which were exhibiting high levels of visible surface damage. The analysis was performed through the use of a “computer-driver, laser-based CyberScan 206 three-dimensional inspection system”. This study found volumetric wear rates for components ranging from 24mm^3/year to 4088mm^3/year, corresponding to a minimum of 16mm^3/1 x 10^6 cycles and a maximum of 4542mm^3/1 x 10^6 cycles. When compared to other studies it appears that the higher values shown are not representative of the majority of retrieved TKR components. It was noted by the authors that the components showing large amounts of volumetric wear had very short implantation times, which could suggest that these components suffered mechanical failure as opposed to wearing (Benjamin, Szivek, Dersam, Persselin, & Johnson, 2001).

This section has presented studies considering volumetric wear on retrieved TKR components. Volumetric wear rates are in the range of 1mm^3/1 x 10^6 cycles to 4088mm^3/1 x 10^6 cycles, representing a very different level of wear, although the higher levels here must be considered in the context of the gross damage they exhibited.

2.3.3 Summary

Table 1 summarises the typical volumetric wear rates found in the studies detailed in this section.

Author	Simulated/Retrieved (S/R)	Volumetric Wear Measured (mm^3/1 x 10^6 cycles)
Teeter et al.	S	11.3 - 34.3
Flores-Hernandez et al.	S	3.8
Schwiesau et al.	S	3.1 - 12.1
Johnson et al.	S	2.8 - 15.4
Brockett et al	S	2.3 - 4.0
Blunt et al	S	5.3 - 9.7
Blunt et al	R	12.5- 20.8
Knowlton & Wimmer	R	1.0 - 21.0
Knowlton et al	R	10.4 - 17.0
Kop & Swarts	R	51.3 - 94.0
Benjamin et al	R	16.0 - 4542.0

Table 1 - Typical TKR wear volumes found in this chapter.

Considering the values shown in Table 1, using the maximum and minimum bounds of each study, the average volumetric wear on a simulated (S) component was found to be 9.46mm^3/1 x 10^6 cycles, with retrieved (R) components exhibiting an average of 478.6mm^3/1 x 10^6 cycles. This is heavily skewed by the Benjamin study. If this study is removed to consider components without a gross amount of wear, the average for retrieved components is 28.5mm^3/1 x 10^6 cycles. The difference between simulated and retrieved components could be attributed to a variety of factors, including component design, the use of crosslinked UHMWPE, different input and loading conditions and cohort size studied.

2.4 Methods of Volumetric Wear Measurement in Total Knee Replacement

The wear of UHMWPE TKR components is a major challenge to the longevity of a prosthesis, with it estimated that wear or surface damage causing a quarter of failures necessitating revision of the TKR (S. M. Kurtz, 2004). This shows that there is a very pressing need to be able to quantify and understand this wear, evaluate what volumes of wear are acceptable, and what volumes of wear could potentially lead to problems during the components working life.

Many methods can be used to evaluate UHMWPE wear volume. The standardised, and most common method for wear measurement is the use of gravimetric measurement, which evaluates wear volume by measuring a change in the mass of a component and converts this to a wear volume using the density of the component. This method although standardised does suffer from some issues. The most notable of these is the requirement for pre-wear geometry to be known to allow the method to be applied. The absence of pre-wear data renders gravimetric measurement redundant in the case of retrieved components, as changes in mass cannot be evaluated. Another method of wear measurement is based around clinical imaging techniques such as radiography (Devane, Bourne, Rorabeck, Hardie, & Horne, 1995; Martell & Berdia, 1997) or Roentgen stereophotogrammetric analysis (RSA) (Selvik, 1990). These methods involve the in-vivo analysis of TKR components, and rely on a series of chronological clinical images, with implant size and position used to estimate wear volume. These methods again require pre-wear data to be available to be able to measure wear volume.

Modern methods in UHMWPE wear involve the use of metrological equipment to use changes in component geometry to measure wear volume. Numerous authors have used micro-computed tomography (Micro-CT) to evaluate wear volume (Bowden, Kurtz, & Edidin, 2005; Elsner et al., 2015; Engh Jr, Zimmerman, Hopper Jr, & Engh, 2013; Matthew G. Teeter, Naudie, McErlain, et al., 2011), whilst other methods have utilised a coordinate measurement machine (CMM) to create a geometrical method (P. Bills et al., 2005; P. J. Bills, 2007; Blunt, Bills, Jiang, et al., 2008; W. Jiang et al., 2018; Knowlton & Wimmer, 2012). These methods have generally been used in a simulator trial setting, with pre and post wear measurements being compared to evaluate the material loss, in a similar way to Gravimetric measurement. However, a few of these methods have attempted to recreate pre-wear geometry, aiming to remove the necessity for pre-wear data to be available. These methods will be discussed in more detail later in this chapter.

This thesis describes a method that recreates pre-wear geometry to allow for wear volume calculation. As it is an in-vitro method, it is not comparable to clinical imaging base methods and therefore these will not be discussed in any greater detail. As the gravimetric measurement method is the standardised and accepted method, which forms a benchmark for alternative methods, this will be explored in greater detail in the next section.

2.4.1 Gravimetric Measurement

As previously discussed, gravimetric measurement is a laboratory-based wear measurement method that is widely considered the "gold-standard" approach in the measurement of orthopaedic wear and is governed by ISO14242 for THR and ISO14243 for TKR (BSI, 2009). As mentioned in the previous section, gravimetric measurement measures wear by assessing the mass change of a component and its density, corresponding to a volume of material loss. This mass measurement is typically acquired using a high precision microbalance, with the standards requiring a minimum accuracy of ±0.1mg in the equipment used (BSI, 2010).

Gravimetric measurement, although standardised and considered accurate in the context of measurement of simulated components, is not without significant challenges that may affect both the accuracy and range of situations in which the method can be used. When simulating components on TJR simulators such as those discussed earlier, the testing typically takes place within a lubricated environment, aiming to recreate the in-service conditions the components would experience as accurately as possible. In a laboratory setting this is generally achieved through the use of bovine serum, although attempts have been made to create artificial synovial fluid (Bortel, Charbonnier, & Heuberger, 2015; Harsha & Joyce, 2011; Reinders, Sonntag, & Kretzer, 2015). UHMWPE is a porous material, which will readily absorb lubrication fluid during testing. This fluid affects the mass of the measured component. This can be mitigated using soak controls, which are components that are within the simulation environment, often loaded, but do not undergo motion and are therefore not subject to wear, and also by allowing components to rest between simulation and measurement, although this remains a pitfall of the method (S. M. Kurtz, 2004). Figure 9 shows the effect that fluid uptake can have in the measurement of volumetric wear in TKR components (P. Bills et al., 2005).

Figure 9 shows the measurement of wear-simulated TKR components using two different methods, the gravimetric method, and a CMM based method, which will be discussed later. The Y-Axis represents the volume of measured wear, whilst the X-Axis displays the number of cycles of wear testing the components have undergone, in millions of cycles. It is noticeable that in the case of both gravimetric measurements (G1 & G2) the wear volume is negative between 0 and approximately 1.0-1.5 million cycles. The components in this study were rested for 48 hours before measurement to allow an "equilibrium drying condition" to be reached. A negative wear volume in the case of Gravimetric measurement indicates that assuming the density of a

material is constant, the mass of the component has increased. This could be a direct result of fluid uptake within the components.

Although soak controls can be used to mitigate the effect of fluid uptake on wear measurement results, soak control components are not entirely representative of actual components undergoing wear and therefore may prove to be inaccurate. The agitation of lubricant in the area surrounding the component, combined with the removal of material from articular surfaces, therefore changing the geometry of the component during the wear process could affect the fluid uptake of a UHMWPE insert. In addition to this, previous studies have shown that lubricants used in wear simulation experience changes in properties during testing, with protein concentrations, in particular, changing (Good, Clarke, & Anissian, 1996; Harsha & Joyce, 2011).

Another factor that can affect the accuracy of Gravimetric measurement is the presence of embedded third body particles within the component (Liza, Haseeb, Abbas, & Masjuki, 2011). This is the situation in which generally metallic particles have been released from the femoral components of TJR components and have become entrenched within the body of the UHMWPE component. These components are generally of higher density than the UHMWPE material, and the mass of the component will therefore increase and lead to an inaccurate evaluation of wear volume. It has been stated that the embedding of third body particles is a leading factor that can cause a wide variety of failure modes of UHMWPE components (Crowninshield, Wimmer, Jacobs, & Rosenberg, 2006; Muratoglu, Ruberti, et al., 2003). This could lead to a similar effect to that shown in Figure 9, where mass change is inaccurately calculated and subsequent wear volume calculations are adversely affected.

It is worth noting that these factors are far more prevalent in situations of low wear, as shown in Figure 9. As a component wears in a greater volume, the contribution of these factors to the overall mass change evaluation diminishes and therefore the negative effect on accuracy is reduced. With wear rates in TJR components becoming lower and lower through the creation of new technology, there is a need to develop methods that are accurate at lower wear volumes.

In addition to these issues with the gravimetric measurement method, the most obvious issue is a lack of transferability to “real-life” situations, such as the measurement of wear on explanted components. Studies using gravimetric measurement rely on data acquired from the measurement of a component before wearing

occurs to be able to have baseline data from which to calculate mass change (Carmignato, Spinelli, Affatato, & Savio, 2011; Matthew G. Teeter, Naudie, McErlain, et al., 2011). In the case of an explanted component, there is unlikely to be any pre-wear data. Although it may be possible to have manufacturer data for this, manufacturers have specific tolerances that components should be manufactured within, which are standardised, meaning that two "identical" components will inevitably have differences in geometry and mass, meaning the manufacturer supplied values are purely nominal and not necessarily accurate for the worn component (ISO, 2011a).

2.4.2 Coordinate Measurement Machines for TKR wear measurement

Coordinate measurement machines are devices that are used to measure the geometry of components through the use of contact probing. They are extensively used for quality control and measurement applications across the engineering world and are widely accepted as a metrological method (Ferreira, Oliva, & Perez, 2013).

The use of CMM for TKR wear measurement was first attempted by Muratoglu et al in 2003. Muratoglu used a cohort of 3 unworn TKR components which underwent simulated wear, with 5 million cycles of wear testing performed. The components were measured using both the gravimetric and CMM measurement methods at regular intervals of testing to measure both total wear volume and volumetric wear rate.

Gravimetric measurement was performed as per the standardised method previously described. Following simulation and before gravimetric or CMM measurement was conducted, components were allowed to reach thermal equilibrium by resting in a temperature-controlled environment for 48 hours. The superior articulating surface of the TKR components was measured as a single entity, resulting in a cloud of approximately 7300 points with a point spacing of 0.75mm in both the X and Y direction. This point cloud was then used to construct a surface to represent the component at the various stages of wear, no method has been stated for how this surface was determined. The surfaces were then compared and the difference between the two surfaces was calculated and represents the wear volume at each stage of testing.

The study found that average volumetric wear as measured by the CMM method was 41 ± 4mm^3, whilst the gravimetric method produced average volumetric wear of 40 ± 8mm^3. This showed "close agreement"

between the two methods, with the corresponding volumetric wear rates showing especially similar results. (Muratoglu, Perinchief, et al., 2003)

This method shows that the use of CMM measurement can provide a measurement result comparable to the gravimetric method. Although this study showed excellent results and agreement between the two methods, the CMM method in this study suffers from the same issue as the gravimetric measurement method, requiring predicate geometry to be able to apply the method. As previously mentioned, a requirement for pre-wear data for comparison means that volumetric wear measurement for explanted components would not be possible using this method. In addition to this, the described study used a relatively large point spacing, which has the potential to generalise large areas of the surface and does not allow for the measurement of surface features smaller than 0.75mm.

A 2005 study by Bills et al used a similar method to Muratoglu et al to measure volumetric wear on a single RPF TKR component. The component underwent 2.5 million cycles of testing on a knee simulator, to simulate the equivalent of 5 years of in-service wear. Again, pre-test measurements were acquired using both a CMM and the gravimetric method, with repeat tests being taken at regular intervals. Again, components were allowed to "stabilise in controlled conditions" for a minimum of 48 hours between simulation and measurement to allow for equilibrium drying and thermal condition to be reached (P. Bills et al., 2005). This study also used this stabilisation time to allow components to achieve an equilibrium core temperature by storing components in a temperature-controlled environment. It has been suggested by Fisher et al that unloaded relaxation of a component for 48 hours can allow for the recovery of greater than 80% of recoverable component creep, with this figure rising to 90% at 100 hours (Derbyshire, Hardaker, Fisher, & Dowson, 1994). The components in this study were allowed to stabilise for a minimum of 72 hours, with the author estimating that 85-90% of recoverable creep had been recovered before measurement.

To measure the TKR component, a point cloud at a spacing of 0.5mm x 0.5mm was used to measure the surface. The probe used was a Renishaw SP600 scanning probe, which is 89mm in length and can achieve measurement speeds of up to 300mm/s (P. Bills et al., 2005). The authors did not state the measurement parameters that were used in this study, nor was it stated the number of points that were measured. This study measured the lateral and medial articular surfaces of the TKR components as two separate entities. The unworn CMM measurement taken at the beginning of testing was used as the reference geometry for further

measurements to allow for accurate relocation of the data points in subsequent measurements, ensuring that the data points taken would be accurately repeated in the X-Y axis, with the Z-Axis position changing for different wear volumes. A surface was constructed from each measurement using a “simple fitting operation”, with the worn surface being compared to the original unworn surface to measure the volumetric wear at each testing stage. The gravimetric measurement method used is not stated and it can be assumed that the traditional method was used.

Figure 9 shows the results that were gained using this method. As previously discussed, unusual results, potentially attributable to fluid uptake were measured between the beginning of testing and 1.5 million cycles. It was noted that after 1.5 million cycles the wear volume results stabilised (P. Bills et al., 2005). No statistical comparison was made between the CMM and gravimetric results, but it was hypothesised that correlation is seen between the two methods in the interval 1.5-2.5 million cycles. The wear volumes found after 2.5 million cycles were approximately an average of 24mm^3 using the CMM method, with the gravimetric method measuring approximately an average of 17.5mm^3.

This study again shows excellent promise in creating a CMM method for TKR wear measurement, with a greater measurement resolution than that found in the 2003 study, potentially allowing smaller surface geometrical features to be measured. This method again requires pre-wear geometry to be known, to be used as both a reference geometry and as a comparator to worn measurements (P. Bills et al., 2005).

Blunt et al produced a study in 2008, which again compared the effectiveness of a CMM-based method to the gravimetric method using TKR components. This study used a cohort of 6 DePuy LCS Complete components. This study aimed to remove the necessity for pre-wear data to be present in the measurement of volumetric wear. As per the 2005 study from the same research group, stabilisation conditions were consistent, allowing components to achieve both a uniform temperature and fluid absorption level before measurement.

Components were simulated on a knee simulator and measured using the traditional gravimetric method. CMM measurement of the components was performed post-simulation. A CAD model of the component was built and used as a reference geometry tool to ensure repeatability in measurement point location. “Large numbers” of equally distributed points were measured in the unworn zone of the articular surface, no information is supplied as to the method used for this. These measurements were then converted into NURBs

using software and in conjunction with the created CAD model was used to create a surface that could be used as a basis for the unworn component. Using a method similar to the 2005 study, this created unworn surface was then compared to the full measured worn surface and the difference compared to calculate a wear volume. The measurement was performed 6 times with an average taken.

The second strand of this study attempted to apply this method to an explanted TKR component. The component was noted as visibly showing an extreme amount of volumetric wear and that it was not possible to recreate the unworn surface accurately. An unworn component of the same design was used to create a comparator surface.

The study produced results that appear to show good agreement between the Gravimetric and CMM results. No statistical analysis was performed by the original authors. However, a paired samples t-test was conducted by the author of this thesis to compare the results of this study. It was found that there was not a significant difference in the results for gravimetric (M=36.85, SD = 8.51) and CMM (M=40.85, SD=7.03) measurement methods; ($t(6)= -1.871$, $p=0.120$), suggesting that the two methods produce comparable results (Blunt, Bills, & Jiang, 2008).

When considering the explanted component, the volumetric wear rate was unable to be calculated as the implantation time was not known. Using the described method produced a distorted wear volume map and was therefore imported into a second analysis package and manually manipulated to provide a wear volume measurement result. The method resulted in a measured wear volume of $95.6mm^3$ (Blunt, Bills, & Jiang, 2008).

This method differs from the two previous methods in that it attempts to measure volumetric wear without the necessity for pre-wear data. The measurement strategy used was similar to that used in the previously described studies. To measure wear, an attempt was made to recreate the unworn component to act as a comparator to the measured worn component. No information is given as to how worn or unworn areas were differentiated from each other when creating an “unworn” component. The method appears to produce comparable results to the gravimetric method when used on simulated components. However, the method was not transferrable to an explanted component, with pre-wear geometry having to be used to calculate wear volume.

Another method of using a CMM to measure volumetric wear on TKR components was detailed by Knowlton and Wimmer in 2012. Knowlton and Wimmer attempted to create a method of wear measurement through "autonomous mathematical reconstruction". The study consists of different elements, both theoretical and practical.

The initial section of the study details a theoretical approach to measure volumetric wear by idealising a TKR component as a convex hemisphere, which was then triangulated with point spacing varied between 0.25µm and 7.5mm in both X and Y directions. This hemisphere was then tailored for 7 different sizes of a specific TKR design (NexGen, Zimmer), and modelled in the same way.

The study then goes on to digitise three unworn NexGen components using a non-contact optical CMM at a point spacing of 0.1mm x 0.1mm to create a grid of approximately 400,000 points. A filter was applied to the resulting dataset to remove points that were considered to be outlying. To do this, the average Z-height of each 0.2mm x 0.2mm window of the part was computed, and any part falling more than 0.05mm from this mean height was removed from the analysis. No rationale is provided for why this filter was applied. All components were measured in a temperature-controlled environment. The mass of the components was also measured using a micro-balance to allow for gravimetric measurement to be performed.

Material was then removed from the surface of the material using a wood-carving gouge, a form of hand tool. This does not represent clinically relevant data and it is unclear why this method of wear application was chosen for this part of the study. The components were then measured gravimetrically and allowed to rest for 24 hours before CMM measurement. CMM measurement, in this case, involved the tracing of the applied wear scar boundary using the optical CMM. This "gouged" point cloud was then triangulated as per previous sections of this study and the difference between this surface and the original measured surface represented the measured wear volume. This process was repeated five times, with each iteration representing a material loss mass of 10mg. Alongside the triangulation study, the study also applied a mathematical reconstruction method. A curve, representing an idealised NexGen component was fitted to measured points outside the gouged area. These curves were then used to interpolate the original unworn surface within the gouged area (Knowlton & Wimmer, 2012).

The method described in the previous paragraph was then applied to two further studies. The first analysed volumetric wear on a cohort of 6 NexGen components that had been worn using a knee simulator. The method was applied directly as above.

The second study applied the method to a cohort of 9 Miller Galante TKR retrieved components. Components that had experienced delamination or significant edge loading were removed from the study, which was limited to two different sizes of TKR. As there was no pre-wear data available, volume loss was compared to damage scores found in a previous study (M. A. Wimmer, Laurent, Haman, Jacobs, & Galante, 2012). The Hood damage score is a subjective scoring method in which a person ranks a component surface on a scale of 1-3 for 8 wear mechanisms (Schwarze et al., 2020). It would typically be expected that a higher damage score would correlate to a higher wear volume, although this may not be true depending on the mechanisms of wear occurring. For example, the Hood damage score included embedded particles in the surface of the components, but this would not affect the amount of wear.

Statistical analysis was performed to consider the correlation between different elements of this study. The R^2 correlation coefficient was used in most cases to assess for correlation between different methods of measurement. This coefficient is based on a regression model which considers the proportion of a dependent variable that is explained by an independent variable. A good agreement between two variables would yield a value of R^2 approaching 1 (Figueiredo, Júnior, & Rocha, 2011). Paired t-tests were also used to test for statistical significance in the difference between methods in the case of the gouged components.

The theoretical section of this study found that the hemispheric model closely approximated an unworn TKR surface, and used a convergence study to analyse the optimum sampling resolution. The study found that a point spacing of 0.1mm x 0.1mm resulted in a sampling error of less than $0.75mm^3$ across most components (Knowlton & Wimmer, 2012).

Whilst analysing the gouged components, it was found that volume loss calculated using pre-wear data correlated well (R^2=0.97) to gravimetric measurements. It was also found that the wear volumes calculated using the mathematical method also correlated well (R^2=0.954) with gravimetric results. Therefore, there was no significant difference between all three methods.

When the same method was applied to wear simulated components it was found that there was good agreement between the mathematical reconstruction method and gravimetric measurement (R^2=0.981).

It was found that for retrieved components, the magnitude of wear measured correlated well (R^2≥0.97 in both sizes) to the semi-quantitative damage scores, with an increase in damage score typically corresponding to an increased wear volume. Figure 10 shows this graphically. Wear volumes calculated for these components corresponded to wear rates of 39.2 ± 7.2mm^3/year for larger size components and 15.7 ± 2.7mm^3/year for smaller size components (Knowlton & Wimmer, 2012).

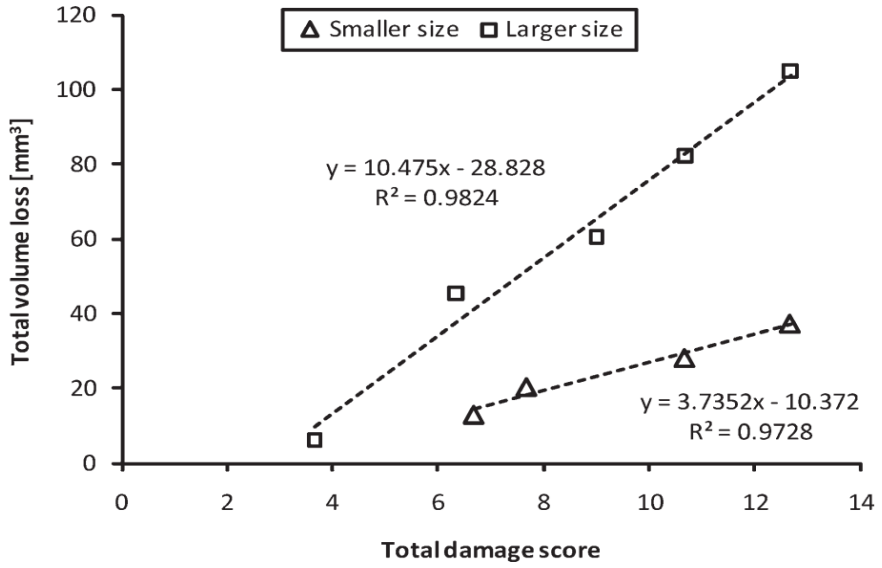

Figure 10 - Graphical representation of volume loss - Hood damage score correlation

This study produces a method of wear measurement that is applicable to both wear simulated and retrieved components, in the case of pre-wear data being unavailable. The theoretical element of the study provides excellent information related to the variation of CMM measurement resolution, finding that a 0.1mm point spacing provides optimum conditions.

The author believes that the section related to the gouged component surface does not accurately reflect the wear characteristics that would be expected from a TKR component, as the application of wear using a hand tool is not comparable to the use of a wear simulator, or in-service conditions. Although the study yields excellent agreement between the two measurement methods, there may have been more appropriate methods used to “create” wear on the articular surface.

A limitation of this method relates to the identification of wear edge location. For this method to be effective the wear edge must be visually identifiable by a CMM operator to effectively trace the wear scar region. This

may not be possible in situations of low-wear. This may also be difficult in the situation of high conformity components, where a large proportion of the articular surface is in contact, as a lower amount of visible unworn area would be available.

The statistical analysis performed illustrates the effectiveness of this method in all studies. Comparison of volumetric wear to Hood damage scores is a sensible comparator, as typically a higher damage score would lead to a higher wear volume, but further analysis of the exact wear mechanisms should be considered to fully consider this relationship.

Jiang et al produced a study in 2018 using a CMM-based method to measure volumetric wear on TKR components. The initial phase of this study involves the digitisation of an unworn DePuy Synthes Sigma TKR component. No information is provided on the measurement parameters used to digitise the component. The CMM point cloud of this component was then converted to a three-dimensional surface (W. Jiang et al., 2018).

Wear region detection was performed by considering the Z-height difference between adjacent measured points. The component was described as "worn out" if this difference was found to be greater than 0.1mm. The author also states that some "clearly wrong" coordinates were removed to enable accurate wear region identification. No explanation is given as to the cause of these data points, or the method used to distinguish them from the global geometry and subsequently remove them. The worn region of a component was then determined autonomously based on this 0.1mm height difference parameter. Worn and unworn areas were isolated using this analysis, with a 5^{th}-order polynomial curve surface fitting algorithm used to generate a representation of the unworn surface. No rationale is provided for the use of this method. Wear volume was calculated through a comparison of this reconstructed unworn surface to the measured worn surface of the component.

This study then applied both a computational and practical method of wear application to the 1 component previously used and used these methods to assess the effectiveness of the reconstruction method. A study was also conducted to consider the effect of scanning resolution.

Wear was applied computationally to the original unworn component measurement to a maximum linear penetration of 0.2mm. Several different wear areas sizes were created with the worn area percentage varying

between 0.29% and 38.55% of the condylar surface. No explanation is given as to the method used to determine the location, magnitude, or geometry of this wear scar.

An experimental method was also used which involved the creation of wear on the articular surface using a 24mm diameter ball-ended cutting tool. This created wear scars with a depth of between 0.1mm and 1mm, the wear scar created is shown in Figure 11. The component was also measured gravimetrically before and after wear application as a comparator. Gravimetric measurement was performed using the standard method.

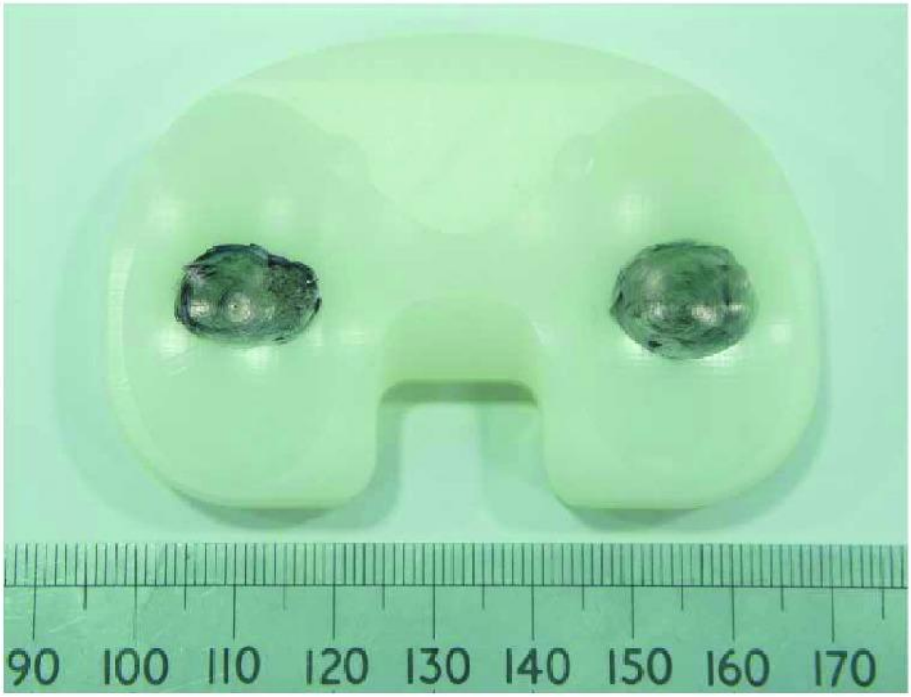

Figure 11 - Wear Scar developed using 24mm Ball-Nose Cutting Tool (W. Jiang et al., 2018)

Lin's concordance correlation coefficient (CCC) was used as a comparator between the two methods. CCC is a correlation comparator used to establish the correlation between a new measurement methodology and a "gold standard" methodology, in this case, Gravimetric measurement, where a result -1 represents a strong negative correlation, a result of +1 represents a strong positive correlation and result of 0 represents no correlation (Lawrence, 1989).

A study was conducted to consider the effect of scanning point spacing with a range between 0.1mm and 2.0mm X-Y grid spacing used on the unworn component measurement. It was found that increasing the point spacing reduced measured points from 31,133 to 90, reduced scan time from 519 minutes to 1.5 mins and

yielded a difference in volumetric wear of up to 8mm^3. It was decided from this study that a scanning interval of 0.2mm was to be used, to balance measurement time with accuracy (W. Jiang et al., 2018).

17 computational configurations of the worn area were used in this study with different wear area percentages generated in each. Volume loss measured using these configurations was found to vary between 0.1mm^3 and 17.4mm^3. The maximum error found between the unworn and computation study was found to be 0.2mm^3, with the CCC found to be 0.9997, showing a close correlation between the results.

Wear volume created using the experimental method ranged from 0.9mm^3 to 19.3mm^3 when measured Gravimetrically, with the applied CMM method evaluating wear volumes ranging between 1.0mm^3 and 19.5mm^3 when initial surface coordinates were used and 0.8mm^3 and 18.2mm^3 when using no pre-wear data. This again corresponded to excellent CCC's of 0.9998 and 0.9960.

Analysis of the results found that for accurate volumetric assessment to be conducted, at least 50% of the component would be required to be unworn, Figure 12 represents this graphically, showing that the accuracy of the developed method decreases with increasing wear area (W. Jiang et al., 2018).

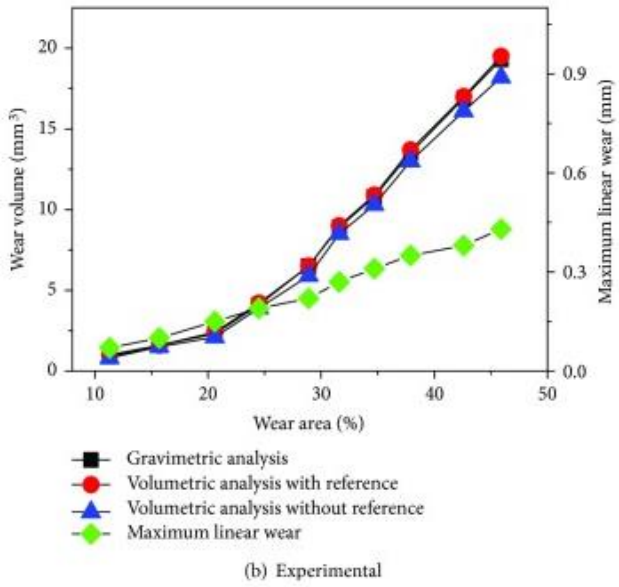

Figure 12 -Graphical Representation of wear area percentage effect on the accuracy of the method developed (Blunt, Bills, & Jiang, 2008; W. Jiang, Ji, Jin, & Dai, 2018; Knowlton, Bhutani, & Wimmer, 2016; Knowlton & Wimmer, 2012; M Kop & Swarts, 2007)

Before considering the limitations of this study, it is important to consider a follow-up study performed by Jiang et al. This study utilised the same method of wear measurement described in the above study, but applied this to a larger cohort of components, a major limitation of the initial study.

In this follow-up study, the method developed was applied to a cohort of 12 wear-simulated components which had been simulated in a previous study (Claire L. Brockett et al., 2016). Gravimetric measurement was performed using the standard method, with resting time before CMM measurement not considered due to the length of time since simulation had occurred. Point spacing for CMM measurement remained at 0.2mm in both X and Y directions based on the previous study.

The study found qualitatively that at low wear volumes, CMM produced comparable results to Gravimetric measurement, with consistent over-estimation by the CMM method at higher wear volumes, as previously seen in the Bills and Blunt studies discussed earlier (P. Bills et al., 2005; Blunt, Bills, & Jiang, 2008). Wear volumes measured in this study using the two methods were in the range of 9.12mm^3 (Gravimetric, Specimen 3) to 52.5mm^3 (CMM, Specimen 9). CCC values for CMM measurement when compared with Gravimetric measurement again showed high levels of correlation (CCC=0.990). The repeatability of CMM measurement was stated as 0.89mm^3, with three measurements performed per component. (Wei Jiang, Ji, Xiao, Jin, & Dai, 2018)

These two studies present a method that was developed to measure volumetric wear on TKR components without the need for pre-wear data (W. Jiang et al., 2018; Knowlton & Wimmer, 2012). The initial study had a major limitation in that measurement was performed on a single component rather than a coherent cohort. This issue was addressed in the second study.

When considering the method by which wear regions are detected, there is a clear issue. Wear regions were identified based on Z-shift between adjacent points, with a difference of 0.1mm used. No rationale was provided for the use of 0.1mm as a differential. This method introduces the concept of a hard wear edge, and that differences smaller than 0.1mm are not considered significant in the evaluation of wear volume. The computational study performed in this research found a maximum linear penetration of 0.2mm. Using the rationale of 0.1mm representing a wear area edge, it would be expected that measuring a linear penetration smaller than this would result in zero wear being measured.

The method of wear application used in the experimental study is comparable to the gouging method used in the previous study by Knowlton and Wimmer, in that it does not represent a clinically accurate wear pattern.

Information provided does not state what percentage of the condylar surface was classed as worn in this situation, but visual examination would suggest it does not exceed the 38.55% used in the computation study.

Previous studies related to the conformity of TKR components have examined the effect of high conformity on wear volumes. These studies typically consider conformity levels in the region of 0.9, or 90% of the component (C. L. Brockett et al., 2018; Schwarzkopf, Scott, Carlson, & Currier, 2015). This would suggest that a wear scar should cover a much greater proportion of the surface. Figure 13 shows wear scars mapped as part of a 2018 study by Brockett et al for a cohort of wear simulated components. As discussed in 2.2, wear simulation methods are widely accepted as producing clinically representative wear.

When Figure 13 is compared to Figure 12, there is a difference in the proportion of the surface that is considered to be worn. This would suggest that the experimental method used in this study, the use of a ball-nose cutting tool has not represented a clinically relevant wear pattern.

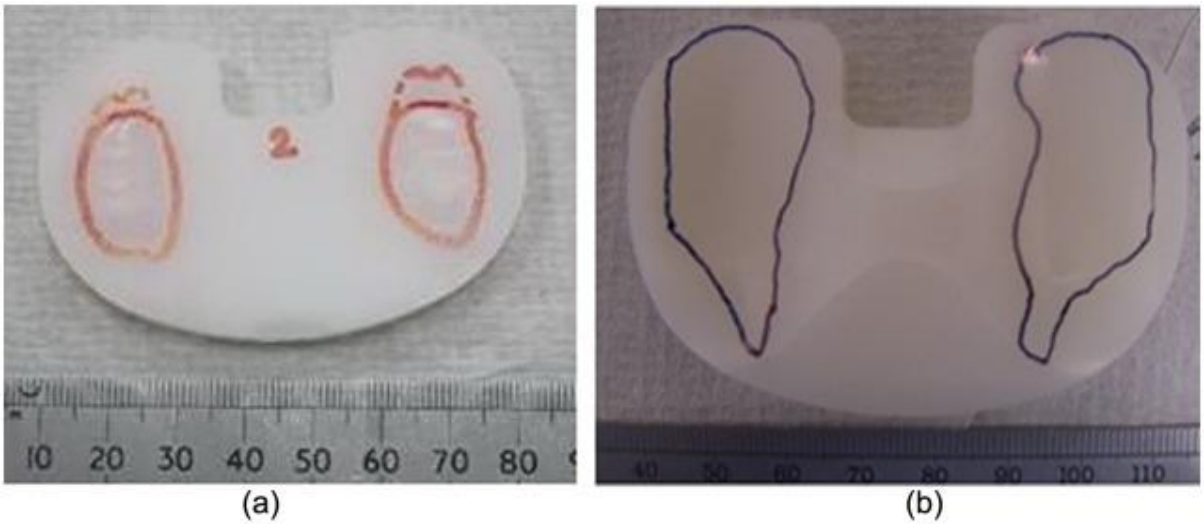

Figure 13 - Example of typical wear scar mapping (C. L. Brockett, Carbone, Fisher, & Jennings, 2018)

The methods described in this section use a variety of approaches to measure volumetric wear using CMM. Point spacing is an important aspect to consider when performing CMM measurements. The studies described in this chapter used point spacings in both X and Y directions of 0.75mm (Muratoglu, Perinchief, et al., 2003), 0.5mm (P. Bills et al., 2005), 0.1mm (Knowlton & Wimmer, 2012) and 0.2mm (W. Jiang et al., 2018). Jiang et al performed a convergence study to consider the effectiveness of scan interval, with 0.2mm considered the greatest balance between measurement accuracy and time constraints. The other studies did not perform this type of analysis.

The Muratoglu, Bills and Blunt studies all require a form of predicate geometry to be known to quantify wear volume. This means that none of the methods developed in those studies would be able to be used for a retrieved component, as pre-wear data would not be available. This is the same issue that is experienced using the gravimetric method. However, there is significant merit in these methods related to the lack of effect from fluid uptake, an issue that can be present using the gravimetric method. Blunt et al attempted to apply the method to a retrieved component, but it was found that the gross levels of wear on the component prevented this from being achieved.

The Knowlton and Jiang methods can both be successfully applied to a retrieved component, as they both employ autonomous reconstruction methods which can use unworn portions of components to reconstruct a full unworn surface. This negates the need for pre-wear data to be available. There are however pitfalls within both methods.

The Knowlton method requires a wear edge that is visible to the operator of the non-contact CMM. If this wear edge is not visible then the wear edge cannot be traced to define the worn or unworn areas, and therefore reconstruction cannot occur.

In the case of the Jiang method, the wear edge is defined by a difference in the Z height of adjacent points greater than 0.1mm. This assumes that there is a sudden step of magnitude greater than 0.1mm at all wear edges. It may be the case that smaller z-shift values could represent a wear edge but be excluded from the analysis. The study also mentions the removal of “clearly wrong” points, without stating the rationale for these to be removed.

The Jiang method has the potential to be applied to retrieved components, but this has yet to happen and therefore it cannot be assumed that the method will produce results comparable to typical wear volumes in retrieved components. The Knowlton method was successfully applied to a cohort of retrieved components, with a good correlation to damage score found.

To improve upon these methods it is critical to perform a more effective and flexible wear edge definition process, such that the wear edge is defined by more than a sudden step-change in Z-position, as well as ensuring that the method is applied to a variety of wear volumes and design.

2.4.3 Micro-Computed Tomography for TKR wear measurement

In the research detailed in this thesis, Micro-CT was used as a precursory technique to facilitate the creation of a computer-aided design 3D model of the TKR component on which wear is to be measured. Micro-CT was not used as a method of quantifying volumetric wear. Despite this, it is still important to consider how Micro-CT has been used on Total Knee Replacement components within the literature, as this will help to inform scanning parameters that are used when digitising the components.

A 2005 study used CT to analyse volumetric wear on a cohort of retrieved UHMWPE acetabular THR components. The components were scanned using a desktop CT scanner at an energy of 45kV (177µA). Unworn components of the same design were also scanned to use as references for wear volume determination. The study concluded that Micro-CT can be used as an "accurate, repeatable and applicable" method for the measurement of volumetric wear on such components. The authors suggested that long scan times and high data density/size were the major limiting factors of such a method (Bowden et al., 2005).

A study in 2011 used Micro-CT for the measurement of volumetric wear on UHMWPE tibial inserts. Again, unworn components were measured as a reference for volume loss calculation. Gravimetric results were also analysed for comparison. Scans were performed at 90kV (40mA), with 1200 individual images taken at approximately 0.3-degree increments. Reconstruction was then performed and volume was calculated to use as the worn reference. The study found high levels of congruency between the results gained in CT measurement and those gained through traditional gravimetric measurement with the authors stating that "no difference" was found between CT and gravimetric measurements, summarising that Micro-CT can provide "precise and accurate" volumetric measurements (Matthew G. Teeter, Naudie, McErlain, et al., 2011).

Outside of TKR, a 2008 study considered the use of Micro-CT for the measurement of spinal disc replacement components, also manufactured from UHMWPE. The components also contained titanium; however, this was removed pre-measurement. The study found that the repeatability of a Micro-CT method for measurement of such components was ±3mm^3. This compared unfavourably with the repeatability of gravimetric measurement, determined to be ±0.007mm^3. It was discussed that Micro-CT has numerous advantages concerning being able to consider the actual density of the part, which gravimetric can only estimate. However pre-wear data was still required as a comparator for volumetric material loss calculation (Vicars, Fisher, & Hall, 2009).

The studies detailed above show that Micro-CT can be used effectively for the measurement of the UHMWPE material used for the TKR and TAR components used in this thesis. It is useful to note the parameters used for scanning in the studies above, and these can be considered when digitising TJR components using Micro-CT.

2.5 Total Ankle Replacement Typical Wear Volumes and Methods of Wear Measurement

As well as considering TKR components it is also important to consider the typical wear rates and measurement methods associated with Total Ankle Replacement. Studies of TAR components of similar size, shape and design are not common due to the formative nature of TAR as an orthopaedic solution; however a selection of studies have been found that can be used as comparators, the volumetric wear rates measured are listed below in Table 2.

Authors	Volumetric Wear Measured (mm^3/1 x 10^6 cycles)	Type of Implant
Reinders et al (2015)	18.2 ± 1.4	HINTEGRA, NewDeal SA
Smyth et al (2017)	1.2 ± 0.6	Zenith, Corin
	25.8 ± 3.1	
Bell et al (2007)	10.4 ± 11.8	Mobility, DePuy
	16.4 ± 17.4	
	3.38 ± 10	
	10.4 ± 14.7	

Table 2 - Example of Volumetric Wear rates for TAR components measured from numerous studies

It can be seen in the literature that a wide variety of volumetric wear rates have been found for TAR components. All three studies in Table 2 assessed wear using the traditional gravimetric method.

The study by Reinders et al investigated volumetric wear on a cohort of 18 Hintegra components, with volumetric wear rates found to be approximately 18.2 ± 1.4mm^3/1 x 10^6 cycles. Smyth et al studied a cohort of Zenith components, inputting multiple kinematic models to simulate anatomical wear. It was found that for simple unidirectional articulation the volumetric wear rate was 1.2 ± 0.6mm^3/1 x 10^6 cycles. However, when AP translation, was introduced to the model this increased to 25.8 ± 3.1mm^3/1 x 10^6 cycles.

Finally, the Bell et al study applied similar methods to Smyth et al by applying multiple kinematic conditions to the components (Carol J. Bell & Fisher, 2007; Jörn Reinders et al., 2015; Smyth et al., 2017). Again, it was found that the addition of AP translation significantly increased wear volume, from 10.6 ± 11.8mm^3/1 x 10^6 cycles to 16.4 ± 17.4mm^3/1 x 10^6 cycles for a cohort of components of Buechel-Pappas design, and from 3.38 ± 10mm^3/1 x 10^6 cycles to 10.4 ± 14.7mm^3/1 x 10^6 cycles for a cohort of Mobility TAR components. It must be

noted that the tolerance of published wear rates in this study was incredible high, leading to a large range of accepted values.

These studies show that wear rates in TAR are relatively comparable to those found in TKR simulation studies, with a range from 1.2mm^3/1 x 10^6 cycles to 25.8mm^3/1 x 10^6 cycles in the studies detailed. Given tolerance bands would expand this range to a maximum of 33.8mm^3/1 x 10^6 cycles with the Bell study noticeably including tolerances which could result in negative wear volumes.

There are currently no published studies that consider volumetric wear measurement of Total Ankle Replacement components using a CMM method. TAR is a relatively new and developing method of joint replacement and as such research in the area lags behind that of both Total Hip Replacement and Total Knee Replacement, and as such the gravimetric method reigns supreme as the typical method of wear volume measurement for TAR components.

2.6 Summary

This chapter has discussed literature in the area of volumetric wear measurement in both TKR and TAR. Firstly, the methods which are used to simulate wear on these components were reviewed, and it has previously been shown that such simulation methods produce wear volumes that are representative of typical TKR and TAR components.

This was further evidenced by the following section which discussed the typical wear volumes that are found in both TKR and TAR. These wear volumes shown in the literature can be used later in the thesis to evaluate volumetric wear results found when pre-wear data is not available. Showing that the volumetric wear rates found are representative of those found by standardised methods will aid in validating the method developed in this thesis.

This chapter also considered existing methods of volumetric wear measurement. This included the gravimetric measurement method and also geometric methods that have been developed using CMM. It has been shown in this chapter that CMM-based methods can produce results comparable to the gravimetric method, whilst requiring less pre-wear data to be known. However, previous studies typically still require pre-wear data, whether in the form of CAD data or otherwise. No method that has been discussed in this chapter can be

described as truly autonomous, often requiring manual input to locate wear edges, or using a simple scalar as the identifying factor as a worn edge.

This thesis will describe the development of a method that requires zero pre-wear geometry to calculate volumetric wear on TKR and TAR components, using a fully autonomous wear edge detection method. This builds on previous studies to help further validate the use of CMM as a wear measurement tool but also furthers previous work to create a robust, adaptable and autonomous method of volumetric wear measurement on TAR and TKR components.

Chapter 3 – Creation of a Method for TKR and TAR Wear Measurement

This chapter describes the development of methods for the measurement of wear on TKR and TAR components through the use of a variety of metrological equipment and software. The apparatus used and information relating to measurement strategies will be discussed, along with how the use of each instrument can be combined with data from other equipment.

Further to this, there will be a discussion of the methods used to process data post-measurement, considering the different approaches that have been attempted to develop a wear measurement method. A major challenge in measuring components when there is no pre-wear data available is the definition of the location of wear areas upon a component. Different methods that have been trialled for this wear edge definition will also be discussed.

This project uses a combination of three major pieces of measurement apparatus. These are the coordinate measurement machine (CMM), the use of Industrial Computed Tomography (CT) and an optical measurement method known as Focus Variation Microscopy (FVM). The following sections will discuss considerations that were made and how measurement strategies were developed for each of these instruments, along with information on how the instruments were used in subsequent studies.

3.1 Industrial Computed Tomography (Micro-CT) and CAD Data Creation

3.1.1 Micro-CT Setup and Operation

Micro-CT was used in this research for the creation of reference geometry to use as a basis for a CMM measurement strategy. The CMM alignment method used and detailed in 3.2 requires a CAD model describing the global geometry of the entire TKR component. This geometry can be gathered through the use of Micro-CT.

The scanner used in this project is a Nikon XTH225 (Nikon Metrology, Tring, UK) scanner, as shown in Figure 14 The scanner has a maximum voltage of 225kV, with a minimum focal spot size of 3µm at 7kV and 225µm at 225kV. The scanner can scan parts of a mass up to 15kg.

Figure 14 - NIKON XTH225 CT Scanner as used throughout this project.

Micro-CT involves the use of an x-ray source and detector in unison to obtain two-dimensions images of a component from a variety of angles which can then be combined to create a three-dimensional reconstruction of a component. Components are sited on a sample manipulator which allows for rotation of the component through 360 degrees. X-Rays are generated and directed through the component and are then collected at a detector. X-Rays that are of insufficient power to penetrate the component being measured will not be collected at the detector and the resulting projection takes the form of a two-dimensional shadowgraph of the component at the specific orientation. The component is then rotated and the next projection is taken (Duliu, 1999; Kak, Slaney, & Wang, 2002).

Three-dimensional reconstruction of the component is performed using filtered back-projection algorithms (Lin & Miller, 2002). Each volumetric pixel, known as a voxel is represented by numerous different angles, and

the sum of this voxel's view from each angle creates a representation of each voxel (Singhal, Grande, & Zhou, 2013). This is then represented as a point cloud of cartesian coordinates.

3.1.1.1 Effect of Voltage and Filtration

Due to the relatively low density of UHMWPE, the x-rays which are required to penetrate the material need relatively low energy and therefore the voltage used for scanning is lower. Studies using Micro-CT to measure UHMWPE generally use a voltage of less than 100kV (Bowden et al., 2005; Matthew G. Teeter, Naudie, McErlain, et al., 2011; Vicars et al., 2009).

Orthopaedic components manufactured from UHMWPE contain locating pins manufactured of a metallic element, often tungsten or tantalum, which require the use of a higher input voltage to achieve x-ray penetration. These locating pins are included to allow for easy contrast on a fluoroscopy x-ray alongside the relatively non-dense UHMWPE material, aiding surgeons in implant alignment and location, they do not perform any mechanical function. This disparity between required scan voltage can cause issues when scanning the TKR components.

Preliminary scans at voltage values comparable to those in the literature (Bowden et al., 2005; Matthew G. Teeter, Naudie, Milner, & Holdsworth, 2011; Vicars et al., 2009) found that there was evidence of scattering in the areas surrounding these locating pins. This scatter is caused due to low energy x-rays produced at this voltage being unable to penetrate the dense metallic material. If these materials were being scanned independently, it would be expected that they would require voltages towards the upper limit of the Micro-CT scanner, due to their high density. The use of such high voltages would allow measurement of the metallic areas of the component, but the high energy x-rays would cause UHMWPE to be invisible to the scan.

TKR components generally have a single locating pin located centrally in the anterior face of the component. This pin is approximately 1mm-2mm in diameter and 5mm in length, and therefore comprise a very small proportion of the component geometry. The TAR components used in this project have three small spherical locating pins (diameter approx. 1mm). These are located both at the anterior (2) or posterior (1) face of the components. Again evidence of significant scattering around these locating pins was noted in scan data.

To counteract this scattering effect a significant amount of copper filtration was used. Filtration reduces the effect of beam hardening. X-Ray beams consist of photons with a variety of energy levels, beam hardening

occurs when lower energy photons are attenuated whilst passing through an object, thus reducing the intensity of the x-ray beam. This can lead to artefacts and inconsistencies in the measurement of components (Meganck, Kozloff, Thornton, Broski, & Goldstein, 2009). Filtration of the x-ray beams through a metallic material before direction at the component causes hardening of the beam, preconditioning and reducing the polychromaticity of the beam reducing the potential for artefacts (du Plessis, Broeckhoven, Guelpa, & le Roux, 2017).

Filters from 0.25mm thickness up to 6mm thickness were trialled, and it was eventually found that a 0.5mm copper filter appeared to display the best balance of contrast between component and background, whilst minimising the effect of ring artefacts on scanning results, as well as reducing the noticeable scatter around the component.

As a result of the use of filtering, the scanning voltage was increased with a level between 150kV/7.1W and 160kV/7.1W used for all components, with a voxel size of 44µm. Scan time for most components was in the region of 120 minutes-180 minutes. Average rotational two-dimensional image spacing was 0.2degrees, leading to approximately 1500 projections to be used for reconstruction.

3.1.1.2 Sample Preparation

Micro-CT does not require extensive sample preparation. All components scanned were cleaned using a cloth soaked in an isopropyl solution and allowed to dry before being fixtured securely using low-density foam, to ensure good contrast between the fixturing material and the UHMWPE (du Plessis et al., 2017). Component orientation in Micro-CT requires that all features of the component are visible in three planes for significant portions of the 360-degree component rotation. In the case of these components, the tibial plateau of the components was placed superior, with the part rotated approximately 45 degrees about both the Z and X axes to ensure component visibility.

3.1.1.3 Use of Scaling Artefacts

Scaling artefacts can be used in Micro-CT scanning to minimise the effect of length measurement error. A scaling artefact was scanned with all TKR and TAR components to allow scaling to be performed, this is shown in Figure 15. The artefact was supplied and manufactured by Orthoplastics (Bacup, UK), and was manufactured of GUR1050 UHMWPE.

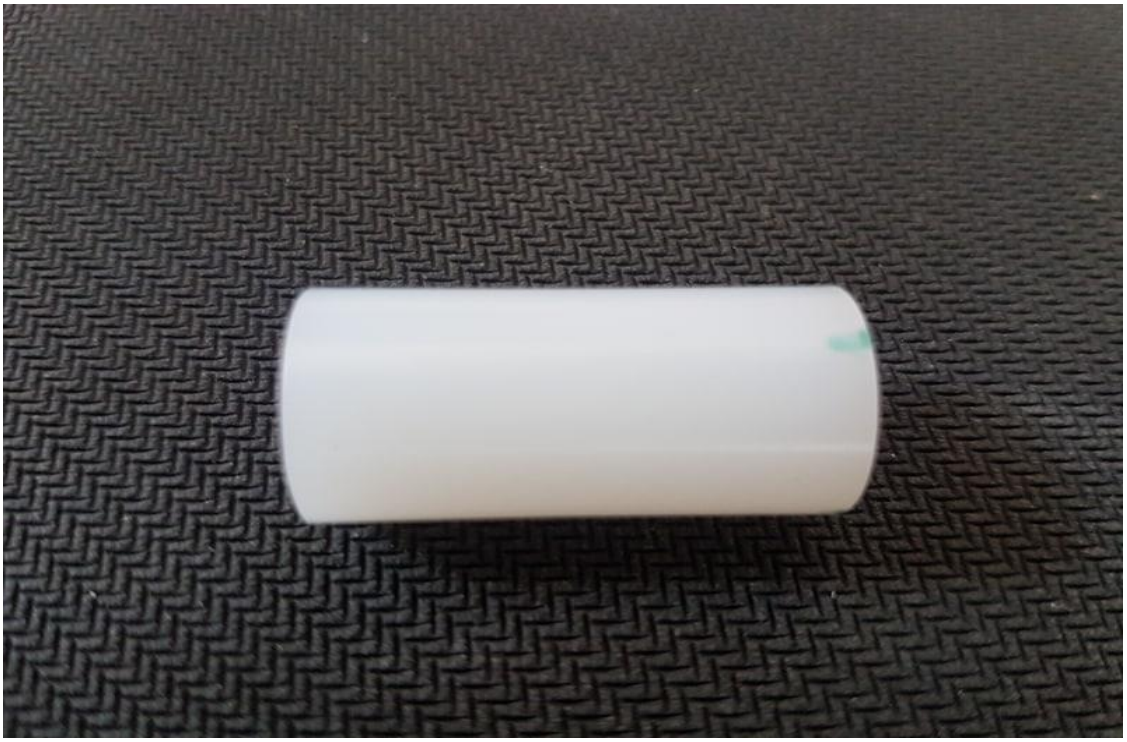

Figure 15 - Example of Scaling Artefact used in CT scans.

The component was 25.4±0.025mm in length, with the diameter being 9.75±0.025mm. The flat surfaces of the component were also within 0.025mm perpendicular. This artefact was suspended within the same fixturing as the components being measured. Scaling was performed post-reconstruction, and it was generally found that minimal scaling (Error < 0.01*Length) was required for all components.

3.1.1.4 Measurement Procedure

The Micro-CT parameters stated in 3.1.1.1 were used for all components, with fixturing performed to ensure that the full component remains within the measurement volume during the full rotation cycle. At this stage, shading correction is performed for the final shadowgraph image. Shading correction increases the contrast between the component and background measurement area, typically by increasing the brightness of the background relative to the part, the exact algorithms used within Nikon software are proprietary.

Preliminary scans are then taken at the initial view and 90 degrees to the initial view. This allows the user to select the region of interest for the measurement, ensuring that the entire component is within the measurement area.

Measurement data is then acquired, with scan durations as discussed previously. Each projection taken is approximately 2MB in size, meaning a scan of 1500 projections creates a subsequent data size of 3GB. Reconstruction of components was then performed in CTPro (Nikon, UK) software and exported in a volume file (.vol) format. Volume Graphics StudioMax (VG Studio) software was used for subsequent processing of the reconstructed scan data. Manual thresholding of the data was performed to remove background data, leaving just measured component data. Cartesian point cloud data was then exported in an ASCII (.txt) format.

3.1.2 Creation of Reference Geometry for CMM using Micro-CT data

As discussed, data is taken from VG Studio in an ASCII format, which represents a point cloud of geometrical data of the component. Figure 16 shows the resulting point cloud from the scan of a PFC component. Figure 16 shows that in addition to the bulk geometry of the component, there is evidence of scatter around the

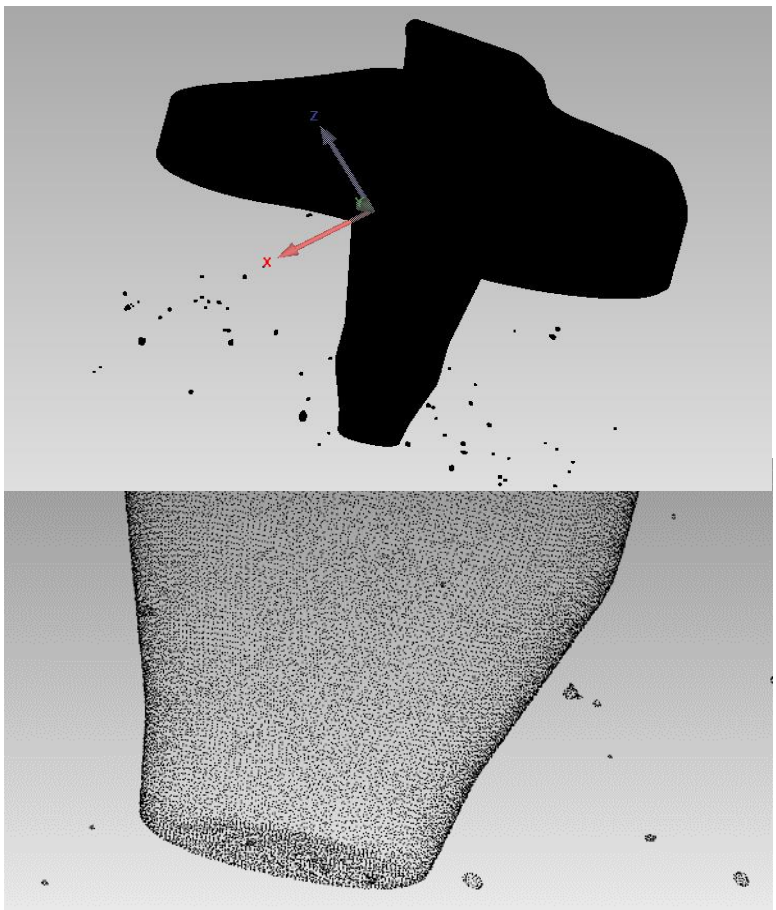

Figure 16 - Example of Point Cloud data taken from VG Studio.

component, displaying as smaller blocks of data isolated from the main body of the component. These are the consequence of including the metallic locating pins within the scan region of interest.

Unfortunately, this is necessary in the case of TKR components because exclusion of the pin would also necessitate exclusion of areas of the articular surfaces of the component, which are integral to the subsequent CMM measurement and wear quantification.

A large number of scatter points were removed using a combination of manual and automatic methods within Geomagic software. The software includes options for the automatic removal of “outliers” and “disconnected components”. These automatic methods apply distance filters to remove data from the point cloud. “Outliers” removes data points that are further than a specified distance from the mean central point of the point cloud, 150mm was used in this study. “Disconnected Components” removes data points that are more than a given distance apart from another data point, 5mm was used in this study. These distances were selected as it was found that using high-sensitivity settings (smaller distances) began to remove data from the main component body, whilst the use of the selected filters removed scatter which was easily identifiable as not part of the main component body. Manual cleaning was performed to remove any further data points that were not part of the main body of the component.

The point cloud data is then converted into a triangular mesh, with the element size equal to the point cloud spacing. For a typical LCS TKR component, the mesh included approximately 100’000 triangulated elements. Manual mesh cleaning was performed in non-critical areas of the components, i.e. not in areas that would be used for CMM alignment. This cleaning involved the manual selection and removal of triangulated area, followed by filling the resultant void with a 4^{th} order best fit polynomial-based fitted surface. As this was only performed in non-critical areas of the component, a basic 4^{th} order polynomial fit was sufficient.

Holes are likely to be present in the areas surrounding the location of surgical location pins due to their exclusion from the CT scan data. These pins are not located in regions of interest for CMM measurement and therefore automatic mesh filling can be performed in these areas. Complex contours may be found around etchings on non-articular faces of the component, often used for component identification in simulation studies.

Markings such as these and also surface damage away from the superior articular surface, for instance, backside damage, may act as useful tools in the case of failure mode identification, but would not be considered relevant when measuring wear on the superior articular surface. It is important at this stage that minimal adjustment is made in the critical areas surrounding the articular surfaces that will be used for alignment and measurement when using CMM.

Following cleaning and smoothing of the mesh in non-critical areas of the component, surfaces were fitted to the model. Using mesh cleaning in non-critical areas simplifies the overall CAD model by reducing the number of surfaces to must be fitted. Although this increases the workflow time at this stage of processing it reduces the workflow time later in the surface fitting process. Surface edge contours were automatically extracted from the model and manually aligned to contours on the mesh. Surface classification (for example freeform/planar) was performed automatically and verified manually. The backside surface of the TKR component was defined as planar to create a base reference plane. Due to the effect of backside wear, it is likely that the backside surface would not be truly planar. It was found that in all cases the maximum deviation in Z-position from the created planar surface was less than 0.2mm. All other surfaces were categorised as freeform.

Surface fitting and stitching were performed semi-automatically in two stages. The first stage was the fitting of surfaces to the contours shown in green in Figure 17.

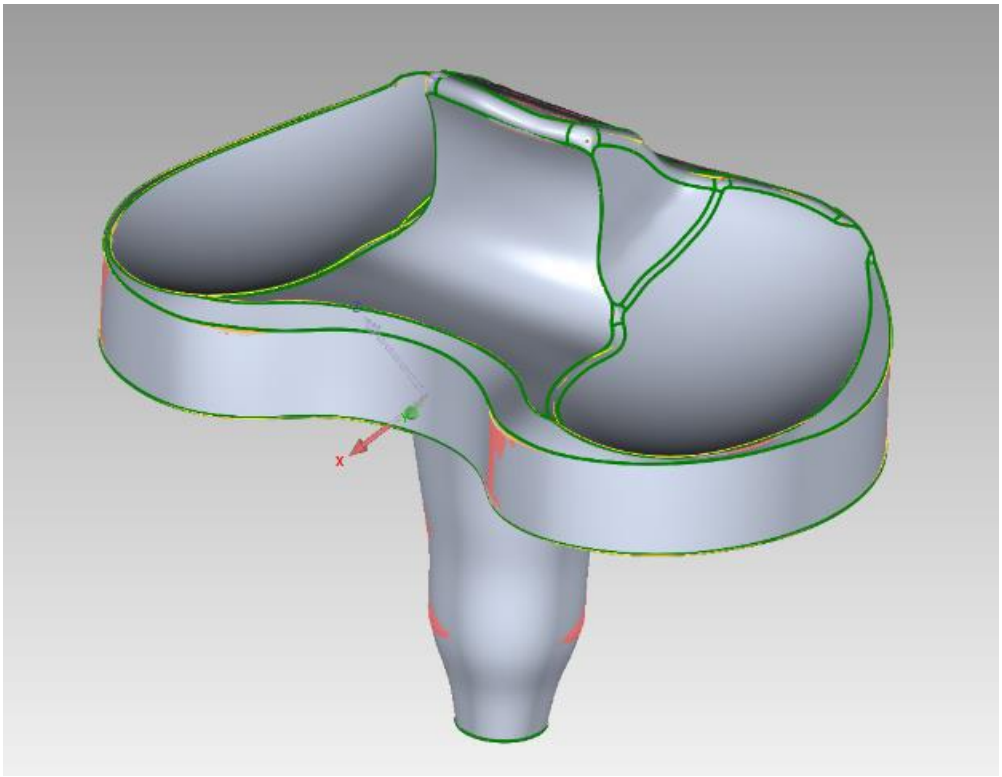

Figure 17 - Surface fitting contours used for surface fitting operation.

Surfaces were fitted to all freeform areas using a cubic interpolating spline curve surface fit. The use of an interpolating spline means that all measured data points lie directly on the generated surface and maintains the integrity of surface edges for relocation using CMM measurement.

These surfaces were then stitched to create a CAD model that can be used for alignment on CMM. This file is exported in a Standard for the Exchange of Product Data (.STEP) type. This is a data file in the EXPRESS data modelling language which contains model information as opposed to coordinate data.

3.2 Coordinate Measurement Machine (CMM)

CMM measurement has been used as a viable and repeatable method of measurement in numerous different areas of orthopaedics and is a logical piece of equipment to use for an accurate definition of component geometry. The equipment used in this project was a Zeiss Prismo CMM (Carl Zeiss AG, Germany), a moving-bridge type CMM as governed by ISO10360-1:2000 (ISO, 2000). It is a CNC machine that is supplied with ZEISS Calypso, ZEISS Gear Pro and ZEISS Holos software. The CMM stylus can move up to 70mm/s in manual mode, with speeds of up to 520mm/s in CNC mode. The VAST XTR 10 gold head requires a minimum probing force of

50mN and can incorporate a stylus up to a maximum length of 350mm and a mass of 500g. Stylus tips can be accommodated down to a minimum diameter of 0.5mm.

3.2.1 CMM Measurement Length Error (E0)

The CMM measurement head is fitted with a ZEISS VAST XTR 10 gold scanning sensor which has a stated length measurement error (E0) defined as:

$$1.5 + \frac{L}{350} \quad (\mu m)$$

Where L represents the measurement length in mm. Assuming that temperature is controlled between 18°C and 22°C. For ambient temperatures between 18°C and 28°C, the length measurement error is defined as:

$$1.8 + \frac{L}{300} \quad (\mu m)$$

. E0 represents a CMM's accuracy at measuring the distance between any two points and is measured by probing two points on a calibration artefact. This must be conducted in a minimum of seven different positions, four of which must be the cross diagonal directions, with the remaining three chosen by the user, with each position measured three times. The CMM is located in a temperature-controlled environment and temperatures measured throughout component testing were found to be maintained between 19°C and 22°C.

The largest individual longitudinal profile measured as part of this study was 31.5mm in length. If this value is inputted to the formula given above, given that temperature was maintained at between 18°C and 22°C this gives a measurement accuracy of 1.59µm. The repeatability range of E0 is defined as 1.1µm (R0), which is calculated from the variability in repeat measurement of E0, which gives a range of values of approximately 1.04µm to 2.14µm for the error in length measurement. Previous studies have suggested that the accuracy required to use a CMM for volumetric wear measurement is approximately 2.0µm (Becker, Schoellhorn, Dirix, & Schmotzer, 2006; Blunt, Bills, & Jiang, 2008), and the CMM used in this study provides this for the maximum measurement length, smaller measurement lengths will provide greater accuracy than 2.0µm.

3.2.2 Stylus System Selection

CMM styli are generally manufactured from tungsten carbide or carbon fibre shafts with a ruby stylus tip. Tungsten carbide shafts are often applied in situations of small stylus length (less than 50mm) or small tip

diameter (under 1mm). Carbon fibre shafts are lighter than tungsten carbide shafts and are typically used in the case of very long stylus shafts, and are suitable for larger ball diameters than tungsten carbide. Ruby stylus tips are used as ruby has a very low coefficient of friction. This stylus material pairing is suitable for the measurement of non-abrasive surfaces, making it suitable for use with UHMWPE.

From the selection of stylus systems available, a 2mm straight stylus was selected as the most suitable option for the measurement of the UHMWPE components used in this project. The stylus is comprised of a carbon fibre stylus shaft with a 2mm ruby stylus tip. Stylus qualification was performed using a manufacturer supplied reference sphere located on the CMM bed.

A grade five, 2mm ruby stylus tip was used for the current research. Grade 5 ruby tips have a maximum permissible probing error (MPE_P) of 1.70µm, with ball sphericity of 0.13µm. MPE_P is found by measuring 25 points on a 20mm calibration sphere with minimal form error (ISO, 2011b). It is recommended that the largest navigable stylus should be used for measurement to negate the effect of surface texture on measurement (Flack, 2014).

It is also recommended that the smallest Effective Working Length (EWL) possible should be chosen, representing the length of the stylus shaft. A longer stylus shaft experiences greater deflection and so the smallest EWL possible should be used (Flack, 2014; Gąska, Gąska, Gruza, Ostrowska, & Sładek, 2017; ISO, 2011b). A stylus with 20mm EWL was used in this study. The stylus was cleaned before stylus qualification and inspected for damage before each measurement run was conducted.

3.2.3 Sample Preparation and Fixturing

CMM does not require significant sample preparation. Components were cleaned using a cloth soaked with an isopropyl based cleaner and allowed to dry before measurement. Components were allowed to stabilise in a temperature-controlled environment for at least 48 hours before measurement to allow components to reach thermal equilibrium (Blunt, Bills, Jiang, et al., 2008). In the case of all components, wear simulation or explantation had occurred at least 100 hours before measurement, allowing for the recovery of at least 95% of recoverable creep (Knowlton & Wimmer, 2012).

When using a contact measurement system such as CMM, fixturing is critical to ensure a component is fixed in such a way to ensure the component does not move during measurement, but still allowing access to the

areas of a component that need to be measured. The fixturing of soft polymeric materials such as UHMWPE is a challenge when using a tactile measurement system as it is also important to ensure that deformation of the component does not occur.

Figure 18 shows the fixture that was created for use with UHMWPE components. The fixture closes around the

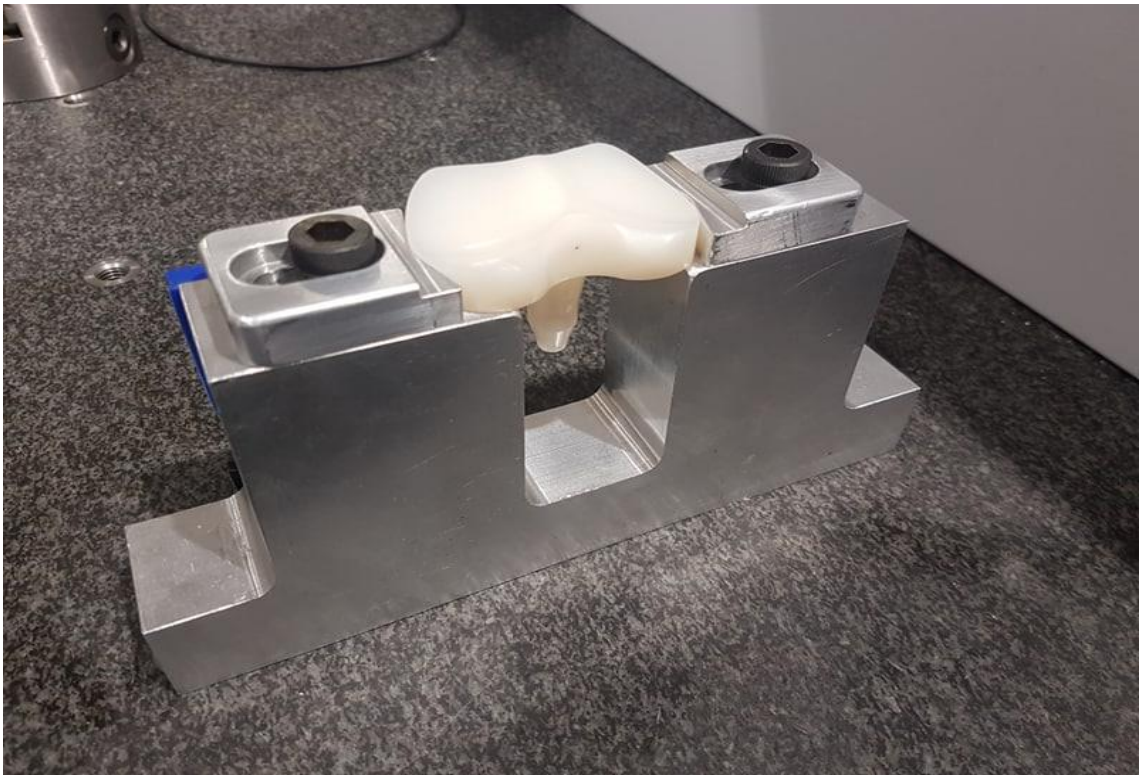

Figure 18 - Example of Fixturing used for TKR components on CMM.

sides with jaws shaped to the outer shape of a typical TKR component, helping to distribute loading on the TKR components, reducing clamping force and reducing the potential for deformation. The fixture was also rigidly fixed to the CMM bed allowing for quick interchange of components. The jaws are released independently meaning that components of the same design can be quickly interchanged without changes in alignment.

The fixture can accommodate TKR designs of multiple different designs, reducing the need for alternate fixtures for each component design.

Figure 19 shows the fixturing that was used for TAR components for CMM measurement. As shown this fixture uses the same principle as the fixture used for TKR components. As shown the fixture rigidly holds the component in place whilst allowing access to the superior articular surface for measurement.

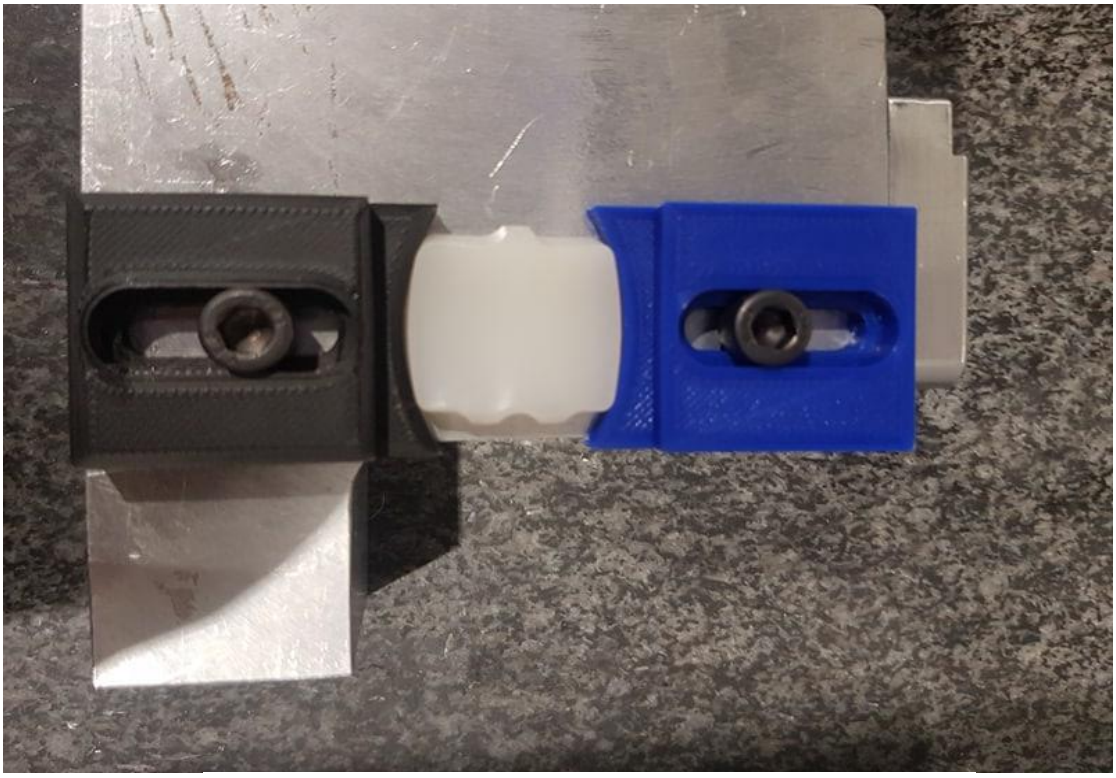

Figure 19 - Example of Fixturing used for TAR components on CMM.

3.2.4 Component Alignment

CMM measurement requires the user to describe accurately the position of a component within the measurement area to define a measurement strategy. ZEISS Calypso software has been used to create the measurement strategy for both TKR and TAR components. The Micro-CT derived CAD model in ".STEP" format was imported into Calypso and aligned to the CMM base coordinate system using the lateral direction as the Y-axis and the longitudinal direction as the X-axis.

An iterative alignment method was applied for both TKR and TAR components. A 3D best fit was conducted based on geometrical features defined by the user. For a TKR component, 8 points around the periphery of the component were defined in Calypso. A minimum of 6 defined alignment points are required for iterative fitting in Calypso, 8 points were defined for TKR components. These points are displayed in Figure 20. These are points that can be visually located by the CMM user. To perform the 3D best fit alignment the 8 points were located visually and then manually probed by the user. Calypso then used the 8 manually probed points and created a Gaussian best fit of the points to the corresponding points on the CAD model.

This fit was then used by the CMM to autonomously re-probe these eight points. The user can visually verify that the fit has been successful if the points correspond to the manually probed points. The probing points shown in Figure 20 is representative of those taken for a DePuy LCS cruciate-retaining style of implant. In the

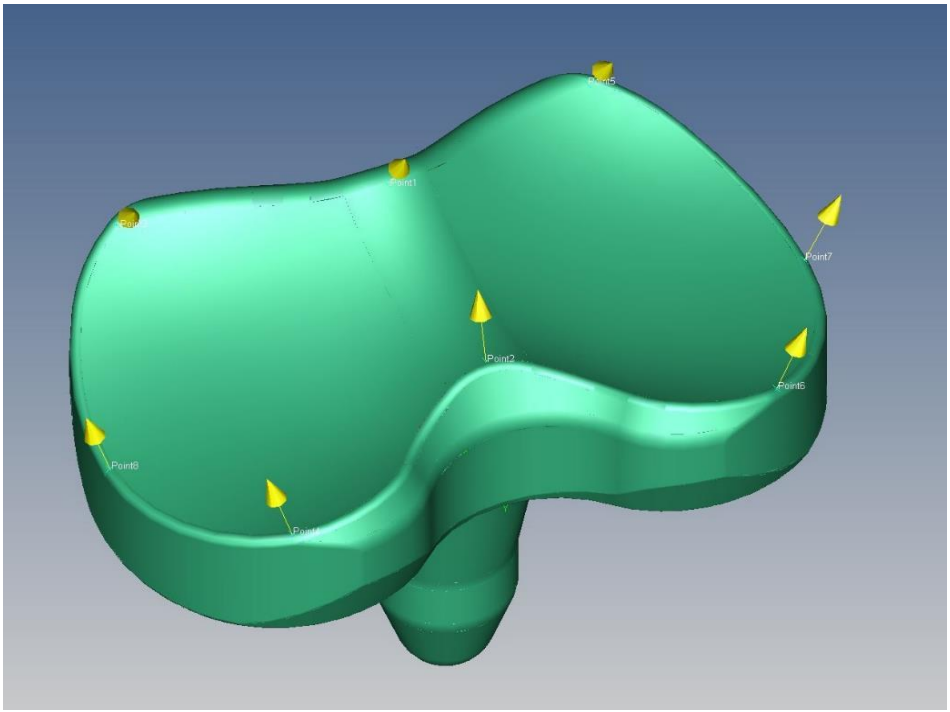

Figure 20 - Display of points used for best fit alignment of TKR components in CMM measurement.

case of posterior stabilised components, the central stabilisation peg provided definitive vertices that were used in alignment. If it was found that the alignment was not proved to be successful, i.e. that the points being probed in CNC mode were incorrect, the alignment points were redefined and the process repeated.

When considering the BOX TAR components used in this project, the method used for alignment was identical. A diagram showing the alignment probing points on such a component is shown in Figure 21.

By using the CAD model as a reference for alignment, it allows for easy definition of further measurement features, as all features are therefore calculated from the CAD model. Likewise, after alignment has been performed the axes of the CMM are aligned with the axes of the component on the CAD model.

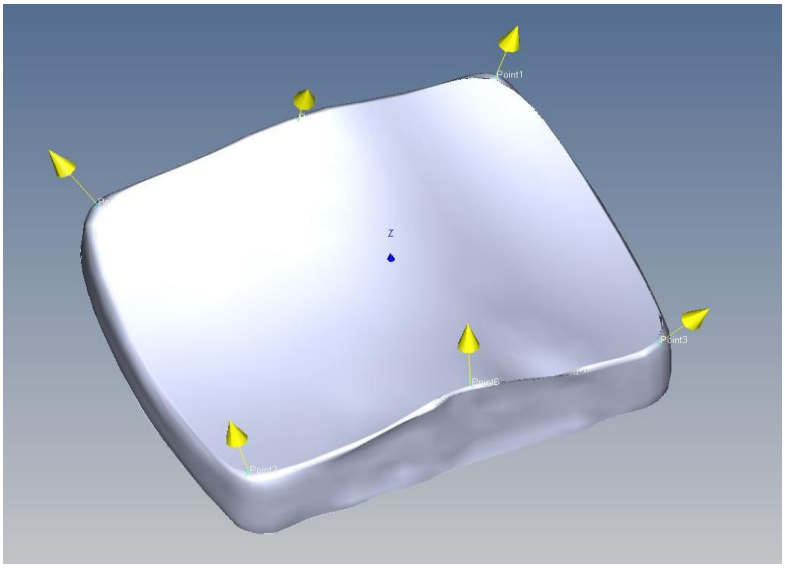

Figure 21 - Location of alignment points for CMM on typical TAR component

3.2.5 Development of Measurement Methodology

With the component fixtured and aligned a methodology was then developed for the measurement of component geometry. Before this can be done other parameters and features must be set to ensure that the measurement is conducted under optimum conditions. The first of these is the positioning of the clearance plane for measurement, as shown in Figure 22. The clearance plane is the definition of a "safe" area, in which

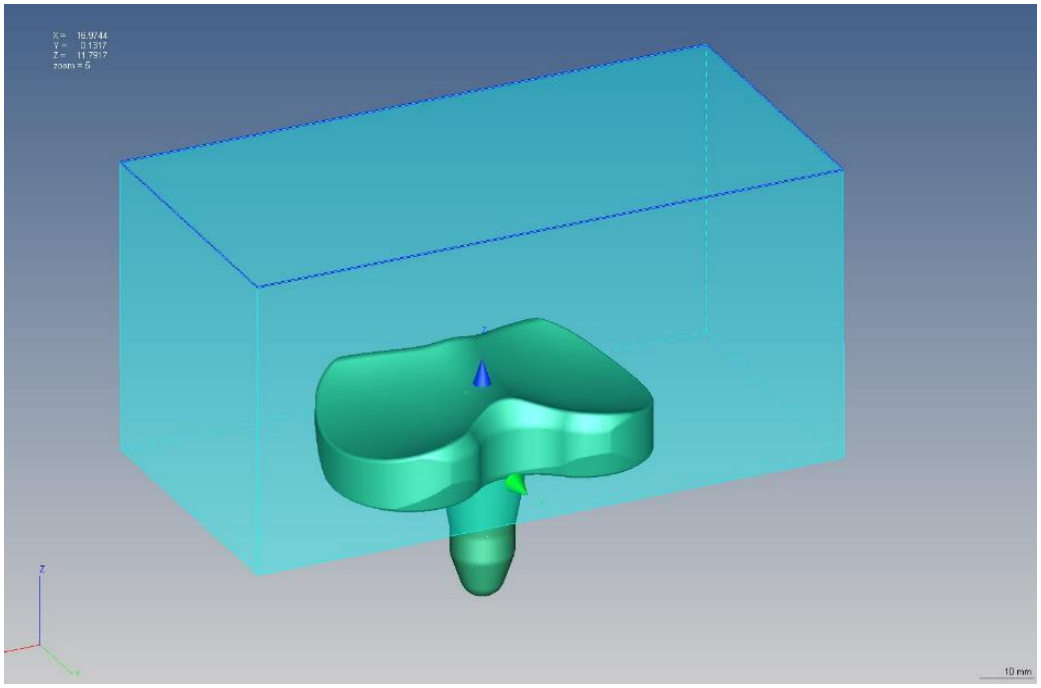

Figure 22 - Demonstration of clearance plane on TKR component

the CMM head can move freely at high speed without the risk of collision. A collision is dangerous in the case of CMM measurement as it could result in costly damage to the stylus or part that is being measured, as well as the wider parts of the CMM machine. Figure 22 shows the clearance plane defined for an LCS TKR component. The clearance plane is described by the component as well as any fixturing surrounding the component. In the case of the component shown in Figure 22, the CMM probe will always approach the articular surfaces of the component in a negative Z-direction, and between measurements will revert to this clearance plane to reduce the risk of collision.

3.2.3.1 Definition of Measurement Geometry

In the case of TKR components, it was decided that it was a sensible option to divide the articular surface along the central line of the component. Although the LCS components, as shown in Figure 18, have a single superior surface, many designs of TKR components do not. For instance, PS type components have a stabilisation peg separating the surfaces, whilst some CR designs have distinct separate articular surfaces.

In all measurements of TKR components, these condylar surfaces are referred to as “left” and “right” corresponding to the location of the condylar surfaces when viewing a TKR component from above with the anterior edge above the posterior edge. When considering TAR components, the articular surface was considered as a single surface.

To create a detailed representation of each condylar surface an X-Y grid of points was created upon each condyle. Previous studies have used point spacings between 0.1mm (Knowlton et al., 2016), 0.5mm (Blunt, Bills, Jiang, et al., 2008) and 0.75mm (Muratoglu, Perinchief, et al., 2003). Knowlton and Wimmer studied CMM point spacing and found that a grid of 0.1mm x 0.1mm provided optimum conditions.

The Bills et al and Muratoglu et al studies were conducted more than 10 years ago, and the point spacing chosen was likely influenced by the limitations of computing power at that time. For this reason, a point spacing of 0.1mm was used between scanning lines on TJR components in this research. Along each scanning line, an initial point spacing of 0.1mm was also used. It was however found that a spacing of 0.05mm could be used without a significant increase in measurement time.

Through the application of this spacing to the surface of a DePuy LCS component, a point cloud of approximately 170,000 points was formed for each condylar surface, which is shown in Figure 23. The

individual scan lines were connected to maintain a single scan path, meaning that the CMM stylus tip remained in contact with the surface being measured throughout, reducing scanning time significantly.

The edge of the point cloud was offset 0.2mm from the edge of the condylar area. This was done to remove the possibility of damage to the stylus from slipping over the edge of the component.

When measuring the component, the X-Y locations of the points defined in the point cloud are probed by the CMM, and the corresponding Z location is measured. This measurement defines a 3D point cloud of cartesian coordinates the corresponds to the articular surface of the component.

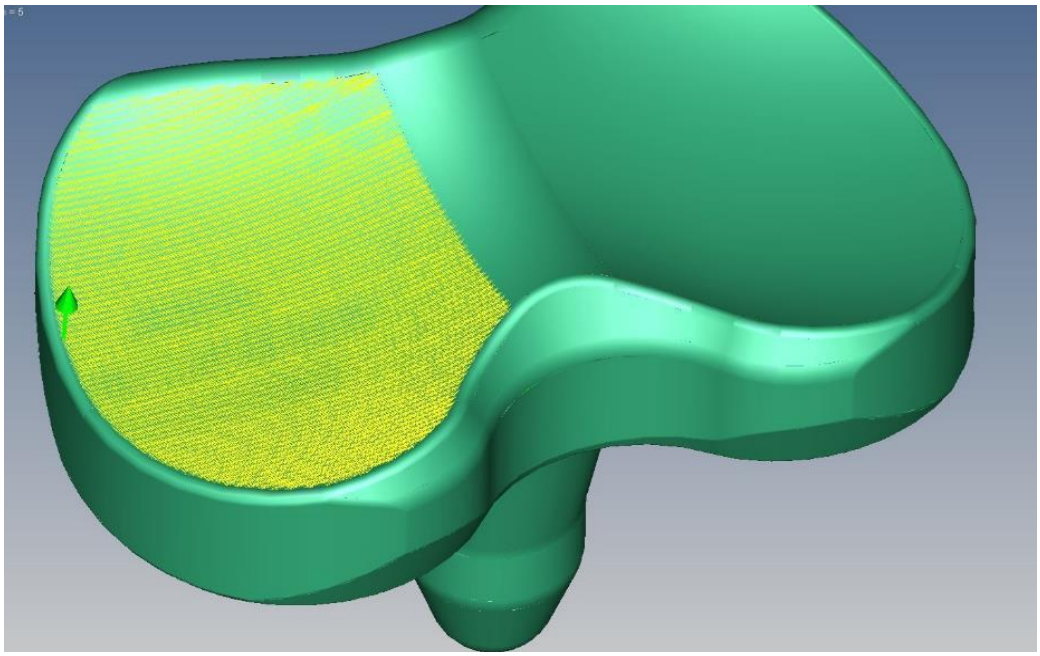

Figure 23 - Representation of grid of measured points on TKR surface

3.2.3.2 Consideration of Probing Force and Measurement Speed

Another consideration in the measurement was probing force. The default probing force of the Prismo machine was 100mN. This is the force with which the stylus tip is pushed into the surface of the component. Figure 24 shows an example of a component surface measured at 100mN and meshed using CATIA to create a triangulated representation of the surface.

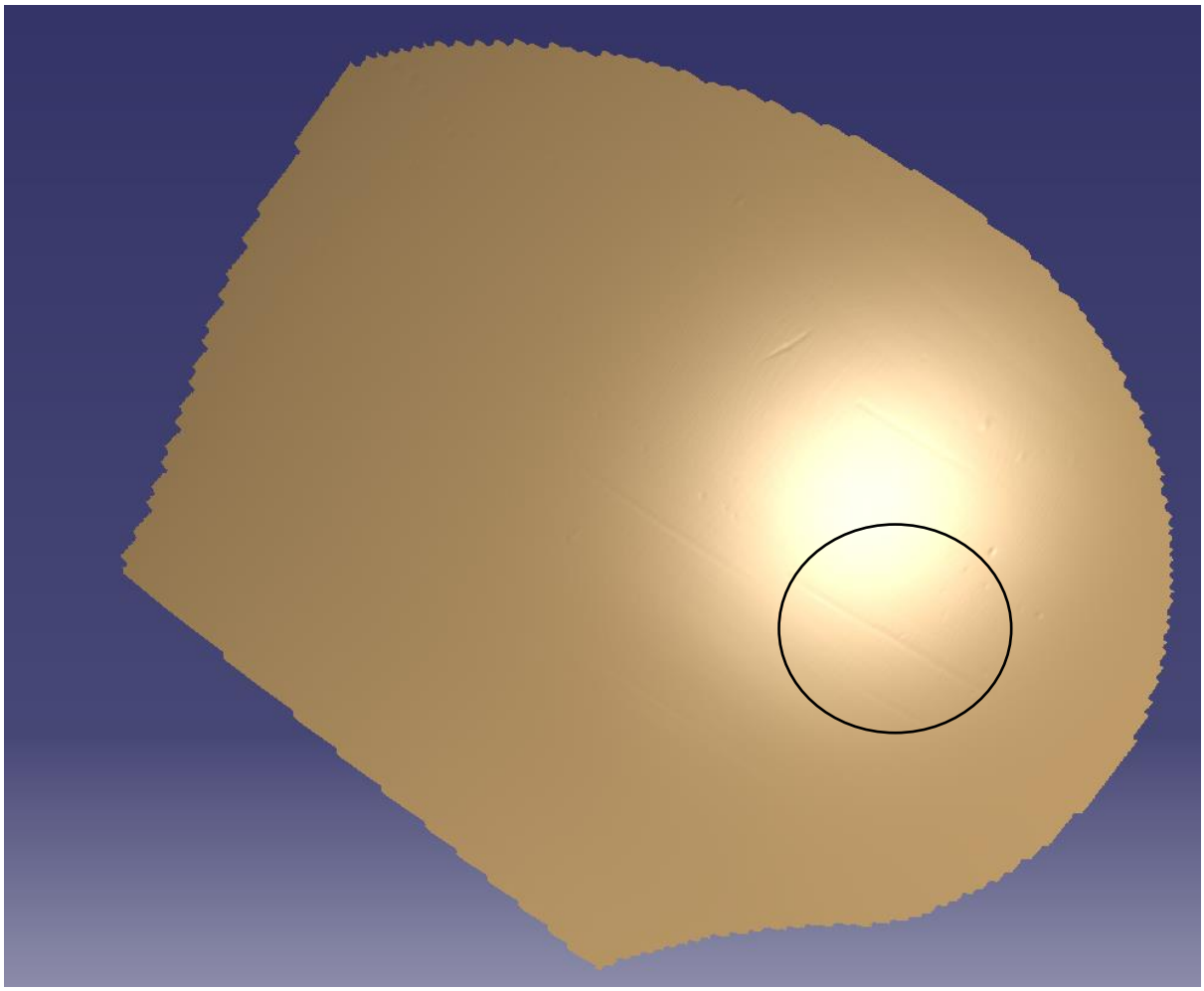

Figure 24- Screenshot of CATIA software showing TKR component condylar surface with evidence of CMM stylus probe skidding, characterised unidirectional channels (an example is circled)

If an insufficient probing force is used, there is potential for the probe to drift or skid along the measured surface in the direction of travel, causing inconsistencies in measurement point spacing. As shown, there are unusual channels that appear to be running across the surface of the component. These are the effect of the stylus tip "skidding" along the surface due to insufficient probing force. Repeating the measurement allowed for visual confirmation that this was occurring. Following this, the probing force was increased to 200mn. It is also important that the probing force remains low enough as to not cause indentation and no evidence was found to suggest that the 200mN probing force was causing any indentation to the measured surface.

Measurement speed can also affect accuracy. It is suggested that a balance should be reached between slow measurement speeds, taking an unreasonable amount of time for data collection, and fast measurement speeds, which can cause vibrational effects. Profile measurements taken for the current research were a maximum of 31.5mm in length and due to this relatively small measurement geometry, a measurement speed in the lower range of CMM capabilities will need to be used. Ali found that a measurement speed of 2mm/s provided the least error (1mm/s – 5mm/s) studied (Ali, 2014), a measurement speed of 2mm/s was therefore used in the current research.

3.2.6 Measurement Procedure

Sample preparation, fixturing and component alignment was performed as described in section 3.2.2, 3.2.3 and 3.2.4. A measurement strategy was created for each type of component. For each component measurement of the left and right condyles was performed in a single measurement run.

The alignment process was conducted for each component, including between components of the same design. This allows for any misalignment between components resulting from fixturing to be removed. Measurement duration was approximately 45 minutes per condylar surface or 90 minutes for an entire TKR component. For TAR components this the measurement duration was approximately 35 minutes. Measurement data from CMM was exported in an ASCII format (either .asc or .txt) consisting of three-dimensional cartesian coordinates. Three repeat measurements were taken consecutively for all components.

3.3 Post-Measurement Data Analysis

3.3.1 Use of CATIA and Profile Extraction

CATIA (Computer-aided three-dimensional interactive application) software is used for computer-aided engineering and design (CAD). CATIA includes a range of tools that can be used for engineering analysis of components and data processing. ASCII data was taken into CATIA's *Digitised Shape Editor* program. This data was then triangulated with the mesh size identical to the point spacing measured on CMM (0.1mm x 0.05mm).

Two-dimensional profile sections were then taken from CATIA using the *Planar Sections* tool. This command sections the mesh at specified intervals. Each mesh section contains a two-dimensional profile which is then exported as an ASCII file. The command was programmed to take an infinite number of profiles at a given separation. An issue with this process is that the use of the infinite command also creates unnecessary profiles

with very little data, these occur at stylus turning points. These profiles are removed from analysis at a later stage of processing that will be discussed in Section 3.5.1.

The direction in which these profiles are taken could potentially affect the wear volume calculated and this must be considered thoroughly before selecting both this and also the profile separation. A study to determine the optimum values for each of these factors was conducted as part of Chapter 4. It was found that in terms of TKR components it was optimum to take the profiles in an anterior-posterior direction at 0.1mm intervals, whilst for TAR components profiles were taken laterally along the components at 0.1mm intervals.

On a typical TKR component, this resulted in 150 profiles on each condylar surface. The smallest full profile extracted on a typical TKR component was approximately 900 points. All these profiles were exported as separate ASCII files in a .txt format.

3.4 Methods for the identification of wear edge location

This section discusses the methods that were applied to attempt to define the location of a wear edge on the TJR components, thus isolating worn and unworn areas of a component. The isolation of definitive worn and unworn regions is a critical challenge to the success of such a method, as the selection of this location could have a major effect on the calculated wear value.

3.4.1 Manual Wear Edge Detection

The first and most logical method for the identification of wear scars upon a component would be the use of visual inspection of a component, as used by Knowlton and Wimmer (Knowlton & Wimmer, 2012). It is generally possible to visibly identify worn areas on UHMWPE components as burnishing makes the worn surface appear polished when compared to unworn areas, and it would be possible to trace this using metrological equipment, in the way that Knowlton and Wimmer did previously.

However, the use of visual inspection is limited due to the high level of manual input and time required to trace such a wear edge. Although it may be easy to identify an area of a component as worn or unworn it is impossible to visually identify the width and precise location of a wear scar and then complex to co-register the location of a two-dimensional profile within the surface of a component. For this reason, visually inspecting the components for wear areas was discounted as a method for wear edge detection in this research.

When viewing a visual representation of a two-dimensional profile plotted against a set of axes, it is possible to visualise the overall shape of a component in this section. It could be hypothesised that a noticeable visible change in the form of this profile, whether a sudden change in slope or any type of visual irregularity could be an indicator that the implant surface has undergone a significant change, for instance from an unworn region to a worn region. Figure 25, taken from Jiang et al (2018), shows an example of how this could appear visually (W. Jiang et al., 2018).

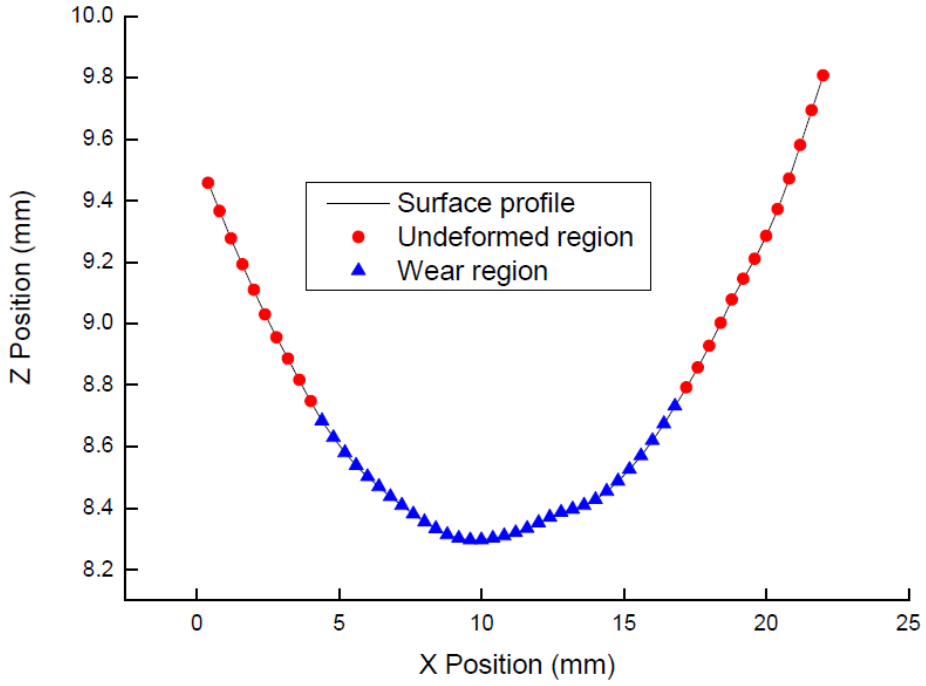

Figure 25 - Visual representation of 2D worn profile (W. Jiang et al., 2018)

If these changes can be visually noted easily it could also be possible to manually select these positions on such a profile with considerable repeatability. It can be seen in Figure 25 that it is not always the case that wear edges are visually identifiable. The repeatability of manual selection was investigated as part of a study in this research and is detailed in Chapter 4. Although the manual selection method was found to be incredibly repeatable and accurate in this situation, the amount of time involved in performing this procedure on approximately 300 profiles per component would be prohibitively excessive.

3.4.2 Automated Wear Edge Detection

The time-consuming nature of manual identification methods means that a step must be made to move towards an automated method of wear edge detection that requires minimal user input, and that can be performed sequentially on all profiles from a component without interruption. Jiang et al attempted this, identifying a worn edge as a Z-shift greater than 0.1mm between adjacent points (W. Jiang et al., 2018).

3.4.2.1 Surface Topographical Analysis

To achieve autonomous wear edge definition, a method that was considered for use was the use of surface topographical measurement to examine surface areal parameters both in worn and unworn areas and report results in a way that could then be numerically integrated into the analysis. Chapter 4 details a comprehensive study that was performed to attempt to distinguish between worn and unworn areas of TKR components using surface topographical parameters. Unfortunately, it was found that whilst there were distinct topographical differences in the areas, the differences were not able to be numerically defined individually and were inconsistent. As a result, pure surface topographical parameter differences were considered an unsuitable way to distinguish between worn and unworn areas of TKR components.

Remaining in the area of surface measurement, it was also considered whether images obtained using surface measurement apparatus could be numerically analysed to ascertain the proportion of a surface that could be considered worn or unworn. To appraise such a method, large surface datasets were taken of the full articular surface of both TKR and TAR components using focus variation microscopy (FVM). These datasets took approximately 8 hours to acquire per component and involved the stitching of multiple datasets. Data was taken using a 10x magnification lens, corresponding to a vertical resolution of 250nm. Components were fixtured using the fixtures shown in Figure 18 and Figure 19, allowing for accurate relocation between component changes. These surface maps were then analysed by 2D visual inspection using tools built into the FVM software.

This method was found to be particularly successful for the identification of wear edges on TAR components. The BOX TAR components used in this project have a very specific pattern imprinted on the unworn surface, as shown in Figure 26. It was also noted that the wear edge on these components was remarkably consistent across the longitudinal direction of the component, with the proportion of component appearing unworn remaining constant at approximately 8% of the lateral width across the component, with equal unworn portions on the medial and lateral extremes. This was found across all sizes of TAR prosthesis and it could therefore follow that 8% of each profile could be considered unworn, with 4% at each extremity.

Figure 26 - Example of Surface Texture of Worn (TOP) and Unworn (BOTTOM) TAR components. Measurement taken using FVM.

Unfortunately, the same success was not replicated when considering TKR components. It was not possible to visually identify worn areas from viewing the two-dimensional surface maps. Unlike the TAR components, the surface macro-texture of unworn TKR areas was identical to the worn macro-texture. This resulted in visual inspection of surface topography measurements being discounted as a method for the identification of worn areas on TKR components.

3.4.2.2 Micro-CT

Micro-CT was also considered as a method for isolating worn areas. The high data density of CT has been applied successfully in other applications as an indicator of surface texture (Plessis et al., 2018; Townsend, Pagani, Blunt, Scott, & Jiang, 2017; Zanini, Pagani, Savio, & Carmignato, 2019). This suggests that there is potential for Micro-CT measurement to be used as a method to identify surface changes, such as those across a wear edge. However, attempts to use CT for this purpose were highly unsuccessful with no visibly identifiable wear edge found.

3.4.2.3 Mathematical Approach

The investigations previously detailed found a method suitable for the characterisation of wear edges in the case of the TAR components but was unfortunately unsuccessful in the case of TKR components. For this reason, numerical methods were explored as a solution for wear edge location identification.

MATLAB software includes a function called *ischange*, which is described as being able to "find abrupt changes in data". By inputting a field of data, the function returns a logical array of values, with 1 corresponding to a change point. As previously stated, the region of change between worn and unworn areas displays characteristics that would be consistent with a sudden change. Within the function there are three different options for the type of change that is to be detected:

- "Mean" – searches for sudden changes in the mean of the data.
- "Variance" – searches for sudden changes in the variance of data.
- "Linear" – searches for sudden changes in the slope and intercept of the data

It would be expected that the unworn areas of components should be uniform and smooth, whilst the worn area is likely to be subject to more changes, such as the polished appearance previously suggested. It could then be suggested that when working across a 2D profile, the changes closest to the two lateral extremities would be the wear edge of the component. It is reasonable to assume that any of the three detection options could be used to locate the wear edge of the component as all three of the change detection parameters would likely undergo a sudden change at the wear edge.

The ischange function finds abrupt data changes by segmenting data iteratively along the length of the data, in this case, a two-dimensional profile. A vector of data is considered to contain a change point when a section of data A is broken down into two segments, A_1 and A_2, and the following is true:

$$C(A_1) + C(A_2) + \tau < C(A)$$

Where C represents a cost function associated with the statistical method chosen (mean, variance, or slope), τ represents a value specified by the *Threshold* input. A cost function is a mathematical operator designed to evaluate how effectively a set of hypothesised data (in this case the actual measured results), fits with the ideal data (in this case the mean for each segment).

In the case of detecting abrupt changes in the mean, the cost function is given by MATLAB as:

$$C(x) = Nvar(x)$$

Where *N* is the number of elements in a vector *x.*

The thresholding value for this function is not well defined in documentation and was not used in the case of this research. Although the name *Threshold* suggests that this affects data accuracy, the *Threshold* value is merely a scalar value that directly affects the number of change points found. MATLAB states that "Increasing the threshold greater than 1 produces fewer change points". The threshold value is as a default value set to 1.

An alternative to the thresholding value is the use of the *MaxNumChanges* input. As suggested by the name, this limits the number of abrupt changes to be found within the dataset being considered. It is important to note that when using the *MaxNumChanges* input, the *Threshold* value is no longer used. If this value is set to 1, the iterative method will cease at the point where the first change point is found.

As previously mentioned, it has been assumed that the change points nearest to the lateral extremities of the condyle would represent the wear edge, as the unworn area will retain its manufactured geometry, whilst the worn area will be freeform. For this reason, the value of *MaxNumChanges* was set to 1, and the data was analysed twice, with iterative analysis beginning from the first and last data points, respectively.

The effectiveness of each method was tested as part of the computational wear study performed in Chapter 5. It was found that using the *mean* and *linear* methods of change detection both provided similar results that corresponded to the location of the known wear edge of the component. It was generally found that the *linear* method appeared to show more repeatable and accurate values and was therefore selected as a suitable method for the wear edge detection on TKR components. It was found that the *variance* method of change detection provided highly inaccurate results with very few if any changes detected across the data.

Numerous different methods have been trialled to attempt to perform wear edge detection in TKR and TAR components. It was found that a simple numerical percentage could be used to define the wear edge in BOX TAR components used in this study. Investigation using surface topographical measurement suggested that 8% of a worn component profile (4% at each extremity) should be used as a basis for the reconstruction of an unworn profile. When considering TKR components it was found that the use of abrupt slope change detection

was effective in detecting wear edges. It was found that searching for sudden changes in slope and intercept detected accurate wear edges in a computational wear simulated component study. These methods can be incorporated into further analysis methods to quantify wear on orthopaedic components.

3.5 Measurement of Two-Dimensional Linear Wear

To calculate volumetric wear on worn components with no pre-wear data, it is necessary to recreate the unworn geometry of the component to use as a reference for comparison. To do this, worn and unworn portions of the component need to be isolated and analysis applied to each. From this, methods need to be applied to find the material loss represented by the difference between these reconstructed forms.

3.5.1 Isolation of Profiles

MATLAB computational mathematics software has been used to perform this process. MATLAB software allows for the creation of a programming script to perform mathematical operations as desired with the potential to create looping features to repeat the operations for multiple iterations. This is particularly useful in the present case, as it is desirable to perform analysis on several hundred profiles in sequence. To do this manually would take an excessive amount of time and be a limiting factor to the success of a wear measurement method. For a method to be successful, it would be beneficial if wear volume calculation could be automated, reducing user input as far as possible.

MATLAB software uses a variety of definitions for different types of features. Numerical data is known as a variable of a given name. A variable can also be text characters, although in the case of this project they are all numerical. MATLAB is designed to allow for quick and powerful calculation of matrix mathematics. Raw Cartesian data is important to MATLAB as an ASCII file. From this file, a [length (data) x 3] matrix is created with each column of the matrix representing X, Y and Z coordinates, respectively. This matrix can then be indexed to use a specific dataset.

As previously mentioned, the profile extraction method used leads to the extraction of numerous tiny incomplete profiles in addition to the full complete datasets. These small profiles are the result of measuring the full data set using CMM as a single scan path. The scan path creates vertices as it changes direction whilst moving from profile to profile. Whilst extracting 2D profiles in CATIA some of these small turning profiles are extracted as profile data but are not desirable to keep in the analysis.

For this reason, a simple filter is applied at the beginning of the script to ignore profiles with a length lower than a set value. In the case of TKR components, this is the aforementioned value of 900. It is at this stage that wear volume calculation methods for TKR and TAR components diverges, with subtly different methods required owing to component geometry and measurement strategy.

3.5.1 Total Knee Replacement Components

In the situation of TKR components, profiles have been taken longitudinally along the anteroposterior direction of the component using CATIA from the measured data taken using CMM. Profiles were spaced at 0.1mm intervals in the medial-lateral direction. As stated, the smallest complete profile has a length of approximately 900 points, anything with a lower value than this is removed at the beginning of the analysis.

The previously mentioned change detection method was performed using the Z-height values across a profile. This change detection creates a logical array of binary values, with 1 corresponding to a change and 0 representing no abrupt change. A minimum of two change points is required for analysis to continue, one towards each extremity of the profile. If the change detection method fails to detect a wear edge on a profile this profile is removed from the analysis. It may be the case that this profile was entirely outside of the wear area and therefore is not relevant to the analysis.

From this, the location index of two change points is exported to a separate variable to represent the location of the profile wear edge. From this, the large data matrix can be segregated to give successive variables representing the worn and unworn Y and Z values. With the worn and unworn data isolated it is then possible to attempt to fit mathematical forms to the data.

3.5.1.1 Curve Fitting

Within MATLAB there is a toolbox of functions designed for the fitting of data to specific curve forms. The toolbox allows for multiple different methods of curve fitting. These can broadly be collated into the following areas:

- Distribution Models
- Exponential Functions
- Fourier Series
- Gaussian Models

- Interpolating Models
- Polynomial Models
- Power Functions
- Rational Equation Models
- Sine Functions
- Spline Models

Some of these data fitting types are unsuitable for the curves taken in this project and can therefore be discounted from the analysis. Three methods were determined to be potentially suitable for use in this research, these were Interpolation Type Models, Polynomials Functions and Spline Models.

Polynomial curve fitting in with MATLAB can be evaluated up to a 9^{th} order. The shape of a typical TKR condyle means that it is logical that there is no requirement to use greater than a 2^{nd} order polynomial for fitting in this situation as there is only a single major turning point within the dataset.

Interpolant fitting is a method of fitting that is performed fully within the ranges of the data. MATLAB facilitates 3 different methods of interpolant fitting for curves. These are listed below with a brief description as taken from MATLAB documentation:

- Linear Interpolation: This method fits a different linear polynomial between each pair of data points for curves.
- Nearest Neighbour Interpolation: This method sets the value of an interpolated point to the value of the nearest data point.
- Cubic Spline Interpolation: This method fits a different cubic polynomial between each pair of data points.

It was decided that cubic spline interpolation was the most suitable method of curve fitting for the datasets gained in this project when compared to linear and nearest neighbour interpolation as it preserves the integrity of the curve shape more robustly than the other two methods. Cubic spline interpolation forms a spline in which all points are in contact with the original dataset. Another method of fitting that has been considered is the use of a smoothing spline. A smoothing spline is characterised by a smoothing parameter *p*. Where a cubic spline has a *p*-value of 1, a smoothing spline value is generally in the region of 0.96 with a *p*-

value of 0.99 representing the smoothest spline that can be fitted through the data. Any *p*-value lower than 1 means that not all sections of the spline will pass through all points.

As a result of the analysis, it was determined that 3 potential methods could be used for curve fitting to data of the shape. These are fitting to a second-order polynomial, cubic spline interpolation and smoothing spline fitting. These three methods were applied to components across several studies detailed in the current research. An example of how the three curve fitting methods are applied is shown in Figure 27. The data used in Figure 27 is a rough sine waveform.

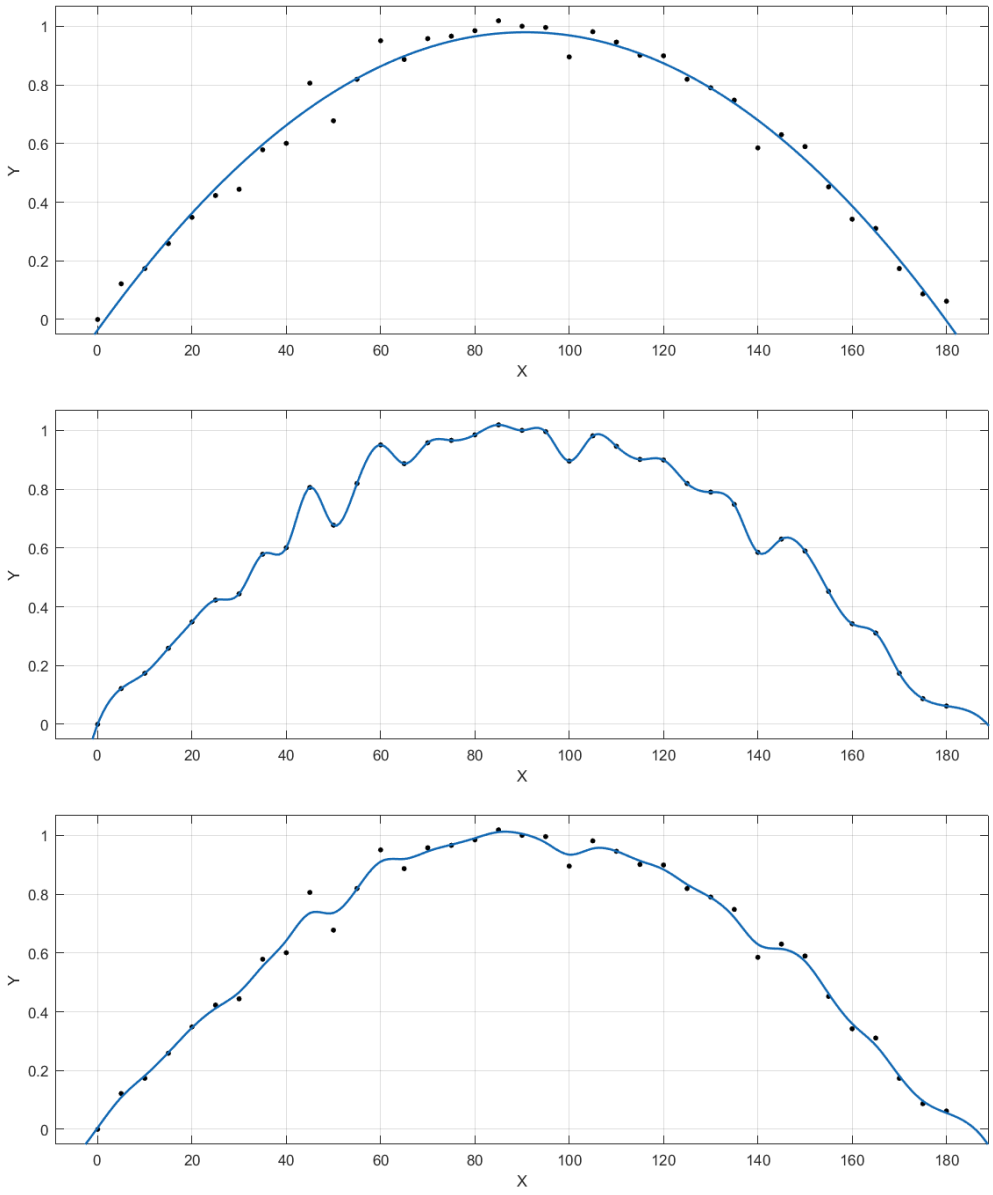

Figure 27 - Example of curve fitting techniques applied on an example data set. Shown are Second-Order polynomial fitting (Top), Cubic Interpolation (Middle) and Smoothing Spline Interpolation (Bottom)

As shown in Figure 27, second-order polynomial fitting applies a single function curve to the dataset. This has the advantage of compensating for erroneous data points but may be insensitive to changes in data. Cubic interpolation applies a piecewise third-order polynomial between each data point, whilst passing through each data point. This has the benefit of being more sensitive to changes in data but may be affected by erroneous data points. The smoothing spline interpolation type curve also forms piecewise polynomials between each point but applies a smoothing parameter to the spine, resulting in a spine that does not pass through each point. This may allow a smoothing spline to reduce the effect of a single erroneous data point when compared to cubic interpolation, but the sensitivity of the smoothing operation may affect the ability to detect small changes in data.

With the worn and unworn data isolated as previously described, the fitting process can be performed on both data sets. Curves were fitted separately on the worn and unworn data and resulted in two separate data sets being created. The wear area across this two-dimensional profile is described by the area between these two splines in the region bounded by the two wear edges.

The evaluation of the area between the two curves was performed using numerical integration methods. Analysis was performed by conducting trapezoidal integration between the two profiles. Trapezoidal integration is an approximation integration technique in which the area of a trapezoid bounded by a curve and the x-axis is calculated between two values of x, as shown in Figure 28. As the values in the x-direction are already defined by the range of y-values, the width of each trapezoid is determined by the spacing between points in this vector. As mentioned, trapezoidal integration is an approximation technique that essentially

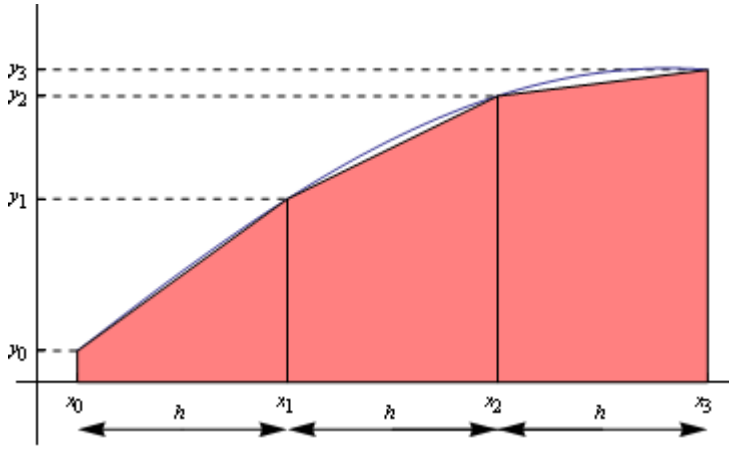

Figure 28 - Visual representation of trapezoidal integration (Imperial College, 2021)

represents the curve as a series of straight lines, contributing slight error to the true value of the area between two curves.

This process is performed for both the worn and unworn curves, giving two values for the wear area in mm^2. By subtracting the unworn profile from the worn profile the resultant area between the two curves can then be calculated. This area calculated in mm^2 corresponds to the material loss area upon that two-dimensional plane. Likewise, the maximum linear penetration within this two-dimensional plane by finding the maximum difference between the two curves.

3.3.2 Total Ankle Replacement Components

The process for wear measurement in a two-dimensional setting for TAR components is relatively similar to that of TKR components. However, the nature of the components and the unworn area location, combined with a difference in measurement strategy means that small differences are required.

In TAR components, the profile data has been taken laterally across the component, meaning that for each profile the Y value remains constant, while the X and Z value fluctuate. Profiles were taken at 0.1mm intervals across the component using CATIA, equating to approximately 300 profiles per component. The number of points in the smallest complete profile of a TAR component was found to be approximately 1200. Similarly to TKR components, profiles of a length shorter than this were discounted from the analysis.

The wear edge isolation method for TAR components is far easier than the aforementioned abrupt slope change detection method used for TKR components. It was found that the TAR components used in this study were approximately 8% unworn across a profile, with the unworn area being similar on both the medial and lateral extremities. This creates the following equation to describe the worn data of the component across a single profile:

$$UnwornData = XData\left(0.04 * length(XData)\right) : XData\left(0.96 * length(XData)\right)$$

XData represents a matrix of all measured X values. The length of XData is the number of points in the profile. For a profile that is 1000 data points in length, the 40^{th} value of XData and the 960^{th} value of XData would be taken to represent the transition between worn and unworn areas on this profile. By using these bounds as

wear edges, two vectors of numbers can be created, one representing worn areas and one representing unworn areas, in the same way as previously displayed for TKR components.

The change detection method applied for TKR components was applied to a profile taken from a TAR component. The change detection methods found wear edges at points corresponding to 4.6% and 3.2% of the components on the medial and lateral sides. This corresponds to 7.8% of the component being unworn, comparing favourably with the percentage found using FVM. For the components used in this research, the wear edge remained at approximately 8% for all profiles measured, the change detection method could however be applied on different cohorts which may require a more complex wear edge definition.

Curve fitting for TAR components was bound by similar conditions to the curve fitting process for TKR components meaning that only certain types of the fitting algorithm were realistically feasible to use for curve fitting. This was limited to polynomial fitting, cubic spline interpolation and smoothing spline fitting. As the articular surface of TAR components has been taken as a single measurement, the geometry is somewhat more complex.

Whereas TKR components were characterised by a single turning point, the measurements taken from TAR appear to have two smaller turning peaks symmetrically located around a larger peak. The presence of three turning points would suggest that if polynomial fitting were to be used, it must be of a 4th order to encompass sufficient turning points.

Cubic interpolation and smoothing splines also have the potential to be used to reconstruct the unworn profiles. However, a major issue with the use of any of the three methods is that the unworn areas of the component are at the lateral extremities and therefore the location of the turning points is not defined, meaning curve fitting may struggle to replicate the surface accurately. For this reason, it was decided that three points around the apex of the central peak would be used in the unworn fitting process to improve the accuracy of the fit.

Following this, the same process was applied to these components as was applied to the TKR components. After evaluation of the curve fitting functions between the wear edges, trapezoidal integration was performed in the region bound by these curves and subtraction was performed to evaluate a wear value across the two-dimensional profile.

It is considered that the method developed is limited in application to the specific cohort of BOX TAR components that have undergone simulated wear. If the method were to be used on an alternate TAR component, different methods of wear edge detection would potentially need to be developed, perhaps in line with those used for TKR components.

3.6 Measurement of Three-Dimensional Volumetric Wear

To calculate volumetric wear in components it is necessary to expand the two-dimensional analysis into a 3D setting. The nature of the components measured means that the surface is freeform across the entire XY plane.

Volumetric wear has been calculated by assuming that the two-dimensional wear-value calculated in the aforementioned stages continues in the region bounded by this profile section and the next profile section that has been calculated. This would be expected to be 0.1mm as this is the original spacing that was taken between profiles. However, due to the method applied, some profiles may have been excluded due to issues with change detection or the length being below the specified threshold. For this reason, the spacing value must be calculated using the static value. This is a simple process that can be integrated into the script.

By multiplying each wear value by the corresponding profile separation and summing the results a value of volumetric wear on that measurement can be calculated. For TAR components this is the total volumetric wear of the superior articular surface component. In the case of TKR components, the two condylar surfaces must be summed to calculate an overall total wear volume for the component.

3.7 Data Analysis Methods

To fully compare results from different measurement methods, a variety of analysis methods were chosen to evaluate the differences between results gained in different methods. Statistical analysis has been conducted alongside qualitative analysis for all studies.

3.7.1 Statistical Methods

Student's t-test was created in 1908 by William Sealy Gosset as a method of hypothesis testing to find statistical significance between two variables (Gosset, 1908), and are considered to be a robust method (Bland,

1995). T-Tests were used in this research for comparison between measurement methods, and also as a comparison between repeat measurements of the same variable.

Where t-tests have been conducted in this research, results will be presented including the mean (M) and standard deviation (SD) of each data set. All tests were performed at a 5% significance level, with results presented as "t(df)= T, p = P", where df refers to the degrees of freedom, T represents the t-value and P is the significance value. A significance value lower than the significant level of 0.05 represents a significant difference between the values. Bland-Altman plots have also been used as a visual representation of this in some studies (Altman & Bland, 1983).

Alongside t-tests, Pearson's product-moment correlation coefficient (Pearson, 1895) has also been reported in some studies. A PPMC of -1 represents a very strong negative correlation between two variables, with +1 representing a very strong positive correlation, and 0 representing no correlation. Results are presented as r(df) = R, p = P, where df is the degrees of freedom, R represents the correlation statistic and P represents the p-value.

3.7.2 Hood Damage Scoring

In the case of retrieved components, alternative volumetric wear measurements are not available as they are for simulated components, due to a lack of pre-wear data. For this reason, retrieved volumetric wear results have been compared statistically to the Hood damage score, as conducted by Knowlton and Wimmer (Knowlton & Wimmer, 2012). The Hood score is a subjective method in which a user scores seven different surface damage mechanisms on a scale of 0-3, equating to a maximum score of 21 (Hood, Wright, & Burstein, 1983). A score of 0 represents the wear mechanism not being present, 1 represents up to 10% of the component surface displaying each wear mechanism, 2 represents between 10% and 50% of the surface displaying each wear mechanism and 3 represents greater than 50% of the surface displaying each wear mechanism. The seven wear mechanisms evaluated are:

- Delamination – layers of fractured material removed from a surface.
- Abrasion – material removal through sliding contact.
- Burnishing – polishing of a surface due to sliding contact.
- Scratching – scratches present on the surface.

- Embedded Particles – aspersions embedded in the component surface (usually CoCr or bone cement).
- Pitting – Small holes or cavities present upon the surface.
- Surface Deformation – plastic deformation of the surface from original geometry.

The Hood score is a subjective measure that is open to inter-user variability. In the current research, Hood damage scores were computed independently by the author and an independent investigator and an average was taken. It would be expected that Hood damage score and volumetric wear would be positively correlated, an increase in Hood damage score would be expected to correspond to an increased volumetric wear rate (Knowlton & Wimmer, 2012). Pearson's product-moment correlation coefficient was used to assess correlation.

Chapter 4 – Comparison of Surface Topographical Parameters between Worn and Unworn areas of TKR components

The content of this chapter relates to a body of work published by the author in Surface Topography: Metrology and Properties (2018). For the full publication please see “Characterisation of wear areas on UHMWPE total knee replacement prostheses through the study of their areal surface topographical parameters”. Full data tables for this study is contained within Appendix A.

4.1 Study Aims & Overview

To quantify volumetric wear on the components using the method employed in the current research, it is vital to know any methods that can be used to distinguish between worn and unworn portions of a TKR component. The study detailed in this chapter presents an approach using surface topographical measurement to differentiate between worn and unworn data by analysing differences in areal surface topographical parameters.

This study also explored whether there is a difference in surface topography between posterior stabilised and cruciate-retaining type prostheses. The cohort used in this study also allowed for an exploration of topographical differences in components that had undergone wear simulation and components that had been retrieved.

This study aimed to be able to isolate areas of a TKR component that are worn and use this information to inform wear edge location for volumetric measurement in further studies.

It was found that significant differences are displayed between different areas of the component although these were found to be inconsistent numerically. Significant differences were found in the surface topography of PS and CR type components. No significant difference was found in surface topographical parameters when comparing wear simulated and retrieved components.

4.2 Study Design

4.2.1 Cohort Definition

A cohort of seventeen UHMWPE TKR tibial components was used for this study. Five of these components were DePuy LCS, a cruciate-retaining design. Seven components were DePuy PFC, a posterior stabilised design that is also of a mobile bearing type. Five components were retrieved components of varying design, consisting

of PS (n=4) and CR (n=1) designs. The retrieved components were supplied by the London Implant Retrieval Centre (LIRC), full details of component design and implantation time are provided in Chapter 7.

4.2.2 Location of Measurement Datasets

Visual inspection identified areas of each component that could be considered worn, these were identified from areas of a polished appearance. Ten datasets were taken for each component, with five on each condyle. A data point corresponding to the lowest Z-height on each condyle was taken as a central point, with measurements taken 10mm from this central point in anterior, posterior, medial and lateral directions. The central point location was dynamic and changed for each component.

This study is indicative of the surface topographical parameters of worn and unworn areas. As each component had undergone differing wear simulation and in-service conditions and therefore exhibited different wear scar geometry it was determined that repeatability of absolute measurement point location between components was not necessary.

The component was aligned to an X-Y coordinate system and the ML and AP directions correspond to the X-axis and Y-axis, respectively. A visual representation of the location of these data points is shown in Figure 29. The diagram in Figure 29 is not to scale and does not accurately reflect the locations of data collection.

Figure 29 - Diagram showing the location of measurement points for surface topography study.

Referring to the nomenclature in Figure 29 combined with a visual inspection of the components, datasets 1,4, 6 and 9 were always found to be classified as worn areas of the component. Datasets 2,3,7 and 10 were found to always be classified as unworn areas. Datasets 5 and 8 were found to vary between worn and unworn

components. Visual analysis of the component was used to determine if points 5 and 8 represented worn or unworn data.

4.2.3 Measurement Method Selection and Parameters

Two surface topographical measurement methods were considered for use in this study, these were Focus Variation Microscopy (FVM) using the Alicona InfiniteFocus® and Correlation Coherence Interferometry (CCI) using the Taylor Hobson Talysurf. Preliminary investigative measurements determined that the FVM instrument was more effective in the measurement of UHMWPE components. It was found that when using CCI there were high levels of data dropout, resulting in high translucency in the UHMWPE surface causing errors in CCI focus. High levels of data dropout in high gradient areas of the TKR components showed that CCI is not optimum for the measurement of such areas. FVM is an effective method for the measurement of steep slope geometry, such as the edge of TKR condyles, and for this reason, was selected as the most appropriate method with which to proceed.

4.2.3.1 Replication

A replication study was performed to investigate the possibility that subsurface texture may be measured for UHMWPE components using FVM due to component translucency. Replication involves the use of high accuracy resin to create an impression of the surface that is to be measured. Often it is the case that the optical light penetrates the top surface of the component and therefore subsurface texture is being measured, leading to incorrect results.

Microset 101RF was used in both a grey and black colour to determine if there was an advantage in using replication in the case of these UHMWPE components. The replication medium has a resolution of 0.1µm and takes between 5 and 60 minutes to cure. A DePuy LCS component was replicated using this replication medium and measured using FVM. It was found that there was no evidence of subsurface texture measurement and it was appropriate to directly measure the TKR components without the need for replication.

4.2.3.2 Sample Preparation and Fixturing

Component preparation for FVM measurement was identical to the process used for Micro-CT and CMM measurement detailed in Chapter 3. The components were allowed to stabilise for a minimum of 48 hours in a

temperature-controlled environment to reach thermal equilibrium. Before measurement components were cleaned using a cloth soaked in an isopropyl based cleaning solution.

Components were fixtured using the fixture shown previously in Figure 18. The central dataset taken for each component was dynamic and related to the specific component geometry, thus re-registration of the component location was not an issue in fixturing.

4.2.3.3 Measurement Parameters

A 20x magnification lens was used in this study, with each measuring approximately 710µm x 520µm in the X-Y plane. The 20x lens has a minimum measurable *Sa* value of 0.075. The lateral resolution was 2.94µm with a vertical resolution of 0.04µm. These parameters were defined to provide a balance between resolution and scanning time.

This study was intended to be indicative of distinct differences in topography between worn and unworn areas and it was decided that individual measurements would be representative of the global geometry. Future development to this study would be to stitch multiple measurement areas to create a larger measurement area as this would help to build a more comprehensive dataset. Each data point was measured once, resulting in ten measurement datasets that correspond to the ten measurement locations shown in Figure 29. These were acquired for each component and exported as ".SUR" files.

4.2.4 Data Processing

Processing of the acquired surface data was performed using Surfstand surface analysis software (University of Huddersfield). Manual pre-processing of the data was performed to individual optical pixels that were misrepresented as spikes. These data spikes were often at least 10 times higher than the mean surface plane and were clear misrepresentations. A linear interpolant filling operation was applied to these measurement voids. A form removal operator (F-operator) was applied to remove underlying geometry from the measurements at a nesting index of 0.2mm. The measurement was fitted to a second order polynomial surface to achieve this. A high pass robust Gaussian filter of 25µm was used to remove optical noise from the dataset whilst maintaining the initial measured surface.

4.2.5 Surface Areal Parameter Selection

ISO-25178 lists the extensive collection of surface areal parameters that can be analysed (ISO, 2012). An initial overview of the results found numerous parameters showed little or no variation across all measurement sets. For this reason, these parameters were excluded from further analysis. With these parameters removed, 9 parameters were selected for further investigation. Parameters were selected which showed variation across results:

The parameters selected were *Sq, Ssk, Sku, Sp, Sv, Sz, Sdq, Sa and Sds*. Although *Sds* is not part of ISO 25178 it was decided that sufficient variation was evident in this parameter. Full details of these parameters along with a brief description of the characteristics they represent are shown in Table 3.

Parameter Symbol	Parameter Name	Description
Sq	RMS Surface Roughness	Root mean square heigh of the scale-limited surface within the definition area
Ssk	Surface Skewness	Determines whether the surface is dominated by peaks or valleys. A value of 0 represents a neutral surface
Sku	Surface Kurtosis	"Sharpness" of peaks or valleys on surface. A value of 3 represents a neutral surface
Sp	Maximum Peak Height	Amplitude of the highest peak upon the surface within the definition area
Sv	Maximum Valley Depth	Amplitude of the deepest valley upon the surface within the definition area
Sz	Maximum Peak-Valley Amplitude	Sum of Sp and Sz. Maximum vertical distance between two points
Sdq	RMS Surface Slope	Average angle of slope across surface. For a completely level surface Sdq is 0
Sa	Surface Roughness	Average surface roughness of component. Interchangeable with Sq and less frequently used in comparison
Sds	Summit Density	Number of peaks per unit area. Of particular interest when considering bearing surfaces.

Table 3 - List of Surface Texture Parameters considered for further analysis.

4.3 Results

The results of this study will be discussed for each surface parameter individually. In discussing each parameter, three different comparisons will be performed; worn vs unworn areas, PS vs CR type prostheses

and wear simulated vs retrieved components. Full raw data from this study is presented in Appendix A. A summary of the average values found for each of the three studies performed is detailed in Table 4.

Parameter	Worn Areas	Unworn Areas	Wear Simulated	Retrieved	Cruciate Retaining	Posterior Stabilised
Sq (µm)	0.63	0.64	0.53	0.67	0.56	0.70
Ssk	-0.25	-0.10	-0.40	-0.47	-0.19	-0.08
Sku	8.44	10.35	10.81	8.80	12.65	6.97
Sp (µm)	4.07	4.88	3.79	4.16	4.22	5.04
Sv (µm)	4.04	5.87	4.79	4.92	4.57	5.21
Sz (µm)	8.12	10.76	8.58	9.08	8.79	10.25
Sdq	0.13	0.16	0.14	0.14	0.14	0.16
Sa (µm)	0.49	0.48	0.40	0.51	0.42	0.55
Sds (/mm^2)	3985.07	4468.53	4142.55	3780.64	4095.87	4520.95

Table 4 - Surface topographical data attained using FVM

4.3.1 RMS Surface Height (*Sq*)

The RMS surface height represents the root mean square value of ordinate values within the defined area. It is equivalent to the standard deviation of heights found on a surface. A lower value of *Sq* indicates a smoother surface.

A paired t-test was performed to compare worn areas to unworn areas. No significant difference in *Sq* was found between worn (M=0.63µm, SD=0.23µm) and unworn (M=0.64µm, SD=0.26µm) areas t(75) = -0.064, p = 0.949. There was no significant difference in *Sq* between worn and unworn areas.

A paired t-test was performed to compare cruciate-retaining components to posterior stabilised components. A significant difference in *Sq* was found between cruciate-retaining (M=0.56 µm, SD=0.24 µm) and posterior stabilised (M=0.70 µm,SD=0.26 µm) type components; t(62) = -3.408, p = 0.001. Posterior stabilised components display rougher surface texture than cruciate-retaining components.

A paired t-test was performed to compare *Sq* for wear simulated components to retrieved components. A significant difference in *Sq* was found between wear simulated (M= 0.53 µm,SD=0.18 µm) and retrieved (M=0.67 µm, SD=0.3 µm) components; t(46) = -2.717, p = 0.009. Retrieved components display rougher surfaces than wear simulated components.

4.3.2 Surface Skewness (*Ssk*)

Surface skewness relates to the height distribution of surface points around its mean plane. An *Ssk* value of 0 would represent a surface where peak and valley average heights across the surface were symmetrical about

the mean plane. An *Ssk* value greater than zero would represent a surface dominated by peaks, whilst a negative value would represent a surface dominated by valleys.

A paired t-test was performed to compare worn areas to unworn areas. No significant difference in *Ssk* was found between worn (M=-0.25 µm, SD=1.27 µm) and unworn (M=-0.1 µm, SD=1.82 µm) areas t(75) = -0.545, p = 0.587. There was no significant difference in *Ssk* between worn and unworn areas.

A paired t-test was performed to compare cruciate-retaining components to posterior stabilised components. No significant difference in *Ssk* was found between cruciate-retaining (M=-0.19 µm, SD=1.96 µm) and posterior stabilised (M=0.08 µm,SD=1.33 µm) type components; t(62) = -0.343, p = 0.733. There was no significant difference in *Ssk* between CR and PS components.

A paired t-test was performed to compare *Ssk* for wear simulated components to retrieved components. No significant difference in *Ssk* was found between wear simulated (M= 0.4 µm,SD=1.51 µm) and retrieved (M=-0.47 µm, SD=1.52 µm) components; t(46) = 0.23, p = 0.817. There was no significant difference in *Ssk* between wear simulated and retrieved components.

4.3.3 Surface Kurtosis (*Sku*)

Surface kurtosis describes the sharpness of peak and valley features on a surface. Figure 30 shows an example of the appearance of a typical profile with changing kurtosis, note that Rku represents Sku on a single two-dimensional profile. Kurtosis uses a neutral value of 3, with values greater than 3 indicating sharper features and those with values lower than 3 being smoother. It was noticeable in this study that nearly all

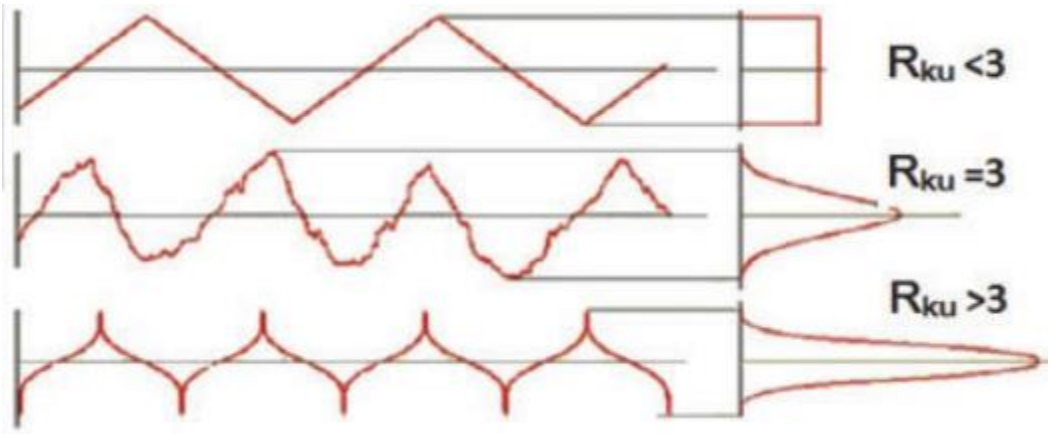

Figure 30 - Representation of Variation in Profile Kurtosis (Duboust et al., 2016)

measurements conducted returned values greater than 3 suggesting that in general the surface measured was dominated by sharp peaks and valleys.

A paired t-test was performed to compare worn areas to unworn areas. No significant difference in *Sku* was found between worn (M=8.44, SD=30.23) and unworn (M=10.35, SD=29.27) areas t(75) = -0.39, p = 0.698. There was no significant difference in *Sku* between worn and unworn areas.

A paired t-test was performed to compare cruciate-retaining components to posterior stabilised components. No significant difference in *Sku* was found between cruciate-retaining (M=12.65 SD=41.75) and posterior stabilised (M=6.97,SD=18.21) type components; t(62) = -0.974, p = 0.334. CR type components do not show significantly higher values of *Sku* than PS type components.

A paired t-test was performed to compare *Sku* for wear simulated components to retrieved components. No significant difference in *Sku* was found between wear simulated (M= 10.81,SD=37.92) and retrieved (M=8.8, SD=20.96) components; t(46) = 0.31, p = 0.757. There was no significant difference in *Sku* between wear simulated and retrieved components.

4.3.4 Maximum Amplitude of Surface Peak (*Sp*)

Sp refers to the maximum amplitude of the highest peak within the defined area on a surface. *Sp* is purely a scalar value of the highest peak above the mean plane of the measurement with higher *Sp* values corresponding to a higher surface peak.

A paired t-test was performed to compare worn areas to unworn areas. No significant difference in *Sp* was found between worn (M=4.07 µm, SD=2.24 µm) and unworn (M=4.88 µm, SD=4.03 µm) areas t(75) = -1.492, p = 0.14. Worn areas do not display significantly lower surface peaks than unworn areas.

A paired t-test was performed to compare cruciate-retaining components to posterior stabilised components. No significant difference in *Sp* was found between cruciate-retaining (M=4.22 µm, SD=3.65 µm) and posterior stabilised (M=5.04 µm, SD = 3.35 µm) type components; t(62) = -1.306, p = 0.196. CR type components do not show significantly lower surface peaks than PS type components.

A paired t-test was performed to compare *Sp* for wear simulated components to retrieved components. No significant difference in *Sp* was found between wear simulated (M= 3.78 µm,SD=2.44 µm) and retrieved

(M=4.16 µm, SD=2.62 µm) components; t(46) = -0.69, p = 0.497. Wear simulated components do not show significantly lower surface peaks than retrieved components.

4.3.5 Maximum Amplitude of Surface Valley (*Sv*)

Sv as a parameter shares great similarity with *Sp* in the sense that it is a single scalar quantity. Where *Sp* is the maximum amplitude of a surface peak, *Sv* represents the maximum amplitude of the deepest valley on a surface. A higher value of *Sv* would represent a deeper surface valley.

A paired t-test was performed to compare worn areas to unworn areas. A significant difference in *Sv* was found between worn (M=4.04 µm, SD=1.97 µm) and unworn (M=5.87 µm, SD=4.38 µm) areas t(75) = -3.381, p = 0.01. Unworn areas display significantly deeper surface valleys than worn areas.

A paired t-test was performed to compare cruciate-retaining components to posterior stabilised components. A significant difference in *Sv* was found between cruciate-retaining (M=4.57 µm, SD=3.66 µm) and posterior stabilised (M=5.21 µm, SD = 3.66 µm) type components; t(62) = -0.955, p = 0.034. PS type components show significantly deeper surface valleys than CR type components.

A paired t-test was performed to compare *Sv* for wear simulated components to retrieved components. No significant difference in *Sv* was found between wear simulated (M= 4.79 µm, SD=4.05 µm) and retrieved (M=4.92 µm, SD=2.71 µm) components; t(46) = -0.165, p = 0.870. There was no significant difference in valley depth between wear simulated and retrieved components.

4.3.6 Maximum Peak-Valley Height (*Sz*)

The surface parameter *Sz* is intrinsically linked to the previous two described parameters. *Sz* represents the maximum distance between a surface peak and a surface valley, and can therefore be described as the overall amplitude of the surface, calculated through the sum of *Sp* and *Sv*. A higher value of S*z* represents a greater peak-valley distance.

A paired t-test was performed to compare worn areas to unworn areas. A significant difference in *Sz* was found between worn (M=8.12 µm, SD=3.01 µm) and unworn (M=10.76 µm, SD=6.51 µm) areas t(75) = -3.162, p = 0.02. Unworn areas display significantly larger peak-valley heights than worn areas.

A paired t-test was performed to compare cruciate-retaining components to posterior stabilised components. A significant difference in *Sz* was found between cruciate-retaining (M=8.79 µm, SD=5.62 µm) and posterior stabilised (M=10.25 µm, SD = 5.37 µm) type components; t(62) = -1.428, p = 0.045. PS type components show significantly greater peak-valley height than CR type components.

A paired t-test was performed to compare *Sz* for wear simulated components to retrieved components. No significant difference in *Sz* was found between wear simulated (M= 8.58 µm, SD=5.13 µm) and retrieved (M=9.08 µm, SD=4.24 µm) components; t(46) = -0.472, p = 0.639. There was no significant difference in peak-valley height between wear simulated and retrieved components.

4.3.7 Surface Peak Density (*Sds*)

The surface peak density is a parameter that is not controlled by ISO25178-2 but showed sufficient variation to warrant being investigated further. *Sds* is described by the number of peaks per square millimetre on a surface. A peak measured by Sds is defined as any point which is above all 8 nearest neighbours and a minimum of 5% of *Sz* above the mean surface plane. Higher values of *Sds* represents a surface with more peaks per unit area.

A paired t-test was performed to compare worn areas to unworn areas. A significant difference in *Sds* was found between worn (M=3985.07/mm^2, SD=722.78 mm^2) and unworn (M=4468.53 /mm^2, SD=946.29 /mm^2) areas t(75) = -4.31, p = 0.001. Unworn areas display a significantly higher surface peak density than worn areas.

A paired t-test was performed to compare cruciate-retaining components to posterior stabilised components. A significant difference in *Sds* was found between cruciate-retaining (M=4095.87 /mm^2, SD=531.18/mm^2) and posterior stabilised (M=4520.95/mm^2, SD = 1118.23/mm^2) type components; t(62) = -2.612, p = 0.011. PS type components show a significantly higher surface peak density than CR type components.

A paired t-test was performed to compare *Sds* for wear simulated components to retrieved components. A significant difference in *Sds* was found between wear simulated (M= 4142.55/mm^2, SD=517.58/mm^2) and retrieved (M=3789.64/mm^2, SD=2642.8/mm^2) components; t(46) = 3.058, p = 0.004. Wear simulated components show a significantly higher surface peak density than retrieved components.

4.3.8 RMS Overall Surface Slope (*Sdq*)

The overall surface slope describes the overall angle of the surface measured within the defined area. It was generally found that all measurements that were taken showed very low surface angles, usually lower than 0.3 degrees. This is likely a result of the F-operator that was applied to each measurement, with the overall difference between angles condensed into a smaller range.

A paired t-test was performed to compare worn areas to unworn areas. No significant difference in *Sdq* was found between worn (M=0.13 deg, SD=0.03 deg) and unworn (M=0.16 deg, SD=0.07 deg) areas t(75) = --3.226, p = 0.002. Unworn areas do not display a significantly higher RMS surface slope than worn areas.

A paired t-test was performed to compare cruciate-retaining components to posterior stabilised components. No significant difference in *Sdq* was found between cruciate-retaining (M=0.14 deg, SD=0.06) and posterior stabilised (M=0.16 deg, SD = 0.06) type components; t(62) = -1.424, p = 0.16. PS type components do not show a significantly higher RMS surface slope than CR type components.

A paired t-test was performed to compare *Sdq* for wear simulated components to retrieved components. A significant difference in *Sdq* was found between wear simulated (M= 0.14 deg, SD=0.05 deg) and retrieved (M=0.13 deg, SD=0.03 deg) components; t(46) = 0.719, p = 0.045. Wear simulated components show a significantly higher RMS surface slope than retrieved components.

4.3.9 Surface Roughness (*Sa*)

Sa is intrinsically linked to *Sq*. Where *Sq* shows the RMS value of the surface height, *Sa* is the mean of the heights of peaks and valleys above or below the mean plane of the surface. A higher value of *Sa* represents a rougher surface.

A paired t-test was performed to compare worn areas to unworn areas. No significant difference in *Sa* was found between worn (M=0.49 µm, SD=0.18 µm) and unworn (M=0.48 µm, SD=0.19 µm) areas t(75) = -0.399, p = 0.691. There was no significant difference in surface roughness between worn and unworn areas.

A paired t-test was performed to compare cruciate-retaining components to posterior stabilised components. A significant difference in *Sa* was found between cruciate-retaining (M= 0.42 µm, SD=0.17 µm) and posterior

stabilised M=0.55 µm, SD=0.17 µm) type components; t(62) = -3.886, p = 0.0001. PS type components show significantly higher surface roughness compared to CR type components.

A paired t-test was performed to compare *Sa* for wear simulated components to retrieved components. A significant difference in *Sa* was found between wear simulated (M= 0.40 µm, SD=0.13 µm) and retrieved (M=0.51, SD=0.22) components; t(46) = -2.667, p = 0.011. Retrieved components show a significantly higher surface roughness than wear simulated components.

4.4 Discussion & Outcomes

The results detailed in 4.3 are summarised below in Figure 31. Situations in which significant differences were found are represented in green.

	Sq	*Ssk*	*Sku*	*Sp*	*Sv*	*Sz*	*Sdq*	*Sa*	*Sds*
Worn vs Unworn									
CR vs PS									
Wear Simulated vs Retrieved									

Figure 31 - Representation of Significant Differences found in Surface Topographical Study. Boxes highlighted green represent where significant differences were found, boxes highlighted white represent situations in which no significant difference was found.

To differentiate subjectively between worn and unworn areas using areal surface texture parameters, there must be a significant difference noted between the two parameters, this was found for four different parameters (*Sv, Sz, Sdq and Sds*).

To differentiate numerically between worn and unworn using areal surface texture parameters, there must be no significant difference in parameters noted between different designs, nor any significant difference noted between different wear application methods, this was found for *Ssk, Sku and Sp.*

This would suggest that worn and unworn areas of a TKR component can be isolated subjectively where a significant difference in surface areal texture parameters. It is however not possible to define the magnitude of change that would represent these two areas, as significant differences were found between components of different design or wear application methods.

The machined unworn surface of TKR components appeared to be rougher than the worn surface, although the difference was not significant. It was found that worn areas typically display lower surface peaks, although

no significant, and significantly shallower surface valleys. The abrasive wearing process may flatten the original surface peaks, resulting in lower values of *Sp* in worn areas.

The articulating motion of a TKR effectively polishes the surface of the UHMWPE insert, causing the aforementioned general smoothing of the surface. Whilst the reduction in surface roughness was found to be non-significant, it was found that unworn areas display significant higher values of *Sds*, representing a larger number of peaks per unit area, again suggesting the abrasion of peaks occurring in worn areas.

PS and CR type TKR components are comparable with little or no difference in clinical performance (Battaglia et al., 2014; Bercik, Joshi, & Parvizi, 2013; Li, Tan, Deng, & Chen, 2014). However, this study found that there are significant differences between the two types of components for almost all studied surface areal texture parameters, except for *Ssk*.

The use of PS type components typically results in increase conformity in the joint articulation (S. J. Song, Park, & Bae, 2019). Increased conformity using a PS type component has previously been shown to cause increased surface damage at a macro-scale (M. A. Wimmer et al., 2012). It is possible to hypothesise that this will lead to changes in surface characteristics at a micro-scale.

Wimmer et al noted that surface pitting and delamination increase with increasing conformity. It was also found that increasing conformity was associated with a reduction in polishing (M. A. Wimmer et al., 2012). These conclusions would appear to agree with the results found in this study. No components used in this study showed evidence of delamination, whilst all components showed evidence of polishing. Some components displayed evidence of pitting on the surface. An increase in pitting has previously been linked to an increase in roughness (Hong & Nagumo, 1997). It was noted in this study that CR type components displayed significantly lower surface roughness (*Sq* and *Sa*) than PS type components.

It can be suggested that polishing would be expected to reduce the surface roughness of a component, with peak abrasion also reducing surface peak height (*Sp*) and reducing the peak-valley height (*Sz*) by lowering the mean surface plan. Significant differences were found between CR and PS type components for all of these parameters.

Wear simulation methods are accepted as an accurate method of replicating in-service wear on TKR components (Abdelgaied et al., 2017; Brandt et al., 2011; Claire L Brockett et al., 2012; Cranin, 1987).

However, this study found significant differences between wear simulated and retrieved components across several surface areal texture parameters (*Sq, Sa* and *Sds).* This suggests that there are significant tribological differences in surface interaction occurring during simulator testing when compared to *in-vivo* wear. There are distinct differences between wear simulation and retrieved component environments i.e. lubrication fluid, component alignment etc. Analysis of how significant differences in surface topography originated for these components would be based purely on speculation as the simulator testing conditions and parameters are not known.

4.5 Summary

The study detailed in this chapter aimed to differentiate between worn and unworn areas on a UHMWPE TKR component using areal surface texture parameters. Although the results do show significant differences in specific parameters between worn and unworn areas, there are no numerically definitive bounds that can be applied to differentiate between the two areas, as significant differences were also found between component designs and wear application methods.

It is interesting that significant differences in surface topography were found between PS and CR type components, as numerous published studies have found no difference in clinical performance between the two designs (Battaglia et al., 2014; Bercik et al., 2013; Li et al., 2014; Wünschel et al., 2013). This comparison is perhaps limited by relatively small sample size, and the cohort of components being biased towards CR type components [CR(n=10); PS(n=7)]. Investigation of a larger, unbiased cohort would be of benefit to this study.

Significant differences were also found when comparing wear simulated and retrieved components. This suggests that surface interaction in wear simulation may not accurately replicate the surface interaction that would occur *in-vivo.* The small sample size for retrieved components (n=5) was a limitation of this study, as was a significant bias in retrieved cohort size when compared to wear simulated components (n=12). Similarly to CR vs PS analysis, this study would benefit from application to a larger, unbiased cohort of components.

This study has shown that wear edge definition using surface areal texture parameters differences is not a viable solution due to inconsistency in parameters across different component designs and wear application methods. All components used in this study exhibit relatively low levels of visual surface damage. Using the Hood score damage index (Hood et al., 1983), the maximum damage score found for any component in this

study was 8. The maximum Hood score is 21. It may be beneficial to expand the cohort for this study to incorporate a wider range of surface damage scores. The cohort was limited to 17 components, with numerous different designs and sizes of components studied. This study may benefit from application to a larger, coherent cohort of consistent design and component geometry.

Chapter 5 – Measurement and Validation of Two-Dimensional Wear Methodology on Computational and 3D printed components

5.1 Study Aims & Objectives

This chapter describes a study to validate the two-dimensional profile volume analysis methodology described in Chapter 3. To validate this measurement method a model was created such that profiles with known geometry could be taken. The two-dimensional analysis method was then applied to these profiles to assess the accuracy of the developed method.

This study aims to validate the developed measurement method by assessing sources of error in the volumetric measurement method.

5.2 Study Content Overview

This study is broken down into many smaller studies to validate a variety of different factors of the volumetric wear measurement method developed in Chapter 3.

1. Assessment of Micro-CT generated CAD model accuracy
2. Manual wear edge location error
    a. Repeatability of manual wear edge selection
3. Automatic wear edge location error
    a. Effect of using automatic wear edge location by comparing wear values found using manual and absolute wear values.
4. Accuracy assessment of curve fitting techniques for two-dimensional wear measurement
    a. Comparison of wear values gained using smoothing spline, cubic interpolation, and second-order polynomial fitting methods to absolute wear values.
5. Accuracy assessment of three-dimensional volumetric wear measurement

5.3 Study Design

5.3.1 CAD Model Accuracy Assessment

A manufacturer supplied unworn CAD model of the DePuy LCS Total Knee Replacement system in the International Graphics Exchange Specification (.IGES) format was used for all studies in this chapter. A worn DePuy LCS component was scanned using Micro-CT as described in 3.1. A CAD model was constructed from

this Micro-CT scan data as described in 3.1. A comparison was made between this CAD model and the manufacturer supplied unworn DePuy LCS CAD model.

Both CAD models were aligned axially to the global coordinate system using the central axis of the backside tibial stem and the planar backside face. Rotational alignment was performed using identifiable points on the component backside face.

Comparison between CAD models was performed by comparing the cartesian location of eight points on the perimeter of the articular surface. These 8 points correspond to the alignment points used in CMM. All points were in unworn areas and therefore should be identical. A comparison was performed to assess for accuracy in the CAD model.

5.3.2 Creation of 3D Printed Test Artefact

The geometry of the unworn articular condylar surfaces was modified using SolidWorks CAD software to simulate a known change in geometry representing wear on the surface of the component. A representation of this surface was then exported in a high-density standard tessellation language (.STL) format, with a triangulated element size of 0.1mm.

The ".STL" file was then manufactured using a BCN3D Sigma 3D printer and is shown in Figure 32. The positioning resolution using the 3D printer was 1.25µm in X and Y and 1µm in Z, with layers built at 0.1mm intervals.

Figure 32 - 3D printed computational wear simulated component manufactured for

After manufacturing, the major outside dimensions in X, Y and Z were verified using a Vernier calliper (±0.01mm) to ensure that these corresponded with the respective dimensions on the computational model. The maximum dimensional error found between the computational model and the manufactured 3D printed component was 0.08mm.

5.3.3 Absolute Wear Value Extraction

Two-dimensional profiles were taken from both the unworn and worn (modified) original CAD models using sectioning tools in Solidworks software. The cross-sectional area found between these unworn and worn profiles represents the absolute value of wear across each two-dimensional profile.

5.3.4 3D Printed Component Measurement

CMM measurement data for the 3D printed component shown in Figure 32 was acquired using the method detailed in 3.2. Two-dimensional profile data was exported using CATIA software as described in 3.3.

5.3.5 Profile Sampling

Ten corresponding profiles were taken from both the computational model and the measured 3D printed component for analysis to represent a sample of profile properties across a component. Four of these profiles were taken from an entirely unworn area. For these four profiles wear value and linear penetration calculated should be equal to zero. The profiles were approximately linearly spaced across the component.

5.3.6 Wear Edge Identification

Two methods were used for wear edge location in this study. The first was the use of manual wear edge location. Profiles were represented graphically in MATLAB software with the wear edge manually located. Six repeat measurements were performed using manual selection as a wear edge detection method and the repeatability of these measurements was assessed.

The automatic wear edge detection method described in 3.4 was also applied to two-dimensional profiles. A study was performed to assess for differences in wear edge location between the absolute, manually selected and automatically detected methods. The x-axis position of the wear edge was taken for each method, with the absolute wear edge location taken as a datum. The x-value difference between absolute, manually selected and automatically detected methods was assessed to consider the accuracy of using each method.

5.3.7 Two-Dimensional Wear Value Measurement Study

To evaluate the accuracy of the two-dimensional measurement method developed in this research several studies were performed to evaluate different curve fitting techniques and to evaluate the effectiveness of curve fitting in both worn and unworn areas of the component by comparing wear values.

The first study compared wear values gained from using smoothing spline, cubic interpolation, and second-order polynomial curve fitting methods. Worn and unworn areas of each profile were isolated using the absolute values of wear edge location taken from the modified CAD model. Curves were fitted to both worn and unworn areas and wear value and wear values were extracted using trapezoidal integration as described in 3.5. Maximum linear penetration was also computed by finding the greatest magnitude of difference between these curves.

5.3.8 Three-Dimensional Volumetric Wear Measurement Study

A final study was performed to assess accuracy in the measurement of volumetric wear on the 3D printed component used in this study. To do this, all profiles on the component were exported at 0.1mm intervals with wear values calculated using the automatic wear edge detection method described in 3.4. Volumetric wear was then calculated using the method described in 3.6. All three curve fitting methods were again compared in this study. These volumetric wear values calculated were then compared to the absolute value of volumetric wear taken from the CAD data. Volumetric wear on the CAD model was assessed by measuring the difference in volume between the original unworn CAD model and the modified (worn) CAD model.

5.4 Results

5.4.1 CAD Model Accuracy

Two CAD models were compared in this study:

1. Manufacturer Supplied DePuy LCS CAD model
2. Micro-CT created CAD model as per 3.1.

Eight points corresponding to those shown in Figure 20 were used for comparison. Cartesian coordinates for each point were taken and the magnitude of difference between the two models was assessed. It was found that the maximum deviation found was approximately 0.05mm in all three directions.

5.4.2 Repeatability of Manual Wear Edge Location

A repeatability study was conducted to evaluate the repeatability of manual wear edge location selection. Wear edge location was selected based on a graphical representation of a curve. Three profiles were used for repeatability analysis, with six repeat measurements of two-dimensional wear value being taken. The results are shown below in Table 5.

Measurement Iteration	Profile 1 (mm^2)	Profile 5 (mm^2)	Profile 8 (mm^2)
1	0.18	17.86	9.26
2	0.18	17.76	9.18
3	0.13	17.86	9.20
4	0.18	17.66	9.15
5	0.19	17.58	9.17
6	0.17	17.77	9.21

Table 5 - Repeatability of Manual Wear Edge Location when measuring two-dimensional wear value

Repeatability was found to be excellent across all three profiles. Profile 1 (M=0.18, SD=0.02, Range = 0.05) showed the greatest repeatability, superior to Profile 8 (M=9.19, SD=0.04, Range = 0.11) and Profile 5 (M=17.75, SD=0.11, Range = 0.28). Table 5 represents wear area measurements taken using smoothing spline curve fitting. The range given in the above statements refers to the full variation range of measurement values taken for each profile.

5.4.3 Accuracy of Wear Edge Location Techniques

The effectiveness of manual and automatic wear edge detection methods has been benchmarked against absolute wear edge locations extracted from Solidworks CAD software. Unworn profiles were excluded from this analysis due to the absence of a wear edge on these profiles. For 6 worn profiles, the X-position of wear edge location was taken using manual and automatic wear edge detection techniques using the mean, variance and linear settings discussed in 3.4. This is shown in the histogram in Figure 33.

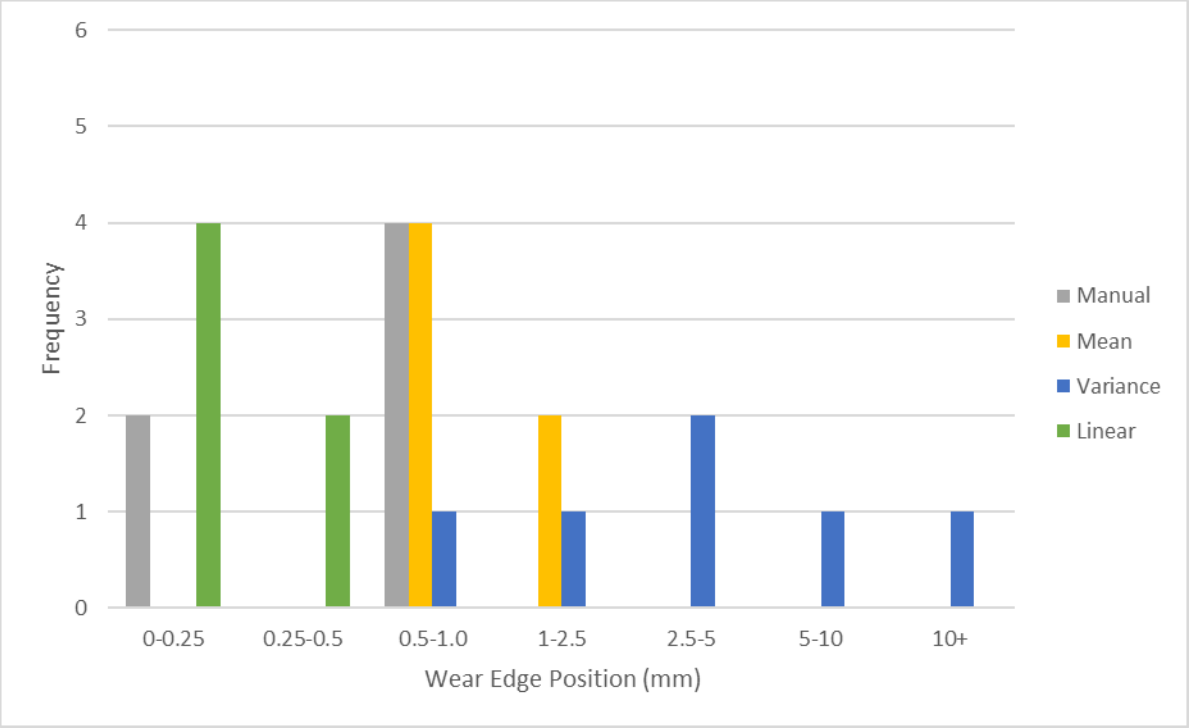

Figure 33 - Histogram showing error in wear edge location position for different wear edge location methods.

Figure 33 shows that the *variance* automatic wear edge detection showed the greatest difference, whilst *linear* automatic wear edge detection in wear edge location when compared to the absolute values. Average values for x-position shift are shown below in Table 6.

Method	Average Deviation (mm)
Manual	0.55
Mean	1.16
Variance	4.74
Linear	0.20

Table 6 - Comparison of average x-position deviation for different wear edge detection methods

Linear automatic wear edge detection displayed the lowest average deviation in x-position from the absolute wear edge location, with an average deviation of 0.2mm. This method of automatic wear edge detection was therefore used in all future studies.

Wear edge location position error was then analysed in the context of sectional wear value analysis. Absolute wear edge location position was input, and curve fitting was performed using cubic interpolation to worn and unworn areas. Wear edge location was then changed to reflect the wear edge position found using automatic

wear edge detection and performed computationally using Solidworks software. The results of this study are summarised in Table 7.

	Absolute Wear Edge Location	Automatic Wear Edge Location (Absolute + 0.2mm)
Profile	Wear Value (mm^2)	Wear Value (mm^2)
1	0.00	0.00
2	0.00	0.00
3	7.68	7.75
4	13.57	13.52
5	17.60	17.66
6	17.17	17.11
7	14.91	15.03
8	8.46	8.44
9	0.00	0.00
10	0.00	0.00

Table 7 - Effect of wear edge location variation on wear value

For profiles 1,2 9 and 10, no wear edge was found using the automatic wear edge location method. This would be expected as these profiles are entirely unworn. This shows that the automatic wear edge detection method does not find wear edges in unworn areas.

A paired t-test was conducted to search for statistically significant differences in wear value between the two methods. No significant difference was found between wear values using the absolute wear edge location (M=7.94, SD=7.53) and wear values found using the automatic wear edge location (M=7.95, SD=7.55), t(9)=-0.681, p=0.513. Wear edge location taken using automatic wear edge detection methods does not lead to significantly different results when compared to absolute wear edge location. The maximum error found equated to 0.12mm^2.

5.4.4 Accuracy of Curve Fitting Techniques

Three curve fitting techniques were trialled in this study: smoothing spline, cubic interpolation, and polynomial fitting (2nd order). Absolute wear edge positions were used to remove the effect of automatic wear edge detection and to isolate errors related to curve fitting. Unworn profiles were again excluded from analysis due to the lack of a wear edge location.

Results for the three curve fitting techniques are shown in Table 8, Table 9 and Table 10.

	Smoothing Spline			
	Wear Value		Maximum Linear Penetration	
Profile	Absolute (mm^2)	Fitted (mm^2)	Absolute (mm)	Fitted (mm)
3	7.68	8.97	0.68	0.99
4	13.57	15.07	1.57	1.56
5	17.60	18.57	2.27	2.81
6	17.17	18.04	2.13	2.49
7	14.91	16.03	2.04	2.37
8	8.46	9.08	0.98	1.26

Table 8 - Wear Value and Maximum Linear Penetration using Smoothing Spline Fitting.

	Cubic Interpolation			
	Wear Value		Maximum Linear Penetration	
Profile	Absolute (mm^2)	Fitted (mm^2)	Absolute (mm)	Fitted (mm)
3	7.68	8.18	0.68	0.81
4	13.57	13.67	1.57	1.33
5	17.60	17.86	2.27	2.54
6	17.17	17.60	2.13	2.50
7	14.91	15.04	2.04	2.33
8	8.46	8.84	0.98	1.45

Table 9 - Wear Value and Maximum Linear Penetration using Cubic Interpolation.

	2nd Order Polynomial			
	Wear Value		Maximum Linear Penetration	
Profile	Absolute (mm^2)	Fitted (mm^2)	Absolute (mm)	Fitted (mm)
3	7.68	8.10	0.68	0.89
4	13.57	16.98	1.57	2.00
5	17.60	17.65	2.27	2.38
6	17.17	17.88	2.13	2.56
7	14.91	13.96	2.04	2.41
8	8.46	9.47	0.98	1.37

Table 10 – Wear Value and Maximum Linear Penetration using 2nd Order Polynomial Fitting.

To assess for statistical significance, paired t-tests were conducted comparing Wear Value and Maximum Linear Penetration for the three methods with the absolute values. The results of this are summarised in Table 11.

Comparison	t-value	Significance (p)
Smoothing Spline Wear Value	-8.325	0.000
Smoothing Spline Linear Penetration	-4.148	0.009
Cubic Interpolate Wear Value	-4.492	0.006
Cubic Interpolation Linear Penetration	-2.108	0.089
Polynomial Fitting Wear Value	-1.302	0.250
Polynomial Fitting Linear Penetration	-5.979	0.002

Table 11 - Paired t-test results comparing curve fitting methods to absolute values.

As shown in Table 11 statistically significant difference was found in some situations.

1. Absolute (M=13.23mm^2, SD=4.27 mm^2) vs Smoothing Spline Wear Value (M=14.29mm^2, SD=4.28mm^2)
2. Absolute (M=1.61mm, SD=0.66mm) vs Smoothing Spline Linear Penetration (M=1.91mm, SD=0.30mm)
3. Absolute (M=13.23mm^2, SD=4.27mm^2) vs Cubic Interpolation Wear Value (M=13.23mm^2, SD=4.20mm^2)
4. Absolute (M=1.61mm, SD=0.66mm) vs Cubic Interpolation Linear Penetration (M=1.83mm, SD=0.73mm)
5. Absolute (M=13.23mm^2, SD=4.27mm^2) vs Polynomial Fitting Wear Value (M=14.01mm^2, SD=4.30mm^2)
6. Absolute (M=1.61mm, SD=0.66mm) vs Polynomial Fitting Linear Penetration (M=1.94mm, SD=0.67mm)

These statistical tests suggest a statistically significant difference between two-dimensional absolute wear values and two-dimensional absolute wear values calculated using the curve fitting techniques in most cases. A non-significant difference was found when comparing linear penetration results using cubic interpolation and also wear value results when using polynomial fitting. . All methods appear to slightly overestimate both wear value and linear penetration when compared to the absolute values.

Direct comparison between the methods to consider their deviation from the absolute values was then conducted. The average difference between absolute and fitted values are shown in Table 12.

	Average Difference (Wear Value,mm^2)	Average Difference (Linear Penetration, mm)
Smoothing Spline	1.06	0.30
Cubic Interpolation	0.30	0.22
2nd Order Polynomial	0.78	0.32

Table 12 - Average Difference in wear value and linear penetration found using different curve fitting techniques.

As shown, cubic interpolation shows the smallest deviation from the absolute values for both wear value and maximum linear penetration.

5.4.5 Measurement of Three-Dimensional Volumetric Wear

A full cohort of two-dimensional profiles was used to calculate volumetric wear on the 3D printed component used in this study. Absolute values of volumetric wear can be calculated as the volume reduction caused by the application of artificial wear to the unworn CAD model. The spatial volume of the LCS component was measured as 24925.18mm^3 before the application of artificial wear. Following application of the artificial wear, this reduced to 24,673.38mm^3, corresponding to a wear volume of 252.80mm^3. This wear volume is higher than the wear volume typically observed in simulated components, but within the range of that found in retrieved components, as discussed in 2.3.

Automatic wear edge detection in a *linear* setting was used as suggested in 5.4.3, and curve fitting was performed using all three methods discussed in 5.4.4. Volumetric wear found using each method are shown in Table 13.

	Wear Volume (mm^3)
Smoothing Spline	262.34
Cubic Interpolation	257.09
2nd Order Polynomial	270.79
Absolute	252.80

Table 13 - Volumetric wear results calculated using varying curve fitting methods.

All three curve fitting methods slightly overestimated the wear volume on the 3D printed component compared to the absolute value. All three methods found volumetric wear values within 7% (2nd Order Polynomial) of the absolute value, with Smoothing Spline (3.7%) and Cubic Interpolation (1.7%) displaying better results. The magnitude of difference between absolute values and each curve-fitting method is shown below in Table 14.

	Difference (mm^3)
Smoothing Spline	-9.54
Cubic Interpolation	-4.29
2nd Order Polynomial	-17.99

Table 14 - Difference in Volumetric wear for different curve fitting methods

5.5 Discussion and Outcomes

The studies performed in this chapter were multi-faceted analyses of the effectiveness of the method discussed in Chapter 3, The accuracy of CAD model creation, wear edge detection and curve fitting techniques were all studied. Application of this method to both two and three-dimensional wear analysis was also performed.

5.5.1 CAD Model Accuracy

The creation of a TKR CAD model using the Micro-CT method developed in 3.1 has been shown in 5.4.1 to produce an accurate representation of the TKR component. It was found that a maximum positional error of 0.05mm was found in locating feature positioning on the surface of the component. This provides important validation of the Micro-CT method described in 3.1 and ensures that CMM alignment to be performed in future studies will utilise an accurate CAD representation of the component.

5.5.1 Wear Edge Detection Techniques

With a clear definition of the wear edge detection method achieved, the final part of this study was focused on analysing the advantage of different curve fitting techniques, namely the use of a smoothing spline, cubic interpolation, or a second-order polynomial. As the data in 5.3.2 shows, the 10 profiles used throughout this study were again used in this part of the study. Wear Value and Linear Penetration for all 10 profiles was calculated using all three curve fitting techniques, and the results were compared back to the computationally calculated values.

When comparing the x coordinate of wear edge position selected using automatic wear edge detection in a *linear* configuration, it was found that the maximum error in location equated to 0.2mm, providing more accurate results than the two other automatic fitting methods, as well as displaying improvement in wear edge location accuracy compared to the manual method, such as the method used by Knowlton (Knowlton & Wimmer, 2012).

This error in positioning was then applied across a two-dimensional profile and integration was performed to calculate a wear value. No significant difference was found between wear values calculated using automatic wear edge detection when compared to the absolute location of the wear edge, with a maximum error between profiles found to be 0.12mm^2. For this reason, it is suggested that using automatic edge detection by

the methods described in this study provides accurate results for the calculation of wear across a two-dimensional profile.

5.5.2 Curve Fitting Methods

This study has evaluated three different curve fitting methods for the assessment of two-dimensional wear on TKR components (smoothing spline interpolation, cubic interpolation, and second-order polynomial fitting). Absolute values for both wear value and maximum linear penetration were compared to those results found across a series of profiles using the three methods. Significant differences were found in several situations. It was found that second-order polynomial fitting wear value results were not significantly different to the absolute values. It was also found the cubic interpolation maximum linear penetration values were not significantly different to the absolute values.

However, the use of all three curve fitting methods produced wear values that correlated excellently to absolute values when Pearson's product-moment correlation coefficient was computed.

Each method of curve fitting appeared to produce better results when comparing different factors. None of the three curve fitting methods appeared to show a significant advantage when compared to the other two methods. For this reason, it was considered appropriate to retain all methods as options and apply these to a study representing clinical wear, this will be discussed in Chapter 6.

5.5.3 Application to Three-Dimensional Analysis

The method developed in this research was also applied in this study as a method of calculating volumetric wear. The results found for volumetric wear corresponded well with the absolute value acquired computationally for all three curve fitting techniques, with each method producing results within 7% of the absolute value, with the most accurate results produced using cubic interpolation. The accuracy of volumetric wear calculation will be further explored and quantified through application to larger studies of clinically relevant components.

5.6 Summary & Context

This study aimed to provide validation for elements of the method developed in Chapter 3, including Micro-CT CAD model creation, automatic wear edge location and curve-fitting methods.

The artificial wear scar used in this study was designed to be simple and easily quantifiable using SolidWorks software. This size of the wear scar was created to be representative of the wear scar found on a wear-simulated DePuy LCS component based on visual inspection. The geometry within the wear area represented the interaction of the articular surface with a spherical item of diameter equivalent to the size of a DePuy LCS femoral component (approximately 35.5.mm), although no further constraints were applied to ensure clinical relevance. Application of this method to a cohort of wear-simulated and retrieved components would further validate the method.

CAD model accuracy was validated using a study comparing a Micro-CT created CAD model to a manufacturer supplied CAD model. The Micro-CT CAD model was found to provide a high level of accuracy when compared to the manufacturer-supplied model, with less than 0.05mm of positional change.

It has been shown in this study that the application of automatic wear edge location can be used to accurately locate wear edges. To do this, locations of wear edges found using automatic wear edge location were compared to absolute positions taken from a CAD model, with less than 0.2mm of difference in x-position found between these wear edges. This translated to a maximum error of $0.12mm^2$ on a typical two-dimensional profile.

Curve fitting method comparison of smoothing spline interpolation, cubic interpolation and polynomial fitting was also performed in this chapter. Whilst statistically significant differences were found between absolute wear values and measured wear values, it was found that values calculated using curve fitting techniques showed an excellent correlation with those found from CAD. No single method displayed substantial benefits when compared to the other two methods. For this reason, all three curve fitting methods are to be further trialled in another study.

Finally, a calculation of the volumetric wear on the 3D printed component was performed. A wear volume was calculated computationally and taken to be an absolute value. Wear volumes were subsequently calculated using the three different curve fitting methods and compared to this exact value. It was found that the wear volume of the component was approximated by all three methods, again with 7% of the exact value. Cubic interpolation was found to produce the most accurate results of the three methods.

The results shown in this study provide validation of the Micro-CT and automatic wear edge detection methods described in 3.1 and 3.4, respectively. Further analysis is required to validate the accuracy of curve fitting techniques and to determine the optimum method of curve fitting to use. Likewise, the application of this three-dimensional volumetric measurement method to a cohort of clinically relevant components would aid the validation of this method.

Chapter 6 – Measurement of Volumetric Wear on Wear Simulated TKR components

6.1 Study Aims and Objectives

The study detailed in this chapter aims to apply the methods described in Chapter 3 to a cohort of wear-simulated TKR components.

The major aims of this study can be summarised as follows:

- To use the method developed in Chapter 3 to calculate volumetric wear on a cohort of TKR components.
- Following the study in 5.4, to evaluate the accuracy of different curve fitting techniques.

6.2 Study Design

A cohort of 6 TKR components of DePuy Low Contact Stress (LCS) design, a cruciate-retaining type TKR prosthesis, was used in this study. The components included a stabilising peg for use with a tibial tray and were of a mobile bearing type. The components were manufactured from GUR1040 UHMWPE.

6.2.1 Gravimetric Measurement

Wear simulation was performed on the components at DePuy Ltd. between 2003 and 2007 by Dr Paul Bills and was performed as per the requirements of ISO14243-1. Components were loaded at a 60:40 medial-lateral bias, as is typically found clinically. Refreshment of lubrication was performed at 0.2 million cycle intervals. All components underwent a total of 4.95 million cycles of wear simulation and were measured using a microbalance with an accuracy of 0.1mg. Gravimetric measurements were taken at pre-defined intervals approximately equal to every 0.5 million cycles. Only measurements taken at the end of simulator testing were relevant to this study.

6.2.2 CMM Measurement

An LCS component was digitized using Micro-CT and a surface model recreated using Geomagic software. This CAD model was the same CAD model used in the study in 5.4.1, where the accuracy of this CAD model was validated against an unworn manufacturer supplied CAD model.

Component alignment was performed using the points previously detailed and measurement data acquired as per the method detailed in 3.2. Post-measurement processing and wear calculation was conducted as per the procedure detailed in 3.3-3.6. Wear edge detection was performed using automatic wear edge detection as

validated in 5.4.3. Smoothing spline interpolation, cubic interpolation and second order polynomial curve fitting techniques were all used to calculate volumetric wear for these components.

Three repeat measurements were taken non-consecutively, with component alignment performed between each measurement. Measurements were performed over several weeks based on machine availability. No notable change in ambient conditions within the measurement environment was recorded during this duration. Stylus requalification occurred at each measurement session, but not between individual measurements. The CMM did not undergo routine servicing or calibration between any of the measurements taken.

6.2.3 Effect of Profile Spacing

Before the commencement of the volumetric wear calculation process, a study was performed to evaluate the effect of profile spacing taken from CATIA on the calculated wear volume. Profile spacing was varied between 1mm and 0.05mm to consider the optimum profile spacing to provide accurate wear measurement results. A smaller spacing would theoretically correlate to a more accurate approximation of the wear value.

However, decreasing the spacing from say 0.25mm to 0.05mm involves the creation and analysis of five times as many profiles, increasing the required analysis time and computational power. This study assesses the value at which there is no significant accuracy improvement resulting from reducing profile spacing.

6.3 Results

6.3.1 Effect of Profile Spacing on Measurement Results

This study was conducted to determine the optimum value to define profile spacing from CATIA software. To study the effect of profile spacing on wear value a single component measurement, in this case, defined as LCS-1-Right, was used and the profile separation value was varied between 0.05mm and 1.0mm. This was done in intervals of 0.1mm in the region 0.5mm < d < 1.0mm and 0.05mm in the region 0.05mm < d < 0.5mm. Cubic interpolation was used as the method of curve fitting in this study.

Table 15 displays the results that were attained from using different profile sizes. As shown, there was a range of 2.07mm^3 between the largest and smallest wear volume results recorded. It was found that in general wear value reduced with a corresponding decrease in profile spacing.

Profile Spacing (mm)	Wear Volume (mm^3)
1	20.84
0.9	20.41
0.8	20.26
0.7	19.85
0.6	19.66
0.5	19.45
0.45	19.44
0.4	19.41
0.35	19.39
0.3	19.25
0.25	19.16
0.2	19.02
0.15	19.02
0.1	18.95
0.05	18.94

Table 15 - Effect of Profile Spacing on Volumetric Wear

This information is displayed graphically in Figure 34. This displays the decreasing trend of wear values as profile spacing is reduced. It can be seen that a lower amount of fluctuation occurs for profile separation values below 0.1mm.

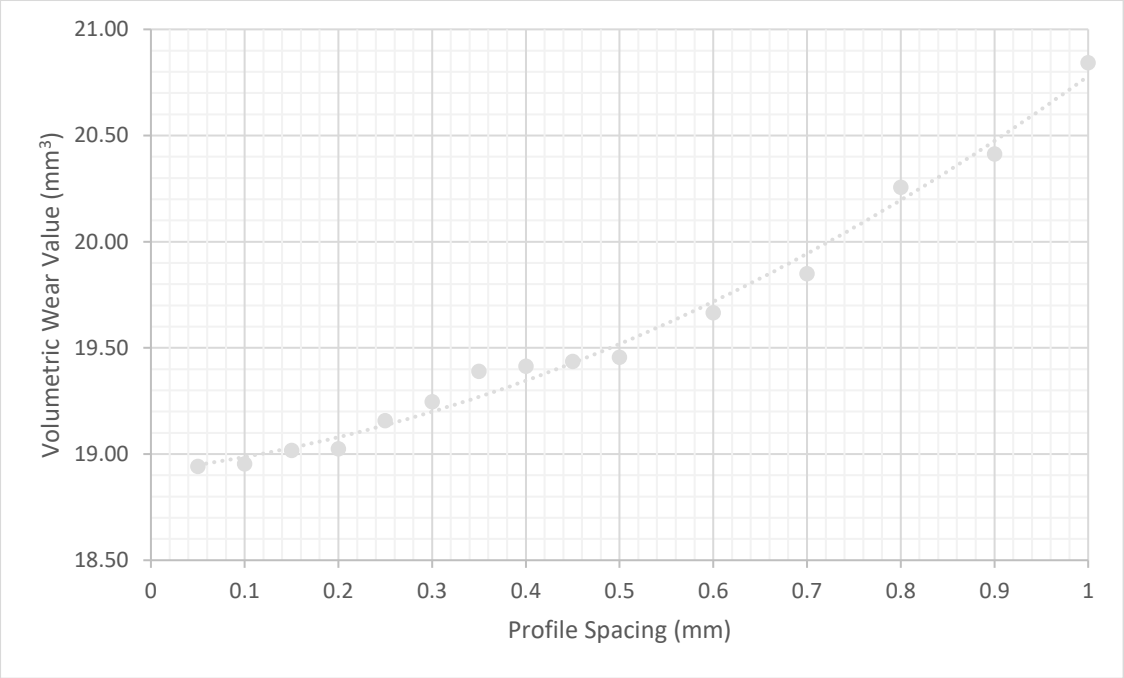

Figure 34 - Graphical Representation of Effect of Profile Spacing on Volumetric Wear

6.3.2 Gravimetric Measurement Results

Gravimetric wear results acquired are shown in Table 16.

	Total Wear (mm^3)
LCS1	30.90
LCS2	26.70
LCS3	46.10
LCS4	43.70
LCS5	30.10
LCS6	43.60

Table 16 - Volumetric Wear results gained using Gravimetric Measurement.

Further analysis of these results will be carried out later in this chapter to consider the accuracy of the method developed in this research. These measurements represent the average of three repeated measurements of each component (LCS1-LCS6) using an identical method. The difference in volumetric wear between components is likely a result of simulator station variation and differing input conditions.

6.3.2 Measurement of Volumetric Wear on LCS components using Cubic Interpolation.

This section and the two subsequent sections present results related to the analysis of wear volume using three different curve fitting techniques. Each section will introduce the results gained from the three repeat measurements of 6 LCS components, and consider the variation across the three measurements. Comparison to Gravimetric results will not take place in this section of the thesis.

The results gained from CMM measurement followed by curve fitting using cubic interpolation are detailed in Table 17.

	Measurement A			Measurement B			Measurement C		
	Left (mm^3)	Right (mm^3)	Total Wear (mm^3)	Left (mm^3)	Right (mm^3)	Total Wear (mm^3)	Left (mm^3)	Right (mm^3)	Total Wear (mm^3)
LCS1	12.73	18.93	**31.66**	13.56	18.94	**32.51**	12.11	20.01	**32.13**
LCS2	15.76	15.87	**31.62**	16.87	17.56	**34.43**	17.84	14.44	**32.28**
LCS3	18.90	22.25	**41.15**	17.05	23.00	**40.05**	18.17	24.00	**42.17**
LCS4	17.57	24.64	**42.21**	19.57	26.48	**46.05**	18.65	26.74	**45.40**
LCS5	15.84	18.63	**34.47**	13.69	13.44	**27.12**	13.70	16.89	**30.59**
LCS6	19.57	24.70	**44.26**	21.69	20.08	**41.76**	20.54	25.00	**45.54**

Table 17 - Results gained from CMM measurement of wear-simulated LCS components, curve fitting performed using cubic interpolation.

As shown, calculated wear volumes in this portion of the study ranged from a minimum of $27.12mm^3$ for LCS5 in measurement B to a maximum of $46.05mm^3$ for LCS4, also in measurement B. Of the 18 measurements taken, volumetric wear was greater in 15 cases (83%) on the right condyle of the component, with the average

left-right bias being 45.1:54.9. The smallest recorded wear volume on a single condyle was 12.11mm^3 (LCS1-Left-C) with the maximum being 26.74mm^3 (LCS4-Right-C). Table 18 shows the standard deviation between the three measurements conducted for each component.

	Average Total (mm^3)	Standard Deviation (mm^3)	Range (mm^3)
LCS1	32.10	0.42	0.84
LCS2	32.78	1.47	2.81
LCS3	41.12	1.06	2.12
LCS4	44.55	2.06	3.84
LCS5	30.73	3.68	7.35
LCS6	43.86	1.92	3.78

Table 18 - Average Volumetric Wear, Standard Deviation and Range of measurements taken using CMM of wear-simulated LCS components, fitting performed using cubic interpolation.

As shown, the maximum variation in measurement was 7.35mm^3 although most measurements were within 3.9mm^3 of other measurement repetitions. The standard deviation of measurements was found to range from 0.42 – 3.67 mm^3. Using the number of component cycles, the volumetric wear rate ranges from between 5.42mm^3/million cycles to 9.21mm^3 per million cycles.

6.3.3 Measurement of Volumetric Wear on LCS components using Smoothing Spline curve fitting.

This section details the results gained from the measurement of wear-simulated components followed by curve fitting performed using smoothing spline fitting, resulting in volumetric wear calculation.

Table 19 contains the volumetric wear results that were gained from the CMM measurement of the wear-simulated components.

	Measurement A			Measurement B			Measurement C		
	Left (mm^3)	Right (mm^3)	Total Wear (mm^3)	Left (mm^3)	Right (mm^3)	Total Wear (mm^3)	Left (mm^3)	Right (mm^3)	Total Wear (mm^3)
LCS1	12.56	19.54	**32.09**	13.57	19.54	**33.11**	12.06	19.02	**31.08**
LCS2	16.44	16.46	**32.89**	15.94	18.58	**34.51**	16.73	19.00	**35.73**
LCS3	24.51	24.10	**48.61**	19.07	21.65	**40.71**	19.06	28.69	**47.74**
LCS4	17.90	23.97	**41.87**	21.67	24.47	**46.14**	18.26	23.99	**42.24**
LCS5	13.27	10.45	**23.71**	14.58	16.54	**31.12**	16.57	17.00	**33.58**
LCS6	20.57	25.69	**46.25**	19.69	21.46	**41.14**	26.98	22.99	**49.96**

Table 19 - Results gained from CMM measurement of wear-simulated LCS components, curve fitting performed using smoothing splines.

As shown, calculated volumetric wear ranges from 23.71mm^3 for measurement A of LCS5 to 49.96mm^3 for LCS6 in measurement C. Volumetric wear was found to be higher in the right condyle of components in 15 of 18 (83%) of measurements, with the average left-right bias being 46.1:53.9. The maximum individual condylar wear volume recorded was 28.69mm^3 (LCS3-Right-C) with the minimum individual value being 10.45mm^3 (LCS5-Right-A). Table 20 shows the average volumetric wear, standard deviation and range of measurements taken in this portion of the study using smoothing spline fitting.

	Average Total (mm^3)	Standard Deviation (mm^3)	Range (mm^3)
LCS1	32.09	1.01	2.03
LCS2	34.38	1.42	2.84
LCS3	45.69	4.33	7.90
LCS4	43.42	2.37	4.27
LCS5	29.47	5.13	9.86
LCS6	45.79	4.43	8.82

Table 20 - Average Volumetric Wear, Standard Deviation and Range of measurements taken using CMM of wear-simulated LCS components, fitting performed using smoothing spline fitting.

As shown, the maximum variation in measurement equated to 9.86mm^3 (LCS5), although the remaining components were shown to be closer with values ranging by less than 8.82mm^3. The standard deviation was found to range between 1.01 and 5.13. Volumetric wear rates calculated were between 4.74mm^3/million cycles and 9.99mm^3/million cycles.

6.3.4 Measurement of Volumetric Wear on LCS components using Second-Order Polynomial Fitting

This section considers the measurement of volumetric wear in the same way as previous sections, however, curve fitting resulting in volumetric values was conducted using second-order polynomial fitting. The results gained from this section of the study are shown in Table 21.

	Measurement A			Measurement B			Measurement C		
	Left (mm^3)	Right (mm^3)	Total Wear (mm^3)	Left (mm^3)	Right (mm^3)	Total Wear (mm^3)	Left (mm^3)	Right (mm^3)	Total Wear (mm^3)
LCS1	14.69	20.65	**35.34**	18.57	19.24	**37.80**	9.99	18.35	**28.34**
LCS2	18.56	19.57	**38.13**	18.31	20.33	**38.64**	16.57	16.90	**33.47**
LCS3	25.56	30.48	**56.04**	14.36	22.87	**37.23**	21.87	26.49	**48.36**
LCS4	19.59	26.58	**46.17**	23.68	30.69	**54.37**	20.87	24.87	**45.75**
LCS5	14.68	16.83	**31.52**	12.90	20.53	**33.43**	16.70	18.06	**34.75**
LCS6	22.77	28.87	**51.64**	23.79	21.01	**44.80**	22.00	29.87	**51.87**

Table 21 - Results gained from CMM measurement of wear-simulated LCS components, curve fitting performed using second-order polynomial fitting.

As shown in Table 21 there was a great range in volumetric wear calculated, ranging from 28.33mm^3 for LCS1 in Measurement C to 56.04mm^3 for LCS3 in measurement A. It was found that the right condyle of components exhibited greater volumetric wear in 17 of 18 situations (94%), with the average left-right bias being 44.9:55.1. The maximum wear for an individual condylar surface was measured as 30.69mm^3 (LCS4-Right-B) with the lower individual value being 6.99mm^3 (LCS1-Left-C). Results for the range and standard deviation of these results are shown in Table 22.

	Average Total (mm^3)	Standard Deviation (mm^3)	Range (mm^3)
LCS1	33.83	4.91	9.46
LCS2	36.75	2.85	5.17
LCS3	47.21	9.46	18.81
LCS4	48.76	4.86	8.63
LCS5	33.23	1.63	3.24
LCS6	49.44	4.02	7.07

Table 22 – Average Volumetric Wear, Standard Deviation and Range of measurements taken using CMM of wear-simulated LCS components, fitting performed using second order polynomial fitting.

The maximum variation in a single component was 18.81mm^3, with other measurements falling below 9.46mm^3. Standard deviation was found to vary between 1.62 and 9.46, with an average standard deviation of 4.62. Volumetric wear rates ranged between 5.67mm^3/million cycles and 11.21mm^3/million cycles.

6.3.5 Statistical Analysis of Volumetric Wear Results

6.3.5.1 Inter-Measurement Variability

Three measurement iterations were conducted for using each curve fitting method. When using Cubic Interpolation, no statistically significant difference was found between repeat measurement iterations, as determined by one way ANOVA $F(2,15)=0.03$, $p=0.964$. Likewise, one way ANOVA determined there was no statistically significant difference found between repeat measurement iterations when using Smoothing Spline Interpolation $F(2,15)=0.18$, $p=0.834$. Finally, one way ANOVA determined that there was no statistically significant difference between repeat measures in the case of second-order polynomial fitting; $F(2,15)=0.152$, $p=0.86$. It was found there was no statistically significant difference between volumetric wear results gained across repeat measurements.

6.3.5.2 Variability in Curve Fitting Method

One-way ANOVA was conducted to assess whether different methods of curve fitting produce significantly different volumetric wear measurement results. No statistically significant difference was found between the

curve-fitting methods; F(2,51)=1.429, p=0.249. There is no statistically significant difference in wear volume found using different curve fitting techniques.

6.3.5.3 Comparison of CMM Measurement results to Gravimetric Measurement results

Paired t-tests were conducted to compare wear measurement results gained using each fitting method to results acquired using gravimetric measurement.

No significant difference was found when comparing volumetric wear results gained using Cubic Interpolation (M=37.52mm^3, SD=6.33mm^3) to volumetric wear results gained using Gravimetric Measurement (M=36.85 mm^3, SD=8.51mm^3); t(5)=-0.470, p=0.658. There is no significant difference between CMM and Gravimetric volumetric wear results when using Cubic Interpolation curve fitting.

No significant difference was found when comparing volumetric wear results gained using Smoothing Spline Interpolation(M=38.47mm^3, SD=7.33mm^3) to volumetric wear results gained using Gravimetric Measurement (M=36.85mm^3, SD=8.51mm^3); t(5)=-1.257, p=0.264. There is no significant difference between CMM and Gravimetric volumetric wear results when using Smoothing Spline curve fitting.

A significant difference was found when comparing volumetric wear results gained using Second-Order Polynomial Fitting (M=41.54mm^3, SD=7.72mm^3) to volumetric wear results gained using Gravimetric Measurement (M=36.85mm^3, SD=8.51mm^3); t(5)=-3.685, p=0.014. There is a significant difference between CMM and Gravimetric volumetric wear results when using Second-Order Polynomial curve fitting.

Pearson's Product Moment Correlation coefficients between volumetric wear results and gravimetric wear results were also calculated. Significant strong correlation was found between Gravimetric measurement and Cubic Interpolation (r(6)=0.930, p=0.007), Smoothing Spline Interpolation (r(6)=0.931, p=0.007) and Second-Order Polynomial Curve Fitting (r(6)=0.931, p=0.007). A graphical representation of the relationship between Gravimetric measurement and the three curve fitting methods is shown in Figure 35.

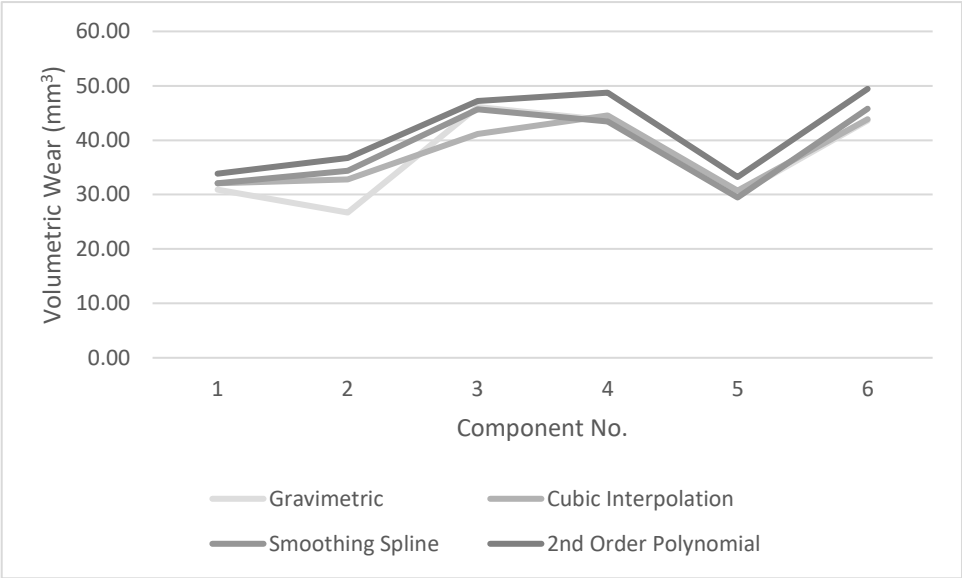

Figure 35 - Graphical Representation of Correlation between Measurement Methods

The total difference between Gravimetric measurement and each measurement method can be calculated to determine which method most closely approximates Gravimetric measurement. These results are shown in Table 23.

	Cubic Interpolation (mm^3)	Smoothing Spline (mm^3)	2nd Order Polynomial (mm^3)
Sum of Error	4.03	9.74	28.12
Sum of Absolute Error	18.02	22.12	56.24

Table 23 - Sum of Difference/Absolute Difference between Gravimetric Measurement and Volumetric wear values acquired using Curve Fitting Techniques

Table 23 shows that the use of Cubic Interpolation most closely approximates Gravimetric measurement when the sum and absolute sum of error is taken. Using the absolute sum as an additional measure counteracts the effect of negative results. Second-order polynomial fitting consistently displays a less accurate approximation of Gravimetric measurement results.

The average volumetric wear rate was also calculated for each component, based on 4.95 million cycles of testing. These results are shown in Table 24.

Gravimetric (mm^3/1 x 10^6 cycles)	Cubic Interpolation (mm^3/1 x 10^6 cycles)	Smoothing Spline (mm^3/1 x 10^6 cycles)	2nd Order Polynomial (mm^3/1 x 10^6 cycles)
6.24	6.48	6.48	6.83
5.39	6.62	6.94	7.42
9.31	8.31	9.23	9.54
8.83	9.00	8.77	9.85
6.08	6.21	5.95	6.71
8.81	8.86	9.25	9.99

Table 24 - Volumetric wear rates found using Gravimetric measurement and Curve Fitting Methods

Paired t-tests were not performed for this data, as the volumetric wear rate was purely calculated as a scalar of the total volumetric wear, and therefore t-test results would be virtually identical.

Bland-Altman plots were constructed to visually assess variation between Gravimetric Measurement and the curve fitting techniques. These plots are shown in

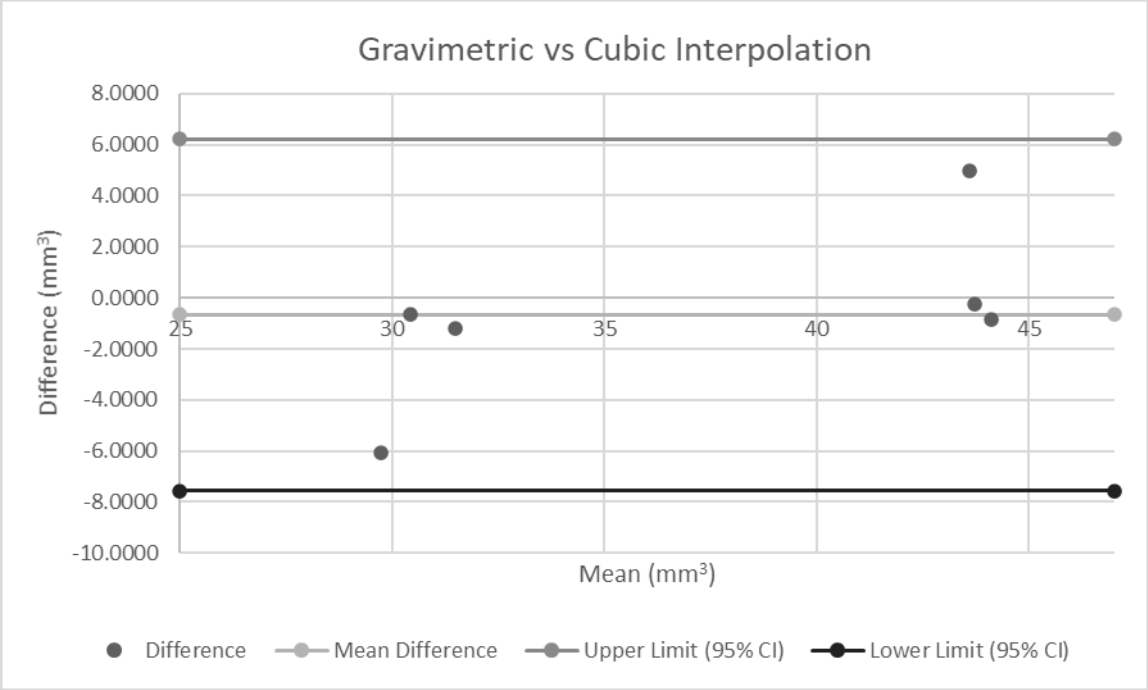

Figure 36 - Bland-Altman Plot for Gravimetric Measurement Volumetric Wear vs Cubic Interpolation Volumetric Wear

Figure 36 displays a Bland-Altman plot for the volumetric wear results acquired using Cubic Interpolation when compared to Gravimetric results. The average difference between methods was found to be 0.67mm^3, with the limits of agreement having a spacing of 13.76mm^3. There is no noticeable increase in variability with an increase in volumetric wear.

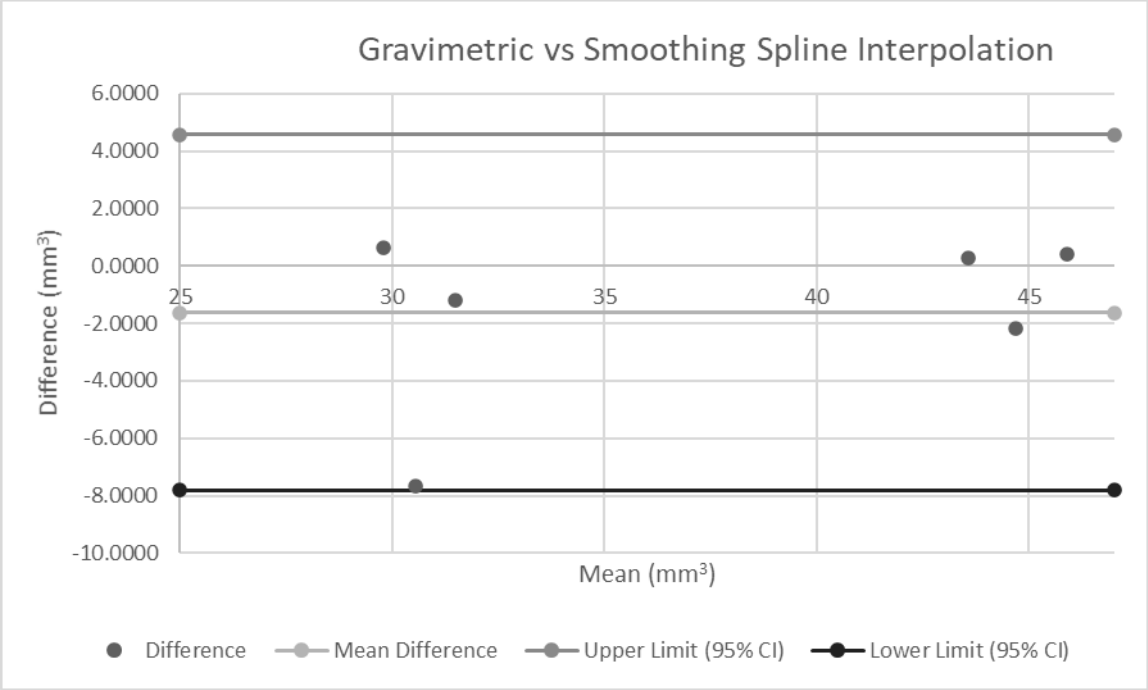

Figure 37 - Bland-Altman Plot for Gravimetric Measurement Volumetric Wear vs Smoothing Spline Interpolation Volumetric Wear

Figure 37 displays a Bland-Altman plot for the volumetric wear results acquired using Smoothing Spline Interpolation when compared to Gravimetric results. The average difference between methods was found to be 1.62mm^3, with the limits of agreement having a spacing of 12.40mm^3. There is no noticeable increase in variability with an increase in volumetric wear.

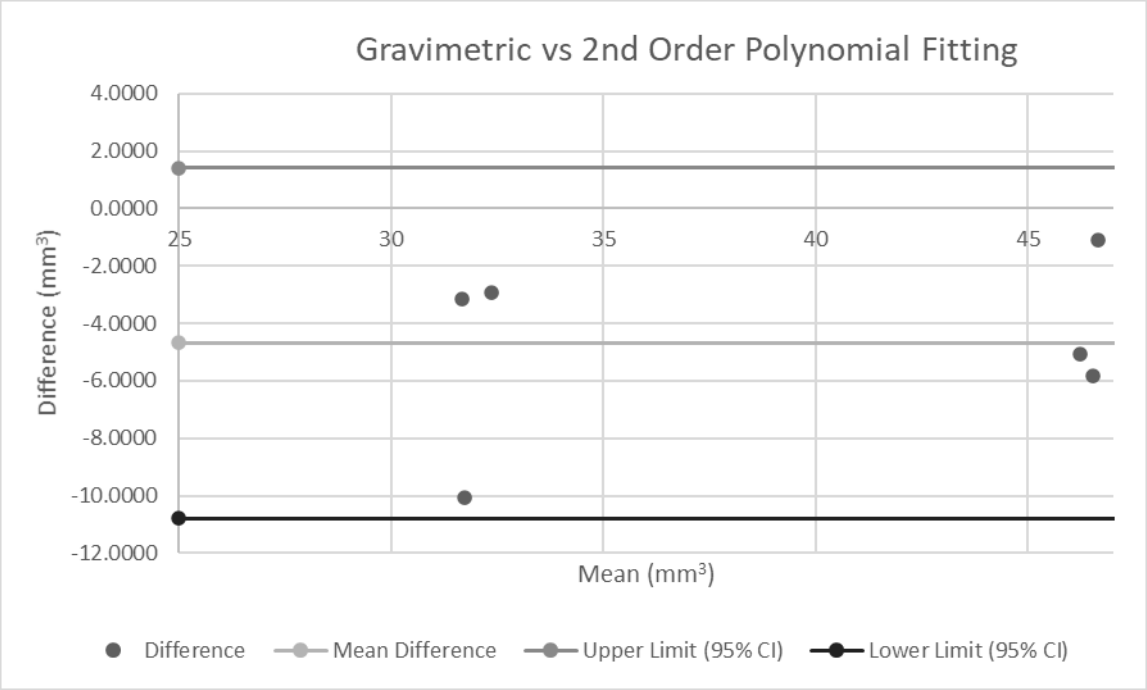

Figure 38 - *Bland-Altman Plot for Gravimetric Measurement Volumetric Wear vs 2nd Order Polynomial Fitting Volumetric Wear*

Figure *38* displays a Bland-Altman plot for the volumetric wear results acquired using Second-Order Polynomial fitting when compared to Gravimetric results. The average difference between methods was found to be 4.69mm^3, with the limits of agreement having a spacing of 12.21mm^3. There is no noticeable increase in variability with an increase in volumetric wear.

All three Bland-Altman plots show that all measured results fall within the 95% confidence limits for each measurement method. This suggests a good agreement between gravimetric measurement and all three curve fitting methods. The components used in this study can be seen to represent two different levels of volumetric wear, these being approximately 30-35mm^3 and 40-50mm^3. These two clusters of data generally showed good agreement, with larger wear volumes typically showing a smaller spread of difference when compared to those with smaller wear volumes.

All three methods produce large 95% confidence intervals equating to approximately a third of the measurement volumes. This suggests that more research should be conducted to draw tangible conclusions from the Bland-Altman diagram. Increasing the sample size by measuring a greater number of components would provide this further rationale.

6.4 Discussion and Outcomes

6.4.1 Evaluation of Profile Spacing

Based on the study described in 6.3.1, it has been shown that there is no advantage in using a profile spacing of less than 0.1mm for volumetric wear analysis. This compares well to the point spacing used by Jiang in modern CMM volumetric wear studies (W. Jiang et al., 2018). As previously mentioned, older studies used much larger point spacings of up to 0.75mm (P. Bills et al., 2005; Blunt, Bills, & Jiang, 2008; Knowlton & Wimmer, 2012; Muratoglu, Perinchief, et al., 2003), but these studies were likely limited by computational power. From the findings in this study, a point spacing of 0.1mm will be used in future studies applying this method.

6.4.2 Inter-Measurement Variability

It was found that there was no statistically significant difference in volumetric wear across 18 repeat measurements using different curve fitting techniques. This shows that the CMM measurement method and subsequent post-processing produces consistent results.

Total values for volumetric wear ranged from 23.71mm^3 (LCS5-A-Smoothing Spline) to 56.04mm^3 (LCS3-A-Polynomial). This equates to wear rates of between 4.80mm^3 and 11.32mm^3. This falls within the range of typical volumetric wear rates found in 2.3.1 for wear simulated components, 2.3mm^3/1 x 10^6 cycles and 34.3 mm^3/1 x 10^6 cycles. Components undergoing 4.95 x 10^6 cycles of simulator testing would be expected to have total volumetric wear amounting to between 11.39mm^3 and 169.79mm^3. Variation between components is likely to be a result of different simulation conditions, these conditions are not known for the components studied.

The TKR components in this study underwent loading in a 60:40 medial-lateral configuration. It was found that volumetric wear on the measured components was recorded at an average bias of approximately 55:45 across all components, with the maximum skew of bias being 65:35. Histograms are shown in Figure 39 and Figure 40 which show this skew, with the Right condyle typically showing greater than 50% total volumetric wear, and the Left condyles showing less than 50% total volumetric wear.

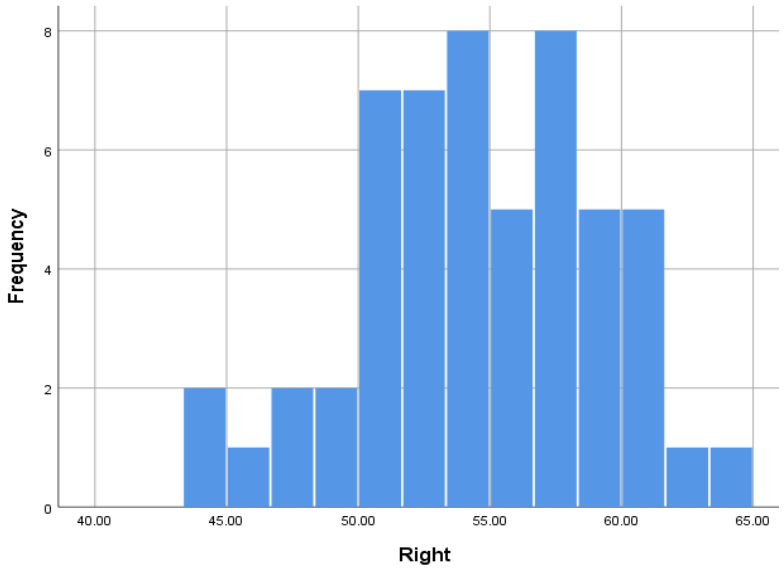

Figure 39 - Histogram Displaying Skew in Medial-Lateral Wear Volumes for Right Condyle

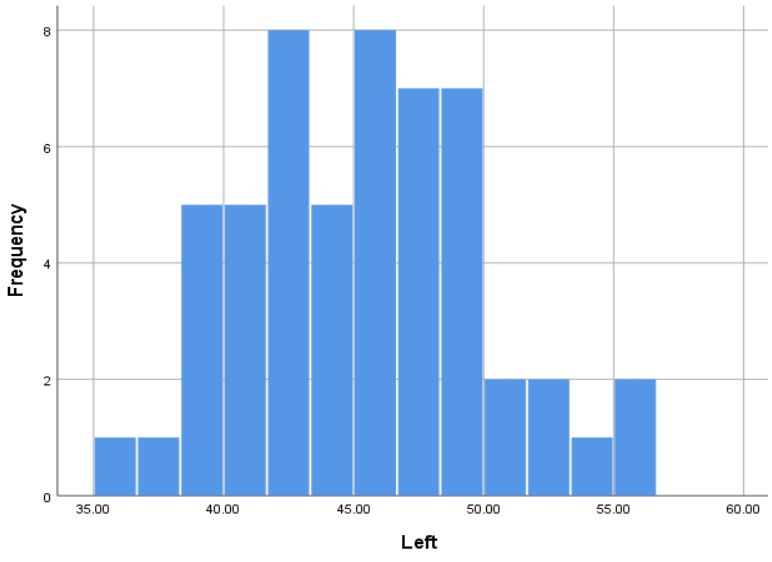

Figure 40 - Histogram Displaying Skew in Medial-Lateral Wear Volumes for Left Condyle

A paired t-test was conducted and significant differences were found in the proportion of volumetric wear found on the Left (M=45.34, SD=4.57) and Right (M=54.65, SD=4.57) condyles of the components studied in this chapter; t(54)=7.47, p=0.001. There is a significant difference in the proportion of volumetric wear attributed to each condyle. These results show that the volumetric wear results gained in this study correlate well with patterns of wear that would be expected given knowledge of simulation testing patterns.

6.4.3 Curve Fitting Techniques

Three curve fitting techniques were used in this study: cubic interpolation, smoothing spline interpolation and second-order polynomial fitting. All three curve fitting techniques were investigated in this study due to a lack of advantage found in the study detailed in Chapter 5.

This study found no statistically significant difference between volumetric wear results produced using all three methods. The magnitude of standard deviation represents the spread or variation within a dataset, therefore a method showing lower standard deviation would be considered to show more consistent results.

Cubic interpolation was found to present the lowest average value of standard deviation (SD=1.77mm^3) with smoothing spline interpolation (SD=3.12mm^3) and Second-order polynomial fitting (SD=4.62mm^3) displaying higher values, suggesting that cubic interpolation curve fitting provides more consistent measurements of volumetric wear when compared to other methods. This hypothesis was further supported when comparing the range between highest and lowest values found across repeat measurements; cubic interpolation = 3.46mm^3, smoothing spline Interpolation = 5.95mm^3 and second-order polynomial fitting = 8.73mm^3. This suggests less variation in measurement when using cubic interpolation curve fitting.

Gravimetric measurement was performed for the six components studied, with total volumetric wear found to be in the range of 26.7mm^3 to 46.10 mm^3, corresponding to a volumetric wear rate between 5.39mm^3/1 x 10^6 cycles and 8.81mm^3/1 x 10^6 cycles. These results compare favourably with the range of typical volumetric wear rates in simulated components found in 2.3.1.

When comparing average values of volumetric wear found using the three curve fitting methods using CMM measurement against gravimetric measurement, a statistically significant difference was found when using second-order polynomial curve fitting. This statistically significant difference suggests that second-order

polynomial fitting is not a suitable method to measure volumetric wear using the method developed in this research.

No significant difference was found between CMM and gravimetric measured volumetric wear when using either cubic interpolation or smoothing spline interpolation. This suggests that both methods provide results comparable with those found using the standardised Gravimetric measurement method. It has typically been found that CMM methods over-estimate volumetric wear when compared to the Gravimetric method. This was found when using both curve fitting methods, with cubic interpolation measurements being an average of 0.67mm^3 higher than gravimetric and smoothing spline interpolation measurement beings an average of 1.62mm^3 higher than gravimetric measurement results.

A t-test was found to test for significant differences arising from using either cubic interpolation or smoothing spline interpolation. No significant difference was found between cubic interpolation (M=37.52, SD=6.33) or smoothing spline interpolation (M=38.47, SD=7.33). There is no significant difference between results gained using either curve fitting method.

To reach a recommendation on the curve fitting method all of the above results can be considered. When compared to gravimetric measurement, there is no significant difference between the use of either method. There is also no significant difference between the use of either method when compared directly against each other. However, it has been shown that cubic interpolation typically provides more consistent results when considering the standard deviation and range of measurements taken. It has also been shown that cubic interpolation produces a typically smaller magnitude of variation from standardised gravimetric results. For this reason, cubic interpolation is recommended as the curve fitting method most appropriate to use in this research.

6.5 Summary and Limitations

Volumetric wear results found using CMM compare excellently with those found using Gravimetric measurement, with no statistically significant difference found between results. Volumetric wear found in this study also falls within the range of volumetric wear rates found in 2.3.1 that is typical of wear-simulated TKR components. Wear volume condylar bias was also found to be consistent with known loading patterns applied during simulation.

It has been shown in this chapter that the CMM measurement method can be applied to wear-simulated components and produce repeatable and accurate results when compared to results attained using the standardised Gravimetric method.

This study is limited by the sample size used for analysis (n=6), as well as the number of repeat measurements taken (n=3). The use of all results acquired has been used for statistical analysis, but this allows repeatability error to be included in significance tests. A more comprehensive test would provide a more comprehensive data set for subsequent analysis. The components studied also exhibited relatively low levels of wear. It would be advantageous to expand the method to include components exhibiting higher levels of wear to fully validate the method across a wider range of volumetric wear values.

Another potential source of error in the measurement of these components are potential issues arising from the length of time between component simulation and component measurement, such as oxidation of the material over time. Oxidation of UHMWPE has been shown in previous studies to adversely affect the success of components in TKR (Collier et al., 1996; Medel et al., 2011). Further studies have considered the effect of oxidation on the mechanical properties of UHMWPE. Although oxidation is shown to adversely affect the mechanical and physical properties of UHMWPE, no evidence is supplied that this affects the geometrical properties of a component (Saverio Affatato, Ruggiero, Jaber, Merola, & Bracco, 2018; C. J. Bell et al., 1998; Hsieh, Barrall, & Xu, 1992).

Chapter 7 – Measurement of Volumetric Wear on Retrieved TKR components

This chapter describes the results arising from applying the aforementioned methods to a cohort of retrieved Total Knee Replacement components. Retrieved describes TKR components that have been removed from service, generally due to either implant or patient failure. Occasionally implants may be retrieved, and a secondary procedure conducted for other reasons such as infection.

Retrieved components are invaluable for research purposes as they are the ideal opportunity to apply methodologies to real-world applications. Often it is the case that retrieved components are of an unknown design, meaning that gravimetric measurement cannot be performed. It is for this reason that methods that reconstruct unworn geometry are developed to be able to quantify wear on such components.

This study provides an ideal opportunity to apply the methods developed through previous chapters to a cohort of clinically relevant retrieved components, in a situation where zero pre-wear information is provided. The reconstruction of pre-wear geometry and subsequent wear volume calculation is a significant challenge in the evaluation of retrieved components, and previous chapters have shown that the method developed throughout this thesis provides accurate and repeatable results for the measurement of wear in this case.

7.1 Study Overview

To evaluate volumetric wear on retrieved TKR components, a cohort of 5 components was supplied by the London Implant Retrieval Centre (LIRC). Among the cohort of 5 components there appeared to be 3 different designs of TKR. Photos of all 5 components showing the variation in design are shown in Figure 41.

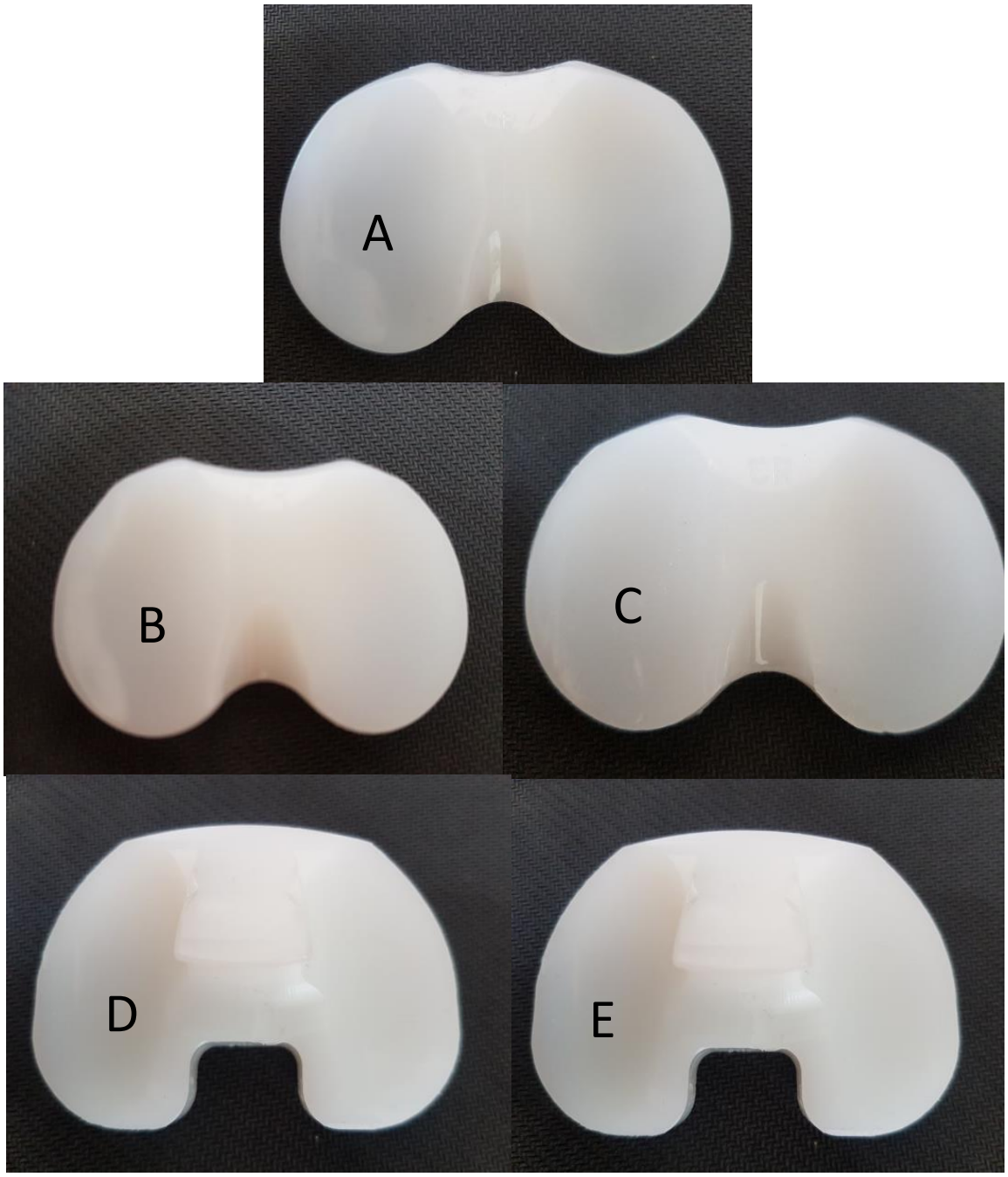

Figure 41 - Photos showing varied design cohort of retrieved TKR components.

As shown, the components displayed consist of both PS and CR type components and were of different sizes and types. All components exhibited significant visual wear on the articular surfaces, with components identified as Poly042 and Poly049 appearing to display particularly high visible wear. Table 25 shows the design and implantation time of all retrieved components. Note that Poly042 was of unknown design as supplied, however bears great resemblance to Poly031, so this component may also be a DePuy PFC Sigma component.

Component ID	Design	Implantation Time (years)	Reference
Poly031	DePuy PFC Sigma	1.25	D
Poly040	Biomet Vanguard	0.25	B
Poly041	Biomet Vanguard	3.25	C
Poly042	Unknown	4.25	E
Poly049	Biomet Vanguard	11.5	A

Table 25 - Representation of Manufacturer, Design and Implantation Time of Retrieved TKR components supplied by LIRC. Letters in reference column correspond to

7.2 Study Design

Digitisation of all 5 components was performed using the Micro-CT method described in Chapter 3. This resulted in the creation of 5 unique CAD models in ".STEP" format. Although multiple components in this study were of the same design, they appeared to be of different sizes and therefore would require a different CAD model to allow for accurate CMM alignment. Alignment on the CMM was performed in the same way as discussed in 3.3, with between 7 and 10 points used on the periphery of the component to perform the alignment. The number of alignment points is dependent on the number of visibly definable features on the component. All measurements were performed three times to assess for repeatability. Between measurements, the component was removed then replaced in the fixture, with alignment performed again.

Post-processing of the measurements taken was performed as per the method discussed in Chapter 3. Automatic wear edge detection was applied as recommended in Chapter 5, and curve fitting was performed using cubic interpolation, as recommended by Chapter 6.

As there is no pre-wear data available for this study, there is no definitive reference value of volumetric wear to compare the measured results to. For this reason, calculated results have been compared to quoted values from the literature for the volumetric wear of retrieved components to ascertain if the values measured are clinically representative.

Inter-variability between repeat measurements was assessed to consider the repeatability of measurement of volumetric wear on retrieved components. In addition to this, all components were scored as per the Hood damage score index (Hood et al., 1983) to provide a further comparison between volumetric wear rates, based on the approach by Knowlton (Knowlton & Wimmer, 2012).

7.3 Results

Table 26 shows the results gained from the volumetric wear calculation of the cohort of retrieved TKR components. As shown, the components generally displayed much greater levels of volumetric wear when compared to the wear-simulated components measured in Chapter 6.

	Left (mm^3)	Right (mm^3)	Total Wear (mm^3)	Left (mm^3)	Right (mm^3)	Total Wear (mm^3)	Left (mm^3)	Right (mm^3)	Total Wear (mm^3)
Poly031	22.45	30.65	53.11	20.59	32.88	53.47	20.87	33.60	54.47
Poly040	12.56	20.57	33.14	14.77	21.22	35.99	13.57	22.75	36.32
Poly041	30.46	45.67	76.13	40.57	35.85	76.42	38.90	47.99	86.89
Poly042	32.18	40.36	72.54	35.57	40.37	75.94	22.87	42.89	65.76
Poly049	54.75	86.45	141.21	40.57	76.46	117.03	60.77	75.90	136.67

Table 26 - Results of Volumetric Wear calculation on cohort of retrieved TKR components

The average value of wear volume alongside the range of wear volumes and standard deviation of data have been extracted from the data shown in Table 26 and are displayed in Table 27.

	Average (mm^3)	Range (mm^3)	Standard Deviation (mm^3)
Poly031	53.68	1.36	0.71
Poly040	35.15	3.19	1.75
Poly041	79.81	10.76	6.13
Poly042	71.41	10.18	5.18
Poly049	131.63	24.18	12.85

Table 27- Statistical Parameters calculated from Results showing Average, Range and Standard Deviation of retrieved TKR volumetric wear results.

Volumetric wear rates were also determined for these components based on the implantation times shown in Table 25, these are shown in Table 28.

	Wear Rate (mm^3/year)
Poly031	42.945
Poly040	140.593
Poly041	24.558
Poly042	16.803
Poly049	11.447

Table 28 - Wear Rates measured for Retrieved Components.

As well as measuring volumetric wear on the components, the components were damage scored based on the Hood score index described in 3.7.2 (Hood et al., 1983). The results of this are shown in Table 29.

As shown, all 5 components showed relatively low levels of surface damage when subjectively assessed. The maximum Hood score is 21, whilst the highest score found among the components studied in this research was 8. Generally, all components showed high levels of burnishing and abrasion, both mechanisms that would be expected from a TKR component post-wearing. No evidence was found of delamination or noticeable surface deformation, in any components assessed, nor was the presence of third body particles. Significant pitting was found in Poly040 which was not present in other components. It is important to note that the Hood score is a subjective scoring index and there may be inter-assessor variability in scoring. The use of such an index does however allow for a comparison between damage score and wear rate to be performed.

	Poly031	Poly040	Poly041	Poly042	Poly049
Burnishing	2	2	2	2	2
Scratching	2	2	2	1	1
Pitting	1	2	0	0	1
Deformation	0	0	0	0	0
Delamination	0	0	0	0	0
Abrasion	2	2	1	1	2
3rd Body Debris	0	0	0	0	0
Total Hood Score	**7**	**8**	**5**	**4**	**6**

Table 29 - Hood Damage Score values for retrieved TKR components.

A comparison between Hood Damage Score and Volumetric Wear Rate is shown in Figure 42. Pearson's product-moment correlation coefficient was computed to assess the relationship between Hood Damage Score and Volumetric Wear Rate for the retrieved TKR components. It was found that there was a strong

positive correlation between the two variables, r = 0.786, n = 5, p = 0.115, showing that components exhibiting greater visible damage also corresponded to increased wear rates.

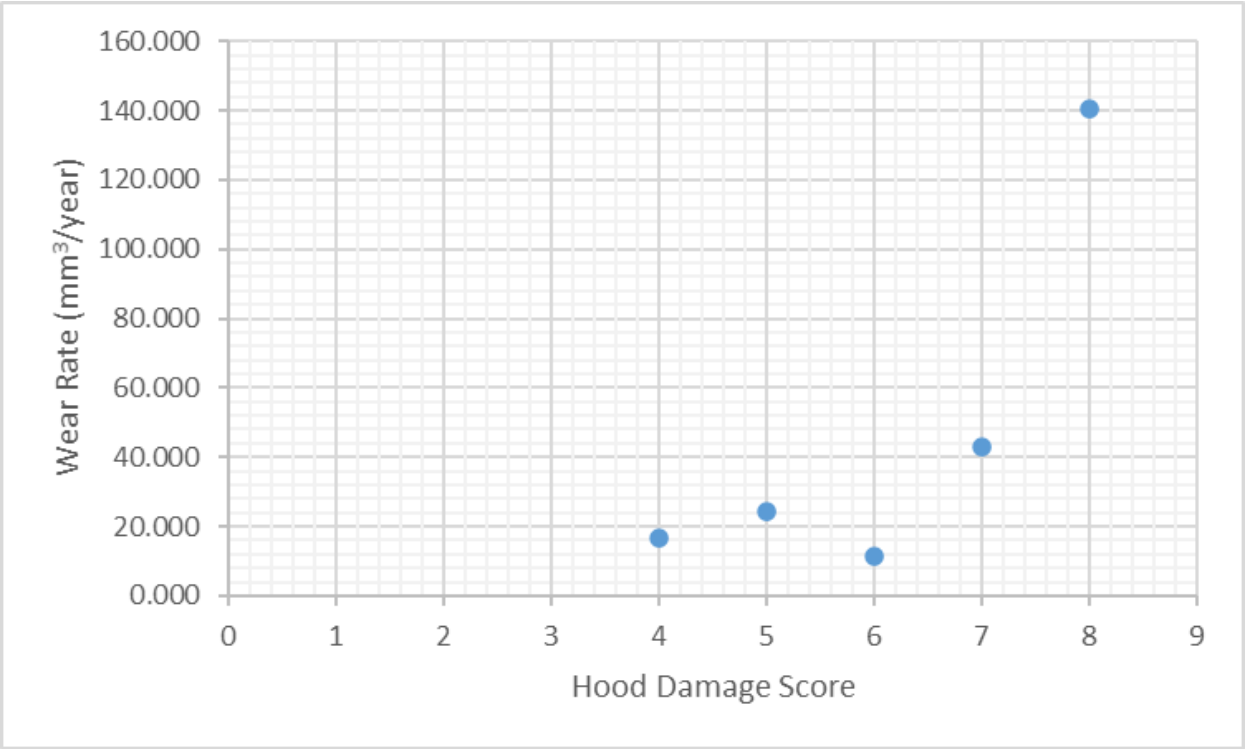

Figure 42 - Comparison between Hood Damage Score and Volumetric Wear Rate for Retrieved TKR components

7.4 Discussion

The previous section has discussed the results gained from the volumetric wear calculation of a cohort of retrieved components. As these are retrieved components of unknown design and origin, definitive volumetric wear values are unavailable for comparison. For this reason, a comparison to retrieved wear values reported in previous literature will be considered. Before this, a consideration of the repeatability of measurements taken will be discussed.

7.4.1 Repeatability of Volumetric Wear Measurements

Figure 43 shows a graphical representation of the variation in volumetric wear values calculated across repeat measurements for all five components. As shown, an increase in wear volume generally appeared to increase

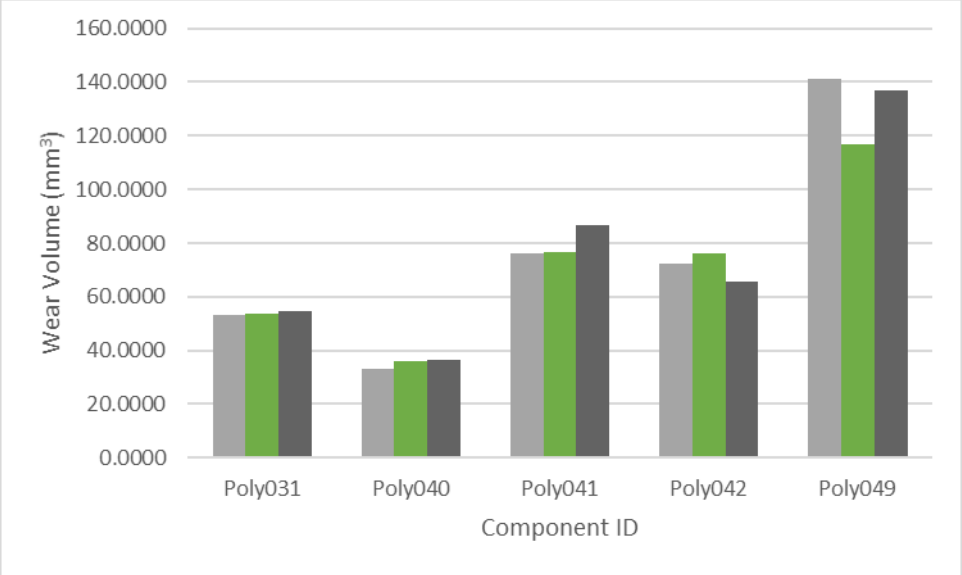

Figure 43 - Graphical representation of results shown in Table 26 showing variation of calculated wear values across repeat CMM measurements for a cohort of retrieved TKR components.

the variability within the dataset. Lower wear volumes such as those demonstrated by *Poly031* and *Poly040* appeared to show better repeatability between measurements.

7.4.2 Assessment of Validity of Results

As discussed in 3.5.2 volumetric wear rates found in the literature range from 1.0mm^3/year to 4542mm^3/year, with an average of 478.6mm^3/year. This is however highly skewed due to excessive wear measured in one study (Benjamin et al., 2001). The average with this study excluded gives an average volumetric wear rate for retrieved TKR components to be 28.5mm^3/year.

The components measured in this study found volumetric wear rates ranging from 11.447mm^3/year to 140.593mm^3/year. The average volumetric wear rate found in this study was 47.269mm^3/year. It is noticeable that Poly040 exhibited an incredibly high wear rate. This may indicate that this component suffered a significant early failure. All other components were implanted for a minimum of 15 months, although this is still a relatively short implantation time. When considering the four components with implantation times of at least 15 months, the average volumetric wear measured equates to 23.938mm^3/year, this compares well to the typical volumetric wear results found for retrieved components found in the literature.

It has been suggested that components typically experience “running-in” wear, meaning that wear rate is typically higher in the initial phase of a components service-life (Blunt, Bills, Jiang, et al., 2008). A Pearson product-moment correlation coefficient was computed to assess the relationship between Volumetric Wear Rate and Implantation Time for the retrieved TKR components. It was found that there was a moderately strong negative correlation between the two variables, r = -0.630, n = 5, p = 0.255. The correlation shows that a lower wear rate is typically associated with a greater implantation time, this is displayed graphically in Figure 44.

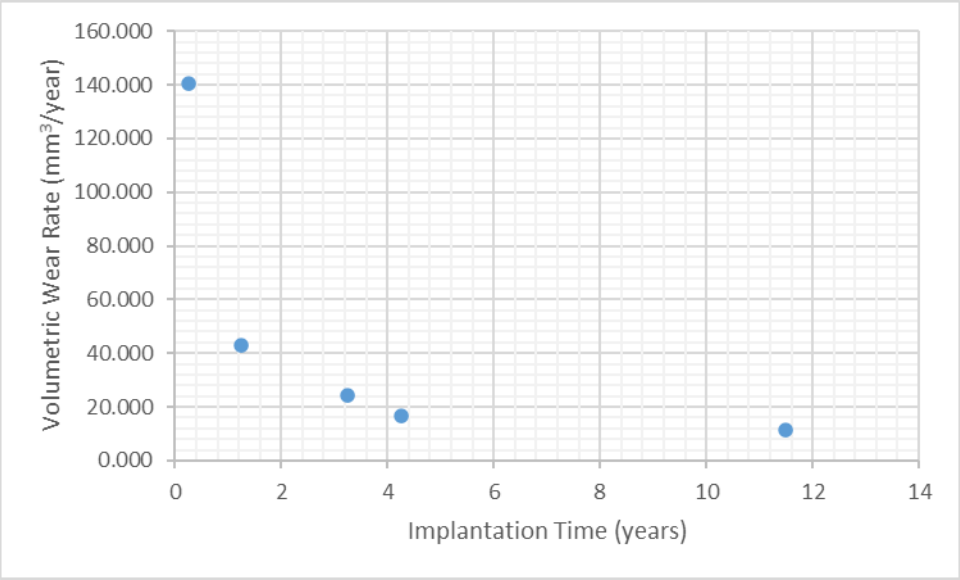

Figure 44 - Graphical representation of the relationship between implantation time and volumetric wear rate

A further consideration is the effect of uneven loading on volumetric wear measurement. As mentioned in Chapter 6, TKR components typically experience loading in a ratio of approximately 60:40 across medial-lateral condyles. For the results found in this study, it was found that the typical bias of volumetric wear was 58.9:41.1. This compares excellently with the typical loading ratios applied to components.

7.5 Summary & Context

The study performed in this chapter has provided a clinically relevant application of the method developed throughout this thesis. It has been found that when applied to a cohort of retrieved components with zero pre-wear information, the method developed can present results that are comparable to typical wear rates suggested in the relevant literature. A strong correlation was also found between surface damage and wear rates.

This study in the wider spectrum of the project provides an important verification of the method as it applies the method to a highly relevant application. The method developed aims to consider wear on components with zero pre-wear data, and whilst previous studies have had either computational or gravimetric comparison results, this study has no “gold-standard” results for comparison. The cohort size in this study is relatively small, and a further study on a greater cohort of retrieved components would provide a more intensive examination of the developed method.

Chapter 8 – Measurement of Volumetric Wear on Wear Simulated TAR Components

8.1 Study Overview

This chapter describes a study to consider the effectiveness of the method described in Chapter 3 when applied to a cohort of wear-simulated total ankle replacement components.

8.2 Study Design

Two cohorts of TAR components were used in this study. Cohort one was 8 BOX TAR components of an unidentified size (identified in this study as TAR_). These components were measured using CMM before the commencement of wear simulation using a TKR wear testing simulator at the University of Leeds Institute of Medical and Biological Engineering (iMBE). The initial proposal for this study was for components to be measured at 0.5 million cycle intervals. Unfortunately, this study did not come to fruition.

Cohort 2 consisted of 8 BOX TAR components, again supplied by iMBE, and will be designated 2a, 2b 2c referring to the type of curve fitting used. The components supplied were of varying size with four medium (identified as TARM_), and four of extra small size (identified as TARXS_). These components had undergone 5 million cycles of simulator wear testing using the TKR simulator. These components were of a different size to those supplied in Cohort 1. Components exhibited clear visual articular wear, with visually identifiable unworn portions at the lateral extremities of the components. One component in each size was fully unworn and used purely as a soak control (TARM4 and TARXS1). Volumetric wear calculation was applied to these components in the same way as all other components to assess for error in wear edge location and fitting technique.

CAD models were created for one component in Cohort 1 and one component of each size in Cohort 2 using the Micro-CT method described in 3.1. CMM measurement was performed using points shown in Figure 21. A single measurement was then performed to encompass the entire superior articular surface, as detailed in Chapter 3. Three repeat measurements were taken to assess repeatability. Components were removed from fixturing between measurement iterations and alignment performed each time. Before measurement, all components were cleaned using a cloth soaked in an isopropyl based cleaner.

Post-processing was performed as detailed in Chapter 3. FVM digitisation of the surface appeared to show that a consistent value of approximately 4% of the profile at the lateral extremities exhibited a clear wear edge. For this reason, 4% of each profile was assumed to be unworn, As previously stated, the central peak of each

profile was included in the unworn analysis to aid curve fitting. Both this 4% value and automatic wear edge location were used.

The exact curve fitting techniques used in Chapters 5-7 could not be applied to the measurements taken in this study, as the two-dimensional profile geometry of TAR components has a different shape to that of the TKR components. For this reason, three curve fitting methods were again analysed for this study: smoothing splines, cubic interpolation, and a fourth-order polynomial fit. Volumetric wear was calculated using the same methods described in Chapter 3. Gravimetric measurement results are not available for the components measured as part of Cohort 2 due to a lack of consistency in component identification during the simulation process.

8.3 Results

The results for this study will be reported segmentally, displaying the results for different fitting methodologies separately. Firstly, the results of measurements on unworn components will be reported, considering the measurement error of the method when applied to these components.

Following on from this, the study of worn TAR components will be discussed, considering results found using percentile and automatic wear edge location separately. These results will then be combined for statistical analysis.

8.3.1 Cohort 1 – Unworn TAR Components

This portion of the study concerns the measurement of a cohort of 8 unworn BOX TAR components. The measured value of volumetric wear on these components should be equal to zero. It follows that any volumetric wear found using the method in this research on these components is a contribution to error in overall measurement. Both percentile and automatic wear edge locations were applied in this study.

8.3.1.1 Percentile Wear Edge Location

Table 30 shows the results that were gained for the measurement of the cohort of unworn components using CMM.

	Cubic Interpolation (mm^3)	Smoothing Spline (mm^3)	4th Order Polynomial (mm^3)
TAR1	1.63	1.63	1.52
TAR2	1.43	1.86	2.24
TAR3	2.47	1.91	0.80
TAR4	0.73	1.35	2.24
TAR5	1.51	1.02	1.65
TAR6	0.96	2.20	1.00
TAR7	1.65	1.46	1.72
TAR8	1.75	2.27	2.03

Table 30 - Volumetric Wear results found for Unworn Components using Percentile Wear Edge Location

Table 31 shows the average, standard deviation, and range of these measurements on a component basis.

	Average (mm^3)	Standard Deviation (mm^3)	Range (mm^3)
TAR1	1.59	0.06	0.11
TAR2	1.84	0.41	0.81
TAR3	1.73	0.85	1.67
TAR4	1.44	0.76	1.51
TAR5	1.39	0.33	0.63
TAR6	1.39	0.70	1.24
TAR7	1.61	0.13	0.26
TAR8	2.02	0.26	0.52

Table 31 - Statistical data relating to wear volume results for the measurement of wear on unworn TAR components using CMM and a variety of fitting techniques.

As shown the average value of volumetric wear in the components ranged from 1.38mm^3 to 2.02mm^3, with an overall average of 1.62mm^3. This value of 1.62mm^3 represents the error present in the use of 4% percentile wear edge location along with the error in curve fitting methods.

8.3.1.2 Automatic Wear Edge Detection

When using automatic wear edge location, volumetric wear calculation failed for all eight components. Chronological analysis of the MATLAB processing script found that the *ischange* function failed to find wear edge locations in the case of all components.

8.3.2 Cohort 2a – Wear Simulated TAR components using Cubic Interpolation.

8.3.2.1 Percentile Wear Edge Location

Volumetric wear results found using percentile wear edge location and cubic interpolation curve fitting are shown in Table 32.

	Measurement A	Measurement B	Measurement C
	(mm^3)	(mm^3)	(mm^3)
TAR M1	85.71	83.98	81.10
TAR M2	75.51	76.83	74.48
TAR M3	77.01	75.04	74.63
TAR M4	1.37	0.54	0.84
TAR XS1	1.63	0.97	1.28
TAR XS2	71.70	73.53	76.03
TAR XS3	75.10	71.04	72.87
TAR XS4	65.04	62.34	60.09

Table 32- Results gained from volumetric wear calculation following CMM measurement of wear-simulated TAR components through the application of percentile wear edge detection and cubic interpolation.

Based on these results, statistical values such as average range and standard deviation can be calculated. These results are shown in Table 33.

	Average	Standard Deviation	Range
	(mm^3)	(mm^3)	(mm^3)
TAR M1	83.60	2.33	4.61
TAR M2	75.61	1.18	2.35
TAR M3	75.56	1.27	2.38
TAR M4	0.92	0.42	0.83
TAR XS1	1.29	0.33	0.66
TAR XS2	73.75	2.17	4.33
TAR XS3	73.00	2.03	4.06
TAR XS4	62.49	2.48	4.95

Table 33 - Statistical parameters for results gained from volumetric wear calculation following CMM measurement of wear-simulated TAR components using percentile wear edge location and cubic interpolation curve fitting.

As shown, a maximum range of approximately 4.95mm^3 was found between repeat measurements. For an unworn medium size component, the average value found was 0.92mm^3, with an extra small component being 1.29mm^3. Considering purely worn components, the average overall wear volume and range found are shown in Table 34 - Average Wear and Average Range found for Medium and Extra Small components across all components measured using percentile wear edge location and cubic interpolation curve fitting. Table 34.

		Cubic Interpolation
Medium	Average Wear (mm^3)	78.25
	Average Range(mm^3)	3.78
Extra-Small	Average Wear (mm^3)	69.75
	Average Range (mm^3)	4.45

Table 34 - Average Wear and Average Range found for Medium and Extra Small components across all components measured using percentile wear edge location and cubic interpolation curve fitting.

8.3.2.2 Automatic Wear Edge Detection

Volumetric wear results found using automatic wear edge location and cubic interpolation curve fitting are shown in Table 35.

	Measurement A (mm^3)	Measurement B (mm^3)	Measurement C (mm^3)
TAR M1	84.01	82.71	79.05
TAR M2	74.19	75.06	73.25
TAR M3	75.05	73.40	73.14
TAR M4	0.00	0.00	0.00
TAR XS1	0.00	0.00	0.00
TAR XS2	69.60	71.90	74.42
TAR XS3	73.30	69.53	71.75
TAR XS4	63.12	61.10	58.20

Table 35 - Results gained from volumetric wear calculation following CMM measurement of wear-simulated TAR components through the application of automatic wear edge detection and cubic interpolation.

Based on these results, statistical values such as average range and standard deviation can be calculated. These results are shown in Table 36.

	Average (mm^3)	Standard Deviation (mm^3)	Range (mm^3)
TAR M1	81.92	2.57	4.96
TAR M2	74.17	0.91	1.81
TAR M3	73.86	1.04	1.91
TAR M4	0.00	0.00	0.00
TAR XS1	0.00	0.00	0.00
TAR XS2	71.97	2.41	4.82
TAR XS3	71.52	1.89	3.77
TAR XS4	60.81	2.47	4.92

Table 36 - Statistical parameters for results gained from volumetric wear calculation following CMM measurement of wear-simulated TAR components using automatic wear edge location and cubic interpolation curve fitting.

As shown, a maximum range of approximately 4.96mm^3 was found between repeat measurements. For all unworn components, no volumetric wear was found. Considering purely worn components, the average overall wear volume and range found is shown in Table 37Table 37.

		Cubic Interpolation
Medium	Average Wear (mm^3)	76.65
	Average Range(mm^3)	3.70
Extra-Small	Average Wear (mm^3)	68.10
	Average Range (mm^3)	4.50

Table 37 - Average Wear and Average Range found for Medium and Extra Small components across all components measured using percentile wear edge location and cubic interpolation curve fitting.

8.3.3 Cohort 2b – Wear Simulated TAR components using Smoothing Spline Interpolation

8.3.3.1 Percentile Wear Edge Location

Volumetric wear results found using percentile wear edge location and smoothing spline interpolation curve fitting are shown in Table 38.

	Measurement A	Measurement B	Measurement C
	(mm^3)	(mm^3)	(mm^3)
TAR M1	84.70	87.69	85.61
TAR M2	78.40	77.64	77.00
TAR M3	75.36	79.34	79.90
TAR M4	1.97	3.08	0.94
TAR XS1	2.27	1.83	1.84
TAR XS2	67.94	65.02	64.91
TAR XS3	73.87	70.87	74.77
TAR XS4	64.23	68.47	69.10

Table 38 - Results gained from volumetric wear calculation following CMM measurement of wear-simulated TAR components through the application of percentile wear edge detection and smoothing spline interpolation.

Based on these results, statistical values such as average range and standard deviation can be calculated. These results are shown in Table 39.

	Average	Standard Deviation	Range
	(mm^3)	(mm^3)	(mm^3)
TAR M1	86.00	1.53	2.99
TAR M2	77.68	0.70	1.40
TAR M3	78.20	2.48	4.54
TAR M4	2.00	1.07	2.14
TAR XS1	1.98	0.25	0.44
TAR XS2	65.96	1.72	3.03
TAR XS3	73.17	2.04	3.90
TAR XS4	67.27	2.65	4.87

Table 39 - Statistical parameters for results gained from volumetric wear calculation following CMM measurement of wear-simulated TAR components using percentile wear edge location and smoothing spline interpolation curve fitting.

As shown, a maximum range of approximately 4.87mm^3 was found between repeat measurements. For an unworn medium size component, the average value found was 2mm^3, with an extra small component being 1.98mm^3. Considering purely worn components, the average overall wear volume and range found is shown in Table 40.

		Smoothing Spline
Medium	Average Wear (mm^3)	80.63
	Average Range(mm^3)	3.46
Extra-Small	Average Wear (mm^3)	68.80
	Average Range (mm^3)	3.93

Table 40 - Average Wear and Average Range found for Medium and Extra Small components across all components measured using percentile wear edge location and smoothing spline interpolation curve fitting.

8.3.3.2 Automatic Wear Edge Detection

Volumetric wear results found using automatic wear edge location and smoothing spline interpolation curve fitting are shown in Table 41.

	Measurement A	Measurement B	Measurement C
	(mm^3)	(mm^3)	(mm^3)
TAR M1	82.06	85.68	83.41
TAR M2	75.70	74.89	74.12
TAR M3	73.10	76.74	77.29
TAR M4	0.00	0.00	0.00
TAR XS1	0.00	0.00	0.00
TAR XS2	65.07	62.25	62.67
TAR XS3	71.12	68.33	72.37
TAR XS4	61.67	66.07	67.08

Table 41 - Results gained from volumetric wear calculation following CMM measurement of wear-simulated TAR components through the application of automatic wear edge detection and smoothing spline interpolation.

Based on these results, statistical values such as average range and standard deviation can be calculated.

These results are shown in Table 42.

	Average	Standard Deviation	Range
	(mm^3)	(mm^3)	(mm^3)
TAR M1	83.72	1.83	3.63
TAR M2	74.90	0.79	1.58
TAR M3	75.71	2.28	4.19
TAR M4	0.00	0.00	0.00
TAR XS1	0.00	0.00	0.00
TAR XS2	63.33	1.52	2.82
TAR XS3	70.61	2.07	4.03
TAR XS4	64.94	2.88	5.41

Table 42 - Statistical parameters for results gained from volumetric wear calculation following CMM measurement of wear-simulated TAR components using automatic wear edge location and smoothing spline interpolation curve fitting.

As shown, a maximum range of approximately 5.41mm^3 was found between repeat measurements. For all unworn components, no volumetric wear was found. Considering purely worn components, the average overall wear volume and range found is shown in Table 43.

		Smoothing Spline
Medium	Average Wear (mm^3)	78.11
	Average Range(mm^3)	3.61
Extra-Small	Average Wear (mm^3)	66.29
	Average Range (mm^3)	4.09

Table 43 - Average Wear and Average Range found for Medium and Extra Small components across all components measured using percentile wear edge location and smoothing spline interpolation curve fitting

8.3.4 Cohort 2c – Wear Simulated TAR components using Fourth-Order Polynomial Curve Fitting

8.3.4.1 Percentile Wear Edge Location

Volumetric wear results found using percentile wear edge location and smoothing spline interpolation curve fitting are shown in Table 44.

	Measurement A	Measurement B	Measurement C
	(mm^3)	(mm^3)	(mm^3)
TAR M1	90.96	94.73	92.00
TAR M2	78.00	76.68	70.47
TAR M3	78.57	72.44	81.04
TAR M4	3.05	2.48	2.76
TAR XS1	2.76	3.60	2.07
TAR XS2	74.04	73.12	69.69
TAR XS3	79.01	74.03	71.99
TAR XS4	63.00	60.00	64.30

Table 44 - Results gained from volumetric wear calculation following CMM measurement of wear-simulated TAR components through the application of percentile wear edge detection and Fourth-Order Polynomial Curve Fitting.

Based on these results, statistical values such as average range and standard deviation can be calculated. These results are shown in Table 45.

	Average	Standard Deviation	Range
	(mm^3)	(mm^3)	(mm^3)
TAR M1	92.56	1.95	3.77
TAR M2	75.05	4.02	7.53
TAR M3	77.35	4.43	8.60
TAR M4	2.76	0.29	0.57
TAR XS1	2.81	0.77	1.53
TAR XS2	72.28	2.29	4.35
TAR XS3	75.01	3.61	7.02
TAR XS4	62.43	2.21	4.30

Table 45 - Statistical parameters for results gained from volumetric wear calculation following CMM measurement of wear-simulated TAR components using percentile wear edge location and Fourth-Order Polynomial Curve Fitting.

		Polynomial
Medium	Average Wear (mm^3)	81.65
	Average Range(mm^3)	5.93
Extra-Small	Average Wear (mm^3)	69.91
	Average Range (mm^3)	5.22

Table 46 - Average Wear and Average Range found for Medium and Extra Small components across all components measured using percentile wear edge location and Fourth-Order Polynomial Curve Fitting.

As shown, a maximum range of approximately 8.60mm^3 was found between repeat measurements. For an unworn medium size component, the average value found was 2.76mm^3, with an extra small component being

2.81mm^3. Considering purely worn components, the average overall wear volume and range found is shown in Table 46.

8.3.4.2 Automatic Wear Edge Detection

Volumetric wear results found using automatic wear edge location and Fourth-Order Polynomial Curve Fitting are shown in Table 47.

	Measurement A	Measurement B	Measurement C
	(mm^3)	(mm^3)	(mm^3)
TAR M1	87.43	91.28	89.21
TAR M2	74.22	73.32	67.62
TAR M3	75.30	68.95	78.23
TAR M4	0.00	0.00	0.00
TAR XS1	0.00	0.00	0.00
TAR XS2	70.93	70.15	66.61
TAR XS3	76.18	70.63	68.23
TAR XS4	60.19	56.36	61.46

Table 47 - Results gained from volumetric wear calculation following CMM measurement of wear-simulated TAR components through the application of automatic wear edge detection and Fourth-Order Polynomial Curve Fitting.

Based on these results, statistical values such as average range and standard deviation can be calculated. These results are shown in Table 48.

	Average	Standard Deviation	Range
	(mm^3)	(mm^3)	(mm^3)
TAR M1	89.31	1.93	3.85
TAR M2	71.72	3.58	6.60
TAR M3	74.16	4.74	9.28
TAR M4	0.00	0.00	0.00
TAR XS1	0.00	0.00	0.00
TAR XS2	69.23	2.30	4.32
TAR XS3	71.68	4.08	7.95
TAR XS4	59.34	2.66	5.10

Table 48 - Statistical parameters for results gained from volumetric wear calculation following CMM measurement of wear-simulated TAR components using automatic wear edge location and Fourth-Order Polynomial Curve Fitting.

As shown, a maximum range of approximately 9.28mm^3 was found between repeat measurements. For all unworn components, no volumetric wear was found. Considering purely worn components, the average overall wear volume and range found is shown in Table 49.

		Polynomial
Medium	Average Wear (mm^3)	78.40
	Average Range(mm^3)	6.18
Extra-Small	Average Wear (mm^3)	66.75
	Average Range (mm^3)	5.79

Table 49 - Average Wear and Average Range found for Medium and Extra Small components across all components measured using percentile wear edge location and Fourth-Order Polynomial Curve Fitting.

8.3.5 Results Analysis

8.3.5.1 Wear Edge Location Method Comparison

Table 50 shows the average volumetric wear results that were found for each worn component in this study, split into different curve fitting methods and wear edge detection methods.

	Cubic Interpolation		Smoothing Spline		Fourth-Order Polynomial	
	4% (mm^3)	Automatic (mm^3)	4% (mm^3)	Automatic (mm^3)	4% (mm^3)	Automatic (mm^3)
TARM1	83.6	81.92	86	83.72	92.56	89.31
TARM2	75.61	74.17	77.68	74.9	75.05	71.72
TARM3	75.56	73.86	78.2	75.71	77.35	74.16
TARXS2	73.75	71.97	65.96	63.33	72.28	69.23
TARXS3	73	71.52	73.17	70.61	75.01	71.68
TARXS4	62.49	60.81	67.27	64.94	62.43	59.34

Table 50 - Average Volumetric wear found for each worn component using different curve fitting and wear edge detection methods

Paired t-tests were conducted to assess for variability between results gained using percentile wear edge detection and automatic wear edge detection.

When comparing results gained using cubic interpolation, a significant difference was found between volumetric wear results found for percentile (M=74, SD=6.79) and automatic (M=72.37, SD=6.80) wear edge fitting techniques, t(5)=29.546, p=0.001.

When comparing results gained using smoothing spline interpolation, a significant difference was found between volumetric wear results found for percentile (M=74.71, SD=7.52) and automatic (M=72.20, SD=7.57) wear edge fitting techniques, t(5)=32.84, p=0.001.

When comparing results gained using the second-order polynomial fitting, a significant difference was found between volumetric wear results found for percentile (M=75.78, SD=9.75) and automatic (M=72.37, SD=9.7) wear edge fitting techniques, t(5)=66.04, p=0.001.

These results show that significant differences were found when using different curve fitting techniques. The average magnitude difference was found to be 1.63mm^3 for cubic interpolation results, 2.51mm^3 for smoothing spline interpolation and 3.21mm^3 for fourth-order polynomial fitting.

As previously mentioned, no wear edge was found when using automatic wear edge detection for the unworn components, as would be expected. Using percentile wear edge location, the average volumetric wear found on unworn component, representing the error, was found to be 1.11mm^3 using cubic interpolation, 1.99mm^3 for smoothing spline interpolation and 2.79mm^3 for fourth-order polynomial fitting.

Assuming that error is carried across into worn components this would represent an overall difference in measurement between wear edge detection methods of 0.52mm^3 for both cubic interpolation and smoothing spline interpolation and 0.42mm^3 for fourth-order polynomial fitting.

8.3.5.2 Curve Fitting Method Comparison

Three curve fitting methods were used in this study. The average volumetric wear found across the three methods, using both wear edge detection methods was 73.19mm^3 for cubic interpolation, 73.46mm^3 for smoothing spline interpolation and 74.18mm^3 for fourth-order polynomial fitting. This represents an overall variability between curve fitting techniques of 0.99mm^3.

Repeatability within the use of a specific curve fitting method can be assessed by considering the range of measurements taken. Across both component sizes, when using 4% percentile fitting it was found that smoothing spline interpolation (R=3.69mm^3) provided a smaller range of values than cubic interpolation (R=4.11mm^3) and fourth-order polynomial fitting (R=5.58mm^3). This was also the case when using automatic wear edge detection, with smoothing spline interpolation (R=3.85mm^3) providing a smaller range of values than cubic interpolation (4.10mm^3) and fourth-order polynomial fitting (R=5.99mm^3).

8.4 Discussion

8.4.1 Evaluation of Wear Edge Detection and Curve-Fitting methods

As gravimetric measurements are not available for the results considered in this study it is not possible to directly compare volumetric wear results acquired to a "gold-standard" measurement practice. This also makes it difficult to assess the absolute accuracy of different wear edge detection or curve fitting methods. It is however possible to assess repeatability in measurement for different methods. It is also possible to compare volumetric wear results found to typical wear volumes found in the literature.

The results found for Cohort 1; a cohort of unworn components showed that error is present in the use of percentile wear edge location. This error was calculated to be 1.62mm^3. For these components, the volumetric wear found should equate to zero as no wear has occurred on the surface. When using automatic wear edge detection, no volumetric wear was found, as no wear edges were detected. This suggests that the automatic wear edge detection method is effective in distinguishing between profiles on which there is no wear, and those on which wear has occurred.

Cohort 2 also contained two components that could be considered unworn. When using percentile wear edge detection the average volumetric wear found ranged from 0.92mm^3 for medium components measured using cubic interpolation to 2.81mm^3 for extra small components measured using fourth-order polynomial curve-fitting, with an average error of 1.89mm^3 for medium components and 2.03mm^3 for extra small components. Again, the use of automatic wear edge detection failed to compute volumetric wear results due to the lack of a detected wear edge.

When comparing the volumetric wear results found for Cohort 2 across all curve fitting techniques it was found that the average difference between using percentile and automatic wear edge detection, ranged between 1.63mm^3 and 3.21mm^3. When the error found in unworn components was considered alongside this, the average difference between wear edge detection methods was found to range between 0.42mm^3 and 0.52mm^3. It was found that when considering average volumetric wear acquired using the two wear edge detection methods that there was a significant difference between percentile and automatic wear edge detection. It would be beneficial to expand this study to include a greater number of unworn components, as

well as to have gravimetric results for comparison to assess whether this unworn error is also present in volumetric wear measurements of worn components.

Three curve fitting methods were used in this study to calculate volumetric wear. As gravimetric measurement results are not available it is not possible to determine which method most accurately calculates volumetric wear. However, each method can be compared to the other methods, and variation in results can be assessed. Paired t-tests showed that there was no significant difference between results gained using all three curve fitting methods when using percentile wear edge location ($0.16 < p < 0.59$). Likewise, no significant difference was found between results gained using all three curve fitting methods when using automatic wear edge detection ($0.85 < p < 0.93$). It was found that smoothing spline interpolation typically produced more repeatable results for volumetric wear, evidenced by a smaller range of values found using both wear edge detection techniques. To be able to explicitly recommend a curve fitting method for use with TAR components it would be beneficial to use a computational method, similar to that in Chapter 5 to consider volumetric wear against a computational model. Another validation method would be the presence of gravimetric measurement data to act as a comparison. From the results found in this chapter, it would be advised to use all three curve fitting methods in a further study to be able to make an explicit recommendation on the optimum technique.

8.4.2 Comparison to Published Literature

In 2.5 it was found that wear-simulated TAR components display typical wear rates of between $1.2mm^3/1 \times 10^6$ cycles and $25.8mm^3/1 \times 10^6$ cycles, with a potential maximum of $33.8mm^3/1 \times 10^6$ cycles. All components in this study underwent five million cycles of simulator testing before measurement. Although these components underwent the same number of cycles, simulator stations often utilise different input conditions and variability between components would therefore be expected. To analyse wear rates for the results in this study, components have been split into medium and extra-small sizes.

For medium components, the maximum volumetric wear found was $92.56mm^3$, with a minimum of $71.72mm^3$. This equates to a wear rate between $14.34mm^3/1 \times 10^6$ cycles and $18.51mm^3/1 \times 10^6$ cycles. The average volumetric wear rate equates to $15.16mm^3/1 \times 10^6$ cycles.

For extra-small components, the maximum volumetric wear found was 75.01mm^3, with a minimum of 59.34mm^3. This equates to a wear rate between 11.87mm^3/1 x 10^6 cycles and 15mm^3/1 x 10^6 cycles. The average volumetric wear rate equates to 13.65mm^3/1 x 10^6 cycles.

As shown, wear rates found across all components fall approximately in the mid-range of typical values found for TAR components. Medium components typically experienced a greater volume of wear when compared to extra-small components, this would be expected due to the larger amount of geometry in contact during the wearing process.

8.4.3 Limitations of Study

The major limitation of this study is the lack of gravimetric data available for comparison to volumetric wear rates found using CMM measurement. The lack of gravimetric data means that statistical significance in the level of volumetric wear results cannot be assessed. Despite this, volumetric wear rates have been found which correlate well with typical values found in the literature.

The sample size used in this study is relatively small and would benefit from being increased. It would also be beneficial to apply this method to TAR components with a wider range of volumetric wear rates. All components used in this study demonstrated similar levels of volumetric wear and therefore the effect of applying the CMM method across a wide range of volumetric wear rates cannot be demonstrated.

8.5 Summary

The study described in this chapter has shown that the CMM method developed has measured volumetric wear rates comparable to those found typically for TAR components in literature for a cohort of wear-simulated TAR components.

The CMM method developed has been shown to provide consistent results using different wear edge detection and curve-fitting methods. The study would benefit from application to a larger cohort and comparison to results gained using gravimetric measurement to fully validate the accuracy of the developed method for TAR components.

Chapter 9 –Discussion and Statement of Novelty

This chapter presents a discussion of the studies that have been performed for this research project. A summary of results that have been gained as part of the studies performed will be presented, whilst the overall aim and objectives stated in Chapter 1 will be referred back to, assessing the success of this research.

The method developed in this project has been applied to several cohort studies on components exhibiting a wide range of designs, sizes, wear application methods and wear volumes. The method has been applied to two cohorts of total knee replacement components; one which had undergone simulated wear and one cohort of retrieved components of differing design. A cohort of total ankle replacement components was also studied.

The method developed in this research uses a combination of metrological equipment combined with mathematical analysis to calculate volumetric wear on the condylar articular surfaces of UHMWPE total joint replacement components. Micro-computed tomography has been used for the creation of CAD geometry that can be used for CMM alignment. A previous study by Jiang et al which performed autonomous wear volume calculation used a manufacturer supplied CAD model (W. Jiang et al., 2018). Manufactured TKR components are subject to form error which could lead to an unworn manufacturer supplied CAD model not providing an accurate representation of a component (Blunt, Bills, Jiang, et al., 2008). The use of a bespoke CAD model in this research represents a novel approach to component alignment using CMM for TKR and TAR wear measurement. The Micro-CT CAD creation process was shown to produce an accurate representation of a DePuy LCS component when compared to a manufacturer supplied component.

The Micro-CT to CMM method was further investigated during Chapter 5 in a study using a computationally simulated worn component. This computationally simulated model provided exact references for wear volume in both two and three-dimensional analyses. Application of the practical CMM method to a high-accuracy 3D printed version of this simulated worn component found that the method developed produced accurate and repeatable results for wear value across a two-dimensional profile. Volumetric wear results gained from this study were also found to provide accuracy to within 7% of exact wear volume. It must be noted that the simulated worn component created was designed for easily quantifiable geometry as opposed to being clinically relevant.

The CMM method was applied to two clinically relevant cohorts of TKR components in this research. The first was a cohort of wear-simulated components, for which results calculated using the standardised gravimetric

measurement method were readily available. It was found that the developed method produced volumetric wear measurement results that showed no statistically significant difference to gravimetric results. Volumetric wear results also showed excellent agreement with the medial-lateral loading ratio applied to the components during wear simulation.

The second cohort of TKR components on which the method was applied was a cohort of retrieved TKR components of different designs. As these components had been explanted, gravimetric measurement results were not available for these components. This is the case with all explanted components, which represent the most clinically relevant components on which volumetric wear needs to be studied. The method developed in this research requires zero pre-wear data to be able to calculate volumetric wear on TKR components.

With gravimetric results not available for analysis, comparisons were made between typical wear volumes found for explanted components in literature, as well as comparison to surface damage scores using the Hood damage score index (Hood et al., 1983). Volumetric wear rates found using the CMM method for the component studied were found to be consistent with volumetric wear rates found in the literature. An excellent positive correlation was also found between volumetric wear and damage score.

Several critical elements required exploration to create the method detailed in this research. The first of these is an accurate description of the location of a component wear edge. Numerous methods were trialled to distinguish between worn and unworn areas on a single component.

A study was performed in Chapter 4 which attempted to differentiate between worn and unworn areas using surface topographical parameters. Although statistically significant differences were found between worn and unworn areas, significant differences were also found between components of differing design, as well as between wear simulated and retrieved components. This concluded that there was not an exact range of surface topographical parameter values that could be used to definitively represent worn and unworn areas.

Micro-CT was also trialled as an unsuccessful wear edge location method. An automatic wear edge detection methodology was developed by detecting sudden changes in linear slope across a data set. Analysis of this automatic wear edge detection method in the Chapter 5 study found excellent agreement between the exact location of a wear edge and the location found using automatic wear edge detection. Likewise, automatic wear edge detection using the method developed was found to be superior to manual selection methods, such as

the method used by Knowlton (Knowlton & Wimmer, 2012). Previous studies have used unworn components (P. Bills et al., 2005; Blunt, Bills, Jiang, et al., 2008), manual methods (Knowlton & Wimmer, 2012) or a single numerical value (W. Jiang et al., 2018) to locate wear edges. The two-dimensional to three-dimensional method used in this study represents a novel approach for wear edge identification.

The use of different curve fitting methods was also explored during this research. With worn and unworn areas isolated, curve fitting was performed to each area to produce a worn area between these curves. The study in Chapter 6 found that the use of cubic interpolation and smoothing spline interpolation produced results showing no statistically significant difference to results gained used gravimetric measurement. Greater accuracy and repeatability in cubic interpolation curve fitting results led to the recommendation of cubic interpolation as the optimum curve fitting method for TKR components.

Jiang et al applied curve fitting techniques to volumetric wear calculation but only evaluated varying degrees of polynomial fitting (W. Jiang et al., 2018). Polynomial fitting methods are prone to accuracy deterioration when working outside measured data. This could produce issues in reconstructing the central unworn portion of the component, which is necessary for comparison against the measured worn data. Indeed, it was shown in all studies in this research that polynomial fitting showed less accurate and less reliable results when compared to two different spline fitting techniques.

This study represents the first application of a CMM reconstruction-based method that can be used to measure volumetric wear on total ankle replacement components. Although gravimetric measurement results were not available for the TAR components studied in Chapter 8, application of the method to such components found wear rates highly comparable with those found in the literature. This included the use of the automatic wear edge detection method developed in this research. Different curve fitting techniques were again used in Chapter 8 with smoothing spline interpolation generally showing the most repeatable results.

The overall aim of this project was stated in Chapter 1 to be:

I. To create an accurate, repeatable, and transferrable method for the measurement of volumetric wear on the articular surfaces of UHMWPE TKR and TAR components through the use of verified and repeatable metrology equipment.

II. To accurately quantify volumetric wear on any TKR or TAR component without the presence of any type of pre-wear information, using only information attained from the worn component.

The first aim has been achieved throughout the studies detailed, with the method developed in this thesis for volumetric wear quantification producing accurate results when compared to standardised wear measurement methods, whilst also being transferrable to a wide spectrum of components.

No pre-wear data was used in the calculation of wear in either Chapter 6, Chapter 7, or Chapter 8. Results in all chapters were found to be either not significantly different to Gravimetric measurement results, or highly comparable to volumetric wear rates shown in published literature. This shows that the method developed in this research can be used to quantify volumetric wear on any component without the use of any pre-wear data, particularly useful in the case of retrieved components.

9.1 Statement of Novelty

The project detailed in this thesis fills a critical knowledge gap in the evaluation of volumetric wear in retrieved TKR and TAR components, with the creation of a method for the volumetric wear measurement of TKR and TAR components without the requirement for any pre-wear data to be known. Although studies have been conducted to measure volumetric wear on retrieved components, it is generally the case that some amount of pre-wear information has been used to measure this material loss.

The method developed in this thesis requires no pre-wear information at any stage of analysis to quantify volumetric wear on the articular surface of such components. This project calculates wear volume on TKR and TAR components through segmentation of measured CMM data into two-dimensional sectional profiles which are then analysed individually and combined to calculate a value for volumetric wear.

The automatic wear edge detection method developed in this study across two-dimensional profiles represents a novel approach to the identification of wear edge location. Previous studies use either manual methods of wear edge location or a single numerical as the defining factor in wear edge location. This automatic wear edge detection method has been shown to produce a more accurate location of wear edge points than manual methods and is adaptable to multiple designs of components, as shown in the studies throughout this thesis.

The Micro-CT-CMM method used also provides a novel approach to CMM alignment for volumetric wear measurement, with CAD models from Micro-CT accurately representing the worn component. Previous studies by Jiang et al have required the use of a manufacturer supplied CAD model for CMM alignment. In the case of retrieved components, the design of the component may not be known and it may not be possible to attain a manufacturer supplied CAD model. The Micro-CT-CMM method used negates this requirement allowing for adaptability to any TKR design.

Previous studies have only evaluated a single curve fitting technique when considering the effectiveness of CMM volumetric wear measurement methods. The current research applied several curve fitting techniques using different methodologies to calculate volumetric wear in both TKR and TAR components. The application of multiple curve fitting methods builds on previous studies using solely polynomial curve fitting to allow for a wider assessment of different curve fitting methods to describe TKR and TAR geometry.

TAR components are a relatively new and unexplored area of orthopaedics and typically Gravimetric methods are used for volumetric wear measurement. This research represents the first application of a truly autonomous method of volumetric wear calculation to TAR components, requiring no pre-wear data.

The method developed in this research presents a novel approach to the measurement of volumetric wear on UHMWPE TKR and TAR components through the application of a novel Micro-CT-CMM measurement method for orthopaedic wear measurement, the application of a novel wear edge detection method and builds on previous research by applying multiple different curve fitting techniques to evaluate the effectiveness of the developed method.

Chapter 10 – Conclusions

This chapter summarises the main conclusions and outcomes that can be drawn from the content of this thesis. These statements consider the method developed and the application of the method to numerous studies and evaluations and summarise the main findings of the study. From the information given in the previous chapters of this thesis, it can be stated that:

- The use of coordinate measurement using a CMM has proven to be a successful tool for the assessment of volumetric wear on Total Knee Replacement and Total Ankle Replacement components of varying design types and wear application methods.
- A variety of measurement techniques have been combined to develop a method for the assessment of wear on TKR and TAR components.
- Micro-CT was found to be a successful method for the CAD digitisation of UHMWPE components. When combined with the use of Geomagic an accurate representation of global component geometry can be developed in ".STEP" format for use in CMM alignment.
- CMM alignment using a best-fit algorithm and bespoke fixturing provided accurate and repeatable measurements of TKR and TAR components.
- A comprehensive post-measurement analysis method has been developed utilising multiple commercial software packages to perform accurate and repeatable measurements of wear on orthopaedic components. Software packages including CATIA, Solidworks, MATLAB, Geomagic and Volume Graphics were used to perform different aspects of analysis.
- Surface topographical measurement of worn and unworn areas of the same component showed significant differences in specific areal texture parameters. Unfortunately, these differences could not be numerically established and integrated into the full volumetric wear calculation method.
- Automatic wear edge detection and location on a two-dimensional longitudinal profile on TKR components using the slope change detection function in MATLAB showed accurate and repeatable results, showing greater accuracy than manual methods.
- For a cohort of TAR components with visible wear edges, automatic wear edge location and detection based on a percentile value provided volumetric wear results comparable to those found in published literature.

- The method developed provided accurate results of volumetric wear in both 2D and 3D on a computationally wear simulated TKR component.
- No significant difference was found between volumetric wear values found using the method developed and results found using Gravimetric measurement results on a cohort of wear-simulated TKR components of the same design.
- Volumetric wear rates calculated for a cohort of retrieved components of multiple different designs were found to be comparable with typical volumetric wear rates published in the literature for retrieved TKR components.
- Measurement of volumetric wear on TAR components was found to display results that were considered comparable with published values for components that had undergone similar simulation durations and methods although further definition is required in curve fitting techniques for TAR components.

Chapter 11 – Further Work

This chapter considers the progress that has currently been made in the application of the developed method to cohorts in studies detailed in previous chapters and on that basis makes suggestions for further work that could be conducted in the area to improve the effectiveness, applications, and accuracy of using the applied method for volumetric wear calculation.

Firstly, it would be advantageous to apply the method used in this study to larger cohorts of components. The studies performed in this thesis used relatively small cohort sizes, meaning that although repeatability and accuracy are shown, there is the potential for restrictive sample sizes to affect confidence in these results. The maximum cohort size used in this study was 8, it would be suggested that a far larger cohort of perhaps more than 20 components would be needed to fully assess the repeatability of volumetric wear calculation.

The surface topography study performed in Chapter 4 showed excellent promise in being able to distinguish between worn and unworn areas of TKR components by isolating differences in surface topographical parameters. As discussed, it was found that the surface topographical parameters did show significant variation between worn and unworn areas, but this could not be represented numerically in a repeatable way.

For this reason, it would be highly suggested that a further study into possible characterisation using surface topographical parameters should be conducted. It would be recommended to perhaps digitise the entire articular surface using an optical measurement technique such as FVM. This may be a time-consuming method, but full digitization would allow for sampling of the entire worn and unworn area of a component, as opposed to single measurement datasets. This would provide a more accurate result of the difference between worn and unworn areas on the same TKR component.

In addition to increasing the size of the measurement area taken, the sample size for this study could also be increased, and potentially include components that have undergone very high levels of wear. All components used in the Chapter 4 study, including the retrieved prostheses, exhibited relatively low levels of visible wear, suggesting that the surface topography between worn and unworn portions is perhaps not too distinct in cases of lower wear. By comparing highly worn components it may be possible to consider the differences more easily between worn and unworn areas.

The study performed in Chapter 5 compared a computationally artificially worn component to a replica of the component that had been manufactured using 3D printing. This study appeared to show excellent promise in

providing reference data to validate measured results. For this reason, it would be suggested that a further study building on this would be of benefit to the overall effectiveness of the wear measurement method. It would be beneficial to perhaps digitise a component with clinically relevant wear on the articular surface and use this as a basis for a component to be 3D printed. This could be achieved through the use of CT in the way it has been used throughout this thesis to create CAD representations of components.

Computational wear volume results can be easily calculated for a CAD model of a component, and if a 3D representation of this was also printed then volumetric wear calculation would be possible using the described method. A more comprehensive study considering repeat measurements of a 3D printed component, as well as considering clinically relevant wear volumes would provide very useful information on the effectiveness of changing wear edge detection or fitting parameters as there is a definitive value to refer back to.

The retrieved component study discussed in Chapter 7 provided interesting results that were comparable with quoted values in the literature of volumetric wear on retrieved TKR prostheses. However, it would be interesting to perform a retrieval study on a cohort of components where pre-wear data is known. This is an idealised study, as retrieved components inherently do not have pre-wear data. However, if the design of the component was known, then manufacturer supplied CAD models of the unworn component form could be used to examine the accuracy of the measurement of such components.

The use of retrieved components could also be used as an interesting study into the volumetric wear of TAR components. Only wear-simulated TAR components have been considered for analysis in this research. Retrieved TAR components of unknown design would provide a thorough investigation into the accuracy of the developed method. Such a study would require the application of alternative methods of wear edge detection for TAR components.

The conducted study into TAR components, as detailed in Chapter 8 used multiple different curve fitting techniques in the calculation of volumetric wear. As shown, no specific method was shown to give more repeatable results across measurements, meaning that no explicitly defined curve fitting method can be recommended based on this study. Further studies could be conducted to further linearise the curve fitting process and determine an optimum method from either those three selected or another method.

Another interesting addition study that could be considered is the use of curve fitting types that are not present as standard within MATLAB software. The author has previously attempted a small study into this, using a third-party MATLAB script to fit the measured 2D profile data to a circular form. Visual analysis suggested that this was unwise for the components in this study and was therefore discounted from the analysis. However, fitting components to an elliptical form would potentially provide an accurate reconstruction of unworn component geometry due to the generally elliptical shape of the surface. The fitting of ellipses to data is very complex and would involve the application of advanced coding in MATLAB.

Finally, the measurement of wear on alternative implant surfaces should perhaps be considered to build up a comprehensive evaluation of volumetric wear on a TKR or TAR component. As mentioned in Chapter 8, the studies performed in this thesis only consider wear on superior articular surfaces of components. In the case of tri-component arthroplasty, as is the most common form in both TKR and TAR, backside wear of the UHMWPE component also occurs. The contribution of this to overall wear volume should not be underestimated and this method may need to be expanded to consider this.

The contribution of deformation and creep to volumetric wear measurement inaccuracy is also a significant challenge in the development of methods such as the one developed in this thesis. As discussed, deformation is unable to be quantified by the method created, and further investigation must be conducted to consider whether methods can be applied to quantify the contribution deformation has the calculated volumetric wear that is found for TKR and TAR components.

Reference List

Abdelgaied, A., Fisher, J., & Jennings, L. M. (2017). A comparison between electromechanical and pneumatic-controlled knee simulators for the investigation of wear of total knee replacements. *Proceedings of the Institution of Mechanical Engineers, Part H: Journal of Engineering in Medicine, 231*(7), 643-651. doi:10.1177/0954411917696519

Affatato, S., Ruggiero, A., Jaber, S. A., Merola, M., & Bracco, P. (2018). Wear Behaviours and Oxidation Effects on Different UHMWPE Acetabular Cups Using a Hip Joint Simulator. *Materials (Basel), 11*(3), 433. doi:10.3390/ma11030433

Affatato, S., Taddei, P., Leardini, A., Giannini, S., Spinelli, M., & Viceconti, M. (2009). Wear behaviour in total ankle replacement: A comparison between an in vitro simulation and retrieved prostheses. *Clinical Biomechanics, 24*(8), 661-669. doi:10.1016/j.clinbiomech.2009.06.006

Ali, S. H. R. (2014). Performance Investigation of CMM Measurement Quality Using Flick Standard. *Journal of Quality and Reliability Engineering, 2014*, 960649. doi:10.1155/2014/960649

Altman, D. G., & Bland, J. M. (1983). Measurement in Medicine: The Analysis of Method Comparison Studies. *Journal of the Royal Statistical Society. Series D (The Statistician), 32*(3), 307-317. doi:10.2307/2987937

Anas, I., Musa, T. A., Kabiru, I., Yisau, A. A., Kazaure, I. S., Abba, S. M., & Kabir, S. M. (2013). Digital radiographic measurement of normal knee joint space in adults at Kano, Nigeria. *The Egyptian Journal of Radiology and Nuclear Medicine, 44*(2), 253-258. doi:https://doi.org/10.1016/j.ejrnm.2013.03.005

Anderson, T., Montgomery, F., & Carlsson, A. (2003). Uncemented STAR total ankle prostheses. Three to eight-year follow-up of fifty-one consecutive ankles. *J Bone Joint Surg Am, 85*(7), 1321-1329.

Barg, A., Knupp, M., Henninger, H. B., Zwicky, L., & Hintermann, B. (2012). Total ankle replacement using HINTEGRA, an unconstrained, three-component system: surgical technique and pitfalls. *Foot Ankle Clin, 17*(4), 607-635. doi:10.1016/j.fcl.2012.08.006

Battaglia, S., Taddei, P., Castiello, E., Tozzi, S., Sudanese, A., & Affatato, S. (2014). Combined effect of the body mass index and implant size on the wear of retrieved total knee prostheses. *Journal of the Mechanical Behavior of Biomedical Materials, 38*, 69-77. doi:10.1016/j.jmbbm.2014.06.012

Becker, A., Schoellhorn, K., Dirix, Y., & Schmotzer, H. (2006). Metal-on-Metal Bearings 1: The influence of 3D measurement accuracy on the calculated wear of a ball head using a new mathematical approach. *ORS Annual Meeting, 52*.

Bell, C. J., & Fisher, J. (2007). Simulation of polyethylene wear in ankle joint prostheses. *Journal of Biomedical Materials Research Part B: Applied Biomaterials, 81B*(1), 162-167. doi:10.1002/jbm.b.30649

Bell, C. J., Walker, P. S., Abeysundera, M. R., Simmons, J. M., King, P. M., & Blunn, G. W. (1998). Effect of oxidation on delamination of ultrahigh-molecular-weight polyethylene tibial components. *J Arthroplasty, 13*(3), 280-290. doi:10.1016/s0883-5403(98)90173-5

Benjamin, J., Szivek, J., Dersam, G., Persselin, S., & Johnson, R. (2001). Linear and Volumetric Wear of Tibial Inserts in Posterior Cruciate-Retaining Knee Arthroplasties. *Clinical Orthopaedics and Related Research®, 392*. Retrieved from https://journals.lww.com/clinorthop/Fulltext/2001/11000/Linear_and_Volumetric_Wear_of_Tibial_Inserts_in.16.aspx

Bercik, M. J., Joshi, A., & Parvizi, J. (2013). Posterior Cruciate-Retaining Versus Posterior-Stabilized Total Knee Arthroplasty. A Meta-Analysis. *Journal of Arthroplasty, 28*(3), 439-444. doi:10.1016/j.arth.2012.08.008

Bills, P., Brown, L., Jiang, X., & Blunt, L. (2005). A metrology solution for the orthopaedic industry. *Journal of Physics: Conference Series, 13*(1), 316-319. doi:10.1088/1742-6596/13/1/074

Bills, P. J. (2007). *The development of a geometric methodology for the determination of volumetric wear in total joint replacements & development of a total knee replacement joint using new and novel measurement techniques.* (Dissertation/Thesis).

Bland, M. (1995). *An Introduction to Medical Statistics*: Oxford University Press.

Blunt, L. A., Bills, P. J., & Jiang, X. Q. (2008). Improvement in the assessment of wear of total knee replacements using coordinate-measuring machine techniques. *Proceedings of the Institution of Mechanical Engineers. Part H, Journal of Engineering in Medicine [H.W. Wilson - AST], 222*(H3), 309. Retrieved from http://hud.summon.serialssolutions.com/2.0.0/link/0/eLvHCXMw3V1bS8MwGA2bD6KI6LzfyItPpWVtsq598GGKUsWBsg19G7HNsNh1sHX4982XNG3m5Q_4NMhgtMkh38nZ-U4QIp7Ttr_tCTR8c3ncpbGf-KDlUFH2GAlY6PmTmPFkNZipoa9TqMf-w8IrmUCqftrEyKr4TeCGn5DdA9aAGTRCfuQcbk6R3izV7rYsG3HFsTTNBRW1p1JHhMGptF5yq0p-XZjk9qkqhgttPdBehJKW9jk0Gktc6CDEhSNY7LywIqXlV_TYCEqE1-iXHgDrsnMdOS-OpXImLdvqDYb6lnSQFblySeHRMWTaNMvUhQRO_TfYQ1pK5a-O_bwifgSGZ0armNSmbrnrcjnmtSlIaipfQ2_ynucZaI6IsWeTdlgXw8qiKE6Ogt6EgSgFEMI-FS9ZXPHcHg2a4oQfwDn_3h9VRV-wKF_FOqrn-

VHaJV8Z7qDtciZxTwFkFzV43kKbxqy20Lqe1D2UG6jBaY7F2uEaNXg2wYAa-JSowYAabKlGS9Tg31CDS9TgGjX76OLudngT2frpx0mWjevJIAdoi0HvRV7IHs3kCGGP8sAlMRdUNKFdnwUx67JEFE7COy7h3jE6_OPXTv785hRt1Ot9htaK-ZKfo-b7MvkCorFpkQ

Blunt, L. A., Bills, P. J., Jiang, X. Q., & Chakrabarty, G. (2008). Improvement in the assessment of wear of total knee replacements using coordinate-measuring machine techniques. *Proceedings of the Institution of Mechanical Engineers, Part H: Journal of Engineering in Medicine, 222*(3), 309-318. doi:10.1243/09544119JEIM289

Bolton-Maggs, B. G., Sudlow, R. A., & Freeman, M. A. (1985). Total ankle arthroplasty. A long-term review of the London Hospital experience. *J Bone Joint Surg Br, 67*(5), 785-790.

Bonnin, M., Judet, T., Colombier, J. A., Buscayret, F., Graveleau, N., & Piriou, P. (2004). Midterm results of the Salto Total Ankle Prosthesis. *Clin Orthop Relat Res*(424), 6-18. doi:10.1097/01.blo.0000132407.75881.a0

Bortel, L. E., Charbonnier, B., & Heuberger, R. (2015). Development of a Synthetic Synovial Fluid for Tribological Testing. *Lubricants, 3*(4). doi:10.3390/lubricants3040664

Bowden, A. E., Kurtz, S. M., & Edidin, A. A. (2005). Validation of a micro-CT technique for measuring volumetric wear in retrieved acetabular liners. *Journal of Biomedical Materials Research Part B: Applied Biomaterials, 75B*(1), 205-209. doi:10.1002/jbm.b.30318

Brandt, J.-M., Charron, K. D. J., Zhao, L., MacDonald, S. J., & Medley, J. B. (2011). Commissioning of a displacement-controlled knee wear simulator and exploration of some issues related to the lubricant. *Proceedings of the Institution of Mechanical Engineers, Part H: Journal of Engineering in Medicine, 225*(8), 736-752. doi:10.1177/0954411911406061

Brockett, C. L., Abdelgaied, A., Haythornthwaite, T., Hardaker, C., Fisher, J., & Jennings, L. M. (2016). The influence of simulator input conditions on the wear of total knee replacements: An experimental and computational study. *Proceedings of the Institution of Mechanical Engineers, Part H: Journal of Engineering in Medicine, 230*(5), 429-439. doi:10.1177/0954411916645134

Brockett, C. L., Carbone, S., Fisher, J., & Jennings, L. M. (2018). Influence of conformity on the wear of total knee replacement: An experimental study. *Proceedings of the Institution of Mechanical Engineers. Part H, Journal of engineering in medicine, 232*(2), 127-134. doi:10.1177/0954411917746433

Brockett, C. L., Jennings, L. M., Hardaker, C., & Fisher, J. (2012). Wear of moderately cross-linked polyethylene in fixed-bearing total knee replacements. *Proceedings of the Institution of Mechanical Engineers, Part H: Journal of Engineering in Medicine, 226*(7), 529-535. doi:10.1177/0954411912445265

Brunner, S., Barg, A., Knupp, M., Zwicky, L., Kapron, A. L., Valderrabano, V., & Hintermann, B. (2013). The Scandinavian total ankle replacement: long-term, eleven to fifteen-year, survivorship analysis of the prosthesis in seventy-two consecutive patients. *J Bone Joint Surg Am, 95*(8), 711-718. doi:10.2106/jbjs.K.01580

BSI. (2009). BS ISO 14243-1:2009: Implants for surgery. Wear of total knee-joint prostheses. Loading and displacement parameters for wear-testing machines with load control and corresponding environmental conditions for test. In: British Standards Institute.

BSI. (2010). BS ISO 14243-2:2009: Implants for surgery. Wear of total knee-joint prostheses. Methods of measurement. In: British Standards Institute.

Buechel, F. F., Sr., Buechel, F. F., Jr., & Pappas, M. J. (2004). Twenty-year evaluation of cementless mobile-bearing total ankle replacements. *Clin Orthop Relat Res*(424), 19-26. doi:10.1097/01.blo.0000132243.41419.59

Carmignato, S., Spinelli, M., Affatato, S., & Savio, E. (2011). Uncertainty evaluation of volumetric wear assessment from coordinate measurements of ceramic hip joint prostheses. *Wear, 270*(9), 584-590. doi:10.1016/j.wear.2011.01.012

Chen, Y., Hallab, N. J., Liao, Y. S., Narayan, V., Schwarz, E. M., & Xie, C. (2016). Antioxidant impregnated ultra-high molecular weight polyethylene wear debris particles display increased bone remodeling and a superior osteogenic:osteolytic profile vs. conventional UHMWPE particles in a murine calvaria model. *Journal of Orthopaedic Research, 34*(5), 845-851. doi:10.1002/jor.23080

Collier, J. P., Sperling, D. K., Currier, J. H., Sutula, L. C., Saum, K. A., & Mayor, M. B. (1996). Impact of gamma sterilization on clinical performance of polyethylene in the knee. *J Arthroplasty, 11*(4), 377-389. doi:10.1016/S0883-5403(96)80026-X

Coventry, M. B., Finerman, G. A., Riley, L. H., Turner, R. H., & Upshaw, J. E. (1972). A new geometric knee for total knee arthroplasty. *Clin Orthop Relat Res, 83*, 157-162. doi:10.1097/00003086-197203000-00030

Cranin, A. N. (1987). Handbook of biomaterials evaluation. Scientific, technical and clinical testing of Implant Materials. Andreas F. von Recum, Editor, New York, 1986, MacMillan. With a forward by Solomon

Pollack and contributions by 61 authors and 10 section editors. Index of 14 pp. $120.00. *J Biomed Mater Res, 21*(9), 1167-1168. doi:https://doi.org/10.1002/jbm.820210909

Crowninshield, R. D., Wimmer, M. A., Jacobs, J. J., & Rosenberg, A. G. (2006). Clinical Performance of Contemporary Tibial Polyethylene Components. *J Arthroplasty, 21*(5), 754-761. doi:10.1016/j.arth.2005.10.012

Culliford, D., Maskell, J., Judge, A., Cooper, C., Prieto-Alhambra, D., Arden, N. K., & Group, C. O. S. (2015). Future projections of total hip and knee arthroplasty in the UK: results from the UK Clinical Practice Research Datalink. *Osteoarthritis and cartilage / OARS, Osteoarthritis Research Society, 23*(4), 594-600. doi:10.1016/j.joca.2014.12.022

Derbyshire, B., Hardaker, C. S., Fisher, J., & Dowson, D. (1994). Assessment of the change in volume of acetabular cups using a coordinate measuring machine. *Proceedings of the Institution of Mechanical Engineers. Part H, Journal of engineering in medicine, 208*(3), 151-158.

Devane, P. A., Bourne, R. B., Rorabeck, C. H., Hardie, R. M., & Horne, J. G. (1995). Measurement of polyethylene wear in metal-backed acetabular cups. I. Three-dimensional technique. *Clin Orthop Relat Res*(319), 303-316. Retrieved from http://europepmc.org/abstract/MED/7554644

du Plessis, A., Broeckhoven, C., Guelpa, A., & le Roux, S. G. (2017). Laboratory x-ray micro-computed tomography: a user guideline for biological samples. *GigaScience, 6*(6), 1-11. doi:10.1093/gigascience/gix027

Duboust, N., Ghadbeigi, H., Pinna, C., Ayvar-Soberanis, S., Collis, A., Scaife, R., & Kerrigan, K. (2016). An optical method for measuring surface roughness of machined Carbon Fibre Reinforced Plastic composites. *Journal of Composite Materials, 51*. doi:10.1177/0021998316644849

Duliu, O. G. (1999). Computer axial tomography in geosciences: an overview. *Earth-science reviews, 48*(4), 265-281.

Eloesser, L. (1913). Implantation of Joints. *California state journal of medicine, 11*(12), 485-491. Retrieved from https://www.ncbi.nlm.nih.gov/pubmed/18736118

https://www.ncbi.nlm.nih.gov/pmc/articles/PMC1640031/

Elsner, J. J., Shemesh, M., Shefy-Peleg, A., Gabet, Y., Zylberberg, E., & Linder-Ganz, E. (2015). Quantification of in vitro wear of a synthetic meniscus implant using gravimetric and micro-CT measurements. *Journal of the Mechanical Behavior of Biomedical Materials, 49*, 310-320. doi:10.1016/j.jmbbm.2015.05.017

Engh Jr, C. A., Zimmerman, R. L., Hopper Jr, R. H., & Engh, G. A. (2013). Can Microcomputed Tomography Measure Retrieved Polyethylene Wear? Comparing Fixed-bearing and Rotating-platform Knees. *Clin Orthop Relat Res, 471*(1), 86-93. doi:10.1007/s11999-012-2513-2

Ferreira, F. A. M., Oliva, J. d. V. y., & Perez, A. M. S. (2013). Evaluation of the Performance of Coordinate Measuring Machines in the Industry, Using Calibrated Artefacts. *Procedia Engineering, 63*, 659-668. doi:https://doi.org/10.1016/j.proeng.2013.08.232

Figueiredo, D., Júnior, S., & Rocha, E. (2011). What is R2 all about? *Leviathan-Cadernos de Pesquisa Polútica, 3*, 60-68. doi:10.11606/issn.2237-4485.lev.2011.132282

Flack, D. (2014). *Measurement Good Practic Guide No. 41*. Retrieved from NPL:

Flores-Hernandez, C., Netter, J., Hermida, J., Steklov, N., Kester, M., & D'Lima, D. (2015). Prediction of Wear in Crosslinked Polyethylene Unicompartmental Knee Arthroplasty. *Lubricants, 2015*, 381-393. doi:10.3390/lubricants3020381

Galhoum, A. E., Wiewiorski, M., & Valderrabano, V. (2017). Ankle instability: Anatomy, mechanics, management and sequelae. *Sports Orthopaedics and Traumatology, 33*(1), 47-56. doi:https://doi.org/10.1016/j.orthtr.2017.01.006

Gąska, P., Gąska, A., Gruza, M., Ostrowska, K., & Sładek, J. (2017). Assessment of impact of stylus length on measurement accuracy for 5-axis coordinate measuring systems. *Mechanik, 90*, 1027-1029. doi:10.17814/mechanik.2017.11.170

Gioe, T. (2007). Knee Arthroplasty in the young patient - Survival in a community registry *Clinical Orthopaedics and Related Research®, 464*, 83-87.

Gluck, T. (1902). Zur Behandlung der Anklose des Kierfergelenkes *Verh. dtsch Ges. Chir. , 1*.

Goldblatt, J. P., & Richmond, J. C. (2003). Anatomy and biomechanics of the knee. *Operative Techniques in Sports Medicine, 11*(3), 172-186. doi:10.1053/otsm.2003.35911

Good, V. D., Clarke, I. C., & Anissian, L. (1996). Water and bovine serum lubrication compared in simulator PTFE/CoCr wear model. *J Biomed Mater Res, 33*(4), 275-283. doi:10.1002/(sici)1097-4636(199624)33:4<275::Aid-jbm7>3.0.Co;2-m

Gosset, W. (1908). The probably error of a mean. *Biometrika, 6* 1-25. doi:10.1093/biomet/6.1.1

Gougoulias, N., Khanna, A., & Maffulli, N. (2010). How successful are current ankle replacements?: a systematic review of the literature. *Clin Orthop Relat Res, 468*(1), 199-208. doi:10.1007/s11999-009-0987-3

Harris, P. F., Ranson, C., & Robertson, A. (2014). *Anatomy for problem solving in sports medicine : The Knee*. Cumbria, UNITED KINGDOM: M&K Update Ltd.

Harsha, A. P., & Joyce, T. J. (2011). Challenges associated with using bovine serum in wear testing orthopaedic biopolymers. *Proceedings of the Institution of Mechanical Engineers. Part H, Journal of engineering in medicine, 225*(10), 948-958. doi:10.1177/0954411911416047

Hintermann, B., Valderrabano, V., Dereymaeker, G., & Dick, W. (2004). The HINTEGRA ankle: rationale and short-term results of 122 consecutive ankles. *Clin Orthop Relat Res*(424), 57-68. doi:10.1097/01.blo.0000132462.72843.e8

Hong, T., & Nagumo, M. (1997). Effect of surface roughness on early stages of pitting corrosion of Type 301 stainless steel. *Corrosion Science, 39*(9), 1665-1672. doi:https://doi.org/10.1016/S0010-938X(97)00072-3

Hood, R. W., Wright, T. M., & Burstein, A. H. (1983). Retrieval analysis of total knee prostheses: A method and its application to 48 total condylar prostheses. *J Biomed Mater Res, 17*(5), 829-842. doi:10.1002/jbm.820170510

Hsieh, Y.-L., Barrall, G., & Xu, S. (1992). Effects of oxidation on mechanical and physical properties of ultra-high-modulus and ultra-high-molecular-weight polyethylene fibres. *Polymer, 33*(3), 536-545. doi:https://doi.org/10.1016/0032-3861(92)90730-K

Huddleston, J. I. (2009). How often do patients with high-flex total knee arthroplasty use high flexion? *Clinical Orthopaedics and Related Research®, 467*, 1898-1906.

Hurowitz, E. J., Gould, J. S., Fleisig, G. S., & Fowler, R. (2007). Outcome analysis of agility total ankle replacement with prior adjunctive procedures: two to six year followup. *Foot Ankle Int, 28*(3), 308-312. doi:10.3113/fai.2007.0308

Imai, K., Ikoma, K., Kido, M., Maki, M., Fujiwara, H., Arai, Y., . . . Kubo, T. (2015). Joint space width of the tibiotalar joint in the healthy foot. *Journal of foot and ankle research, 8*, 26-26. doi:10.1186/s13047-015-0086-5

ISO. (2000). Geometrical Product Specifications (GPS) — Acceptance and reverification tests for coordinate measuring machines (CMM) In *Part 1: Vocabulary*: ISO.

ISO. (2011a). Implants for Surgery - Partial and total hip joint prostheses - Part 2: Articulating surfaces made of metallic, ceramic and plastics materials. (3).

ISO. (2011b). ISO 10360 - Geometrical product specifications (GPS) — Acceptance and reverification tests for coordinate measuring machines (CMM).

ISO. (2012). Geometrical product specifications (GPS) — Surface texture.

Jiang, W., Ji, C., Jin, Z., & Dai, Y. (2018). CMM-Based Volumetric Assessment Methodology for Polyethylene Tibial Knee Inserts in Total Knee Replacement. *Appl Bionics Biomech, 2018*, 9846293. doi:10.1155/2018/9846293

Jiang, W., Ji, C., Xiao, H., Jin, Z., & Dai, Y. (2018). Comparison of CMM and Micro-CT Volumetric Analysis of Polyethylene Tibial Knee Inserts in Total Knee Replacement. *International Journal of Polymer Science, 2018*, 3601480. doi:10.1155/2018/3601480

Johnson, T., Laurent, M. P., Yao, J. Q., & Blanchard, C. R. (2003). Comparison of wear of mobile and fixed bearing knees tested in a knee simulator. *Wear, 255*, 1107-1112. doi:10.1016/S0043-1648(03)00272-2

Jung, H. G., Shin, M. H., Lee, S. H., Eom, J. S., & Lee, D. O. (2015). Comparison of the outcomes between two 3-component total ankle implants. *Foot Ankle Int, 36*(6), 656-663. doi:10.1177/1071100715573716

Kak, A. C., Slaney, M., & Wang, G. (2002). Principles of computerized tomographic imaging. In: Wiley Online Library.

Knecht, S., Estin, M., Callaghan, J. J., Zimmerman, M., & KJ;, A. (2004). The Agility Total Ankle Arthroplasty *Journal of Bone and Joint Surgery, 86*, 1161-1171.

Knowlton, C., Bhutani, P., & Wimmer, M. (2016). RELATIONSHIP OF SURFACE DAMAGE AND VOLUMETRIC WEAR IN RETRIEVED TKR POLYETHYLENE LINERS. *98-B*(SUPP_8), 111-111. doi:10.1302/1358-992x.98bsupp_8.Ista2015-111

Knowlton, C., & Wimmer, M. (2012). An autonomous mathematical reconstruction to effectively measure volume loss on retrieved polyethylene tibial inserts. *Journal of biomedical materials research. Part B, Applied biomaterials, 101*. doi:10.1002/jbm.b.32782

Kofoed, H. (1995). Cylindrical cemented ankle arthroplasty: a prospective series with long-term follow-up. *Foot Ankle Int, 16*(8), 474-479. doi:10.1177/107110079501600803

Kopp, F. J., Patel, M. M., Deland, J. T., & O'Malley, M. J. (2006). Total ankle arthroplasty with the Agility prosthesis: clinical and radiographic evaluation. *Foot Ankle Int, 27*(2), 97-103. doi:10.1177/107110070602700205

Kurtz, S., Ong, K., Lau, E., Mowat, F., & Halpern, M. (2007). Projections of Primary and Revision Hip and Knee Arthroplasty in the United States from 2005 to 2030. *The Journal of Bone & Joint Surgery, 89*(4), 780-785. doi:10.2106/jbjs.f.00222

Kurtz, S. M. (2004). *The UHMWPE handbook: ultra-high molecular weight polyethylene in total joint replacement*. Amsterdam;London;: Elsevier Academic Press.

Lawrence, I. K. L. (1989). A Concordance Correlation Coefficient to Evaluate Reproducibility. *Biometrics, 45*(1), 255-268. doi:10.2307/2532051

Li, N., Tan, Y., Deng, Y., & Chen, L. (2014). Posterior cruciate-retaining versus posterior stabilized total knee arthroplasty: a meta-analysis of randomized controlled trials. *Knee Surgery, Sports Traumatology, Arthroscopy, 22*(3), 556-564. doi:10.1007/s00167-012-2275-0

Lin, C., & Miller, J. (2002). Cone beam x-ray microtomography—a new facility for three-dimensional analysis of multiphase materials. *Mining, Metallurgy & Exploration, 19*(2), 65-71.

Liza, S., Haseeb, A. S. M. A., Abbas, A. A., & Masjuki, H. H. (2011). Failure analysis of retrieved UHMWPE tibial insert in total knee replacement. *Engineering Failure Analysis, 18*(6), 1415-1423. doi:https://doi.org/10.1016/j.engfailanal.2011.04.001

Lord, G., & Marotte, J. H. (1973). [Total ankle prosthesis. Technic and 1st results. Apropos of 12 cases]. *Rev Chir Orthop Reparatrice Appar Mot, 59*(2), 139-151.

Lord, G., & Marotte, J. H. (1980). [Total ankle replacement (author's transl)]. *Rev Chir Orthop Reparatrice Appar Mot, 66*(8), 527-530.

M Kop, A., & Swarts, E. (2007). Quantification of polyethylene degradation in mobile bearing knees: A retrieval analysis of the Anterior-Posterior-Glide (APG) and Rotating Platform (RP) Low Contact Stress (LCS) knee. *Acta Orthopaedica, 78*(3), 364-370. doi:10.1080/17453670710013942

Mansfield, P. J., & Neumann, D. A. (2019). Chapter 11 - Structure and Function of the Ankle and Foot. In P. J. Mansfield & D. A. Neumann (Eds.), *Essentials of Kinesiology for the Physical Therapist Assistant (Third Edition)* (pp. 311-350). St. Louis (MO): Mosby.

Martell, J. M., & Berdia, S. (1997). Determination of polyethylene wear in total hip replacements with use of digital radiographs. *J Bone Joint Surg Am, 79*(11), 1635-1641. doi:10.2106/00004623-199711000-00004

McKellop, H., Shen, F. W., Lu, B., Campbell, P., & Salovey, R. (1999). Development of an extremely wear-resistant ultra high molecular weight polyethylene for total hip replacements. *J Orthop Res, 17*(2), 157-167. doi:10.1002/jor.1100170203

Medel, F. J., Kurtz, S. M., Parvizi, J., Klein, G. R., Kraay, M. J., & Rimnac, C. M. (2011). In vivo oxidation contributes to delamination but not pitting in polyethylene components for total knee arthroplasty. *J Arthroplasty, 26*(5), 802-810. doi:10.1016/j.arth.2010.07.010

Meganck, J. A., Kozloff, K. M., Thornton, M. M., Broski, S. M., & Goldstein, S. A. (2009). Beam hardening artifacts in micro-computed tomography scanning can be reduced by X-ray beam filtration and the resulting images can be used to accurately measure BMD. *Bone, 45*(6), 1104-1116. doi:10.1016/j.bone.2009.07.078

Minoda, Y., Aihara, M., Sakawa, A., Fukuoka, S., Hayakawa, K., Tomita, M., . . . Ohzono, K. (2009). Comparison between highly cross-linked and conventional polyethylene in total knee arthroplasty. *Knee, 16*(5), 348-351. doi:10.1016/j.knee.2009.01.005

Muratoglu, O. K., Perinchief, R. S., Bragdon, C. R., O'Connor, D. O., Konrad, R., & Harris, W. H. (2003). Metrology to quantify wear and creep of polyethylene tibial knee inserts. *Clin Orthop Relat Res*(410), 155-164. doi:10.1097/01.blo.0000063604.67412.04

Muratoglu, O. K., Ruberti, J., Melotti, S., Spiegelberg, S. H., Greenbaum, E. S., & Harris, W. H. (2003). Optical analysis of surface changes on early retrievals of highly cross-linked and conventional polyethylene tibial inserts. *J Arthroplasty, 18*(7), 42-47. doi:10.1016/S0883-5403(03)00293-6

Naal, F. D. (2009). How active are patients undergoing total joint arthroplasty? A systematic review". *Clinical Orthopaedics and Related Research®*. doi:DOI 10.1007/s11999-009-1135-9

NJR. (2018). *15th Annual Report (2018) : National Joint Registry for England Wales, Northern Irelands and the Isle of Man* Retrieved from Hemel Hempstead:

Norgren, B., Dalén, T., & Nilsson, K. G. (2004). All-poly tibial component better than metal-backed: a randomized RSA study. *Knee, 11*(3), 189-196. doi:http://dx.doi.org/10.1016/S0968-0160(03)00071-1

Pearson, K. (1895). Notes on regression and inheritance in the case of two parents. *Proceedings of the Royal Society of London, 58*, 240-242.

Plessis, A. d., Sperling, P., Beerlink, A., Kruger, O., Tshabalala, L., Hoosain, S., & le Roux, S. G. (2018). Standard method for microCT-based additive manufacturing quality control 3: Surface roughness. *MethodsX, 5*, 1111-1116. doi:https://doi.org/10.1016/j.mex.2018.09.004

Popelka, S., Sosna, A., Vavrik, P., Jahoda, D., Bartak, V., & Landor, I. (2016). [Eleven-Year Experience with Total Ankle Arthroplasty]. *Acta Chir Orthop Traumatol Cech, 83*(2), 74-83.

Popelka, S., Vavrik, P., Landor, I., Hach, J., Pech, J., & Sosna, A. (2010). [Our experience with AES total ankle replacement]. *Acta Chir Orthop Traumatol Cech, 77*(1), 24-31.

Ranawat, C. S., Ranawat, A. S., Mohanty, S. S., Goldsmith, S. E., Rasquinha, V. J., & Rodriguez, J. A. (2005). Experience With an All-Polyethylene Total Knee Arthroplasty in Younger, Active Patients With Follow-up From 2 to 11 Years. *J Arthroplasty, 20*(3), 7-11. doi:10.1016/j.arth.2005.04.027

Reinders, J., Sonntag, R., & Kretzer, J. P. (2015). Synovial fluid replication in knee wear testing: an investigation of the fluid volume. *J Orthop Res, 33*(1), 92-97. doi:10.1002/jor.22736

Reinders, J., von Stillfried, F., Altan, E., Sonntag, R., Heitzmann, D. W. W., & Kretzer, J. P. (2015). Force-controlled dynamic wear testing of total ankle replacements. *Acta Biomater, 12*(1;C;), 332-340. doi:10.1016/j.actbio.2014.10.036

Rodriguez, J. A., Baez, N., Rasquinha, V., & Ranawat, C. S. (2001). Metal-backed and all-polyethylene tibial components in total knee replacement. *Clin Orthop Relat Res*(392), 174-183. doi:10.1097/00003086-200111000-00021

Salemyr, M., Muren, O., Ahl, T., Bodén, H., Chammout, G., Stark, A., & Sköldenberg, O. (2015). Vitamin-E diffused highly cross-linked polyethylene liner compared to standard liners in total hip arthroplasty. A randomized, controlled trial. *International orthopaedics, 39*(8), 1499-1505. doi:10.1007/s00264-015-2680-3

San Giovanni, T. P., Keblish, D. J., Thomas, W. H., & Wilson, M. G. (2006). Eight-year results of a minimally constrained total ankle arthroplasty. *Foot Ankle Int, 27*(6), 418-426. doi:10.1177/107110070602700606

Schmalzried, T. P., Szuszczewicz, E. S., Northfield, M. R., Akizuki, K. H., Frankel, R. E., Belcher, G., & Amstutz, H. C. (1998). Quantitative assessment of walking activity after total hip or knee replacement. *J Bone Joint Surg Am, 80*(1), 54-59.

Schwarze, M., Eckert, J., Walker, T., Jäger, S., Kretzer, J., & mueller, u. (2020). Bearing Thickness Is Not a Predictive Factor for Damage and Penetration in Oxford Unicompartmental Knee Arthroplasty—A Retrieval Analysis. *Materials, 13*. doi:10.3390/ma13204589

Schwarzkopf, R., Scott, R. D., Carlson, E. M., & Currier, J. H. (2015). Does Increased Topside Conformity in Modular Total Knee Arthroplasty Lead to Increased Backside Wear? *Clinical Orthopaedics and Related Research®, 473*(1), 220-225. doi:10.1007/s11999-014-3648-0

Schwiesau, J., Schilling, C., Utzschneider, S., Jansson, V., Fritz, B., Blömer, W., & Grupp, T. M. (2013). Knee wear simulation under conditions of highly demanding daily activities - Influence on an unicompartmental fixed bearing knee design. *Medical Engineering and Physics, 35*(8), 1204-1211. doi:10.1016/j.medengphy.2012.12.015

Selvik, G. (1990). Roentgen stereophotogrammetric analysis. *Acta Radiol, 31*(2), 113-126.

Shetty, A. A., Tindall, A., Ting, P., & Heatley, F. W. (2003a). The evolution of total knee arthroplasty. Part 1: introduction and first steps. *Current Orthopaedics, 17*(4), 322-325. doi:10.1016/S0268-0890(03)00093-8

Shetty, A. A., Tindall, A., Ting, P., & Heatley, F. W. (2003b). The evolution of total knee arthroplasty. Part II: the hinged knee replacement and the semi-constrained knee replacement. *Current Orthopaedics, 17*(5), 403-407. doi:10.1016/S0268-0890(03)00107-5

Singhal, A., Grande, J. C., & Zhou, Y. (2013). Micro/nano-CT for visualization of internal structures. *Microscopy Today, 21*(2), 16-22.

Smyth, A., Fisher, J., Suñer, S., & Brockett, C. (2017). Influence of kinematics on the wear of a total ankle replacement. *Journal of Biomechanics, 53*, 105-110. doi:https://doi.org/10.1016/j.jbiomech.2017.01.001

Song, E. K., Moon, J. Y., Seon, J. K., & Hyoun, Y. J. (2013). *The Evolution of Modern Total Knee Prostheses*: INTECH Open Access Publisher.

Song, S. J., Park, C. H., & Bae, D. K. (2019). What to Know for Selecting Cruciate-Retaining or Posterior-Stabilized Total Knee Arthroplasty. *Clinics in orthopedic surgery, 11*(2), 142-150. doi:10.4055/cios.2019.11.2.142

Takahashi, Y., Tateiwa, T., Shishido, T., Masaoka, T., Kubo, K., & Yamamoto, K. (2016). Size and thickness effect on creep behavior in conventional and vitamin E-diffused highly crosslinked polyethylene for total hip arthroplasty. *Journal of the Mechanical Behavior of Biomedical Materials, 62*, 399-406. doi:10.1016/j.jmbbm.2016.05.020

Tam, T., & Bhatnagar, A. (2016). 1 - High-performance ballistic fibers and tapes. In A. Bhatnagar (Ed.), *Lightweight Ballistic Composites (Second Edition)* (pp. 1-39): Woodhead Publishing.

Teeter, M. G., Naudie, D. D. R., McErlain, D. D., Brandt, J.-M., Yuan, X., MacDonald, S. J., & Holdsworth, D. W. (2011). In Vitro Quantification of Wear in Tibial Inserts Using Microcomputed Tomography. *Clin Orthop Relat Res, 469*(1), 107-112. doi:10.1007/s11999-010-1490-6

Teeter, M. G., Naudie, D. D. R., Milner, J. S., & Holdsworth, D. W. (2011). Determination of Reference Geometry for Polyethylene Tibial Insert Wear Analysis. *J Arthroplasty, 26*(3), 497-503. doi:10.1016/j.arth.2010.01.096

Teeter, M. G., Parikh, A., Taylor, M., Sprague, J., & Naudie, D. D. (2015). Wear and creep behavior of total knee implants undergoing wear testing. *J Arthroplasty, 30*(1), 130-134. doi:10.1016/j.arth.2014.08.001

Townsend, A., Pagani, L., Blunt, L., Scott, P. J., & Jiang, X. (2017). Factors affecting the accuracy of areal surface texture data extraction from X-ray CT. *CIRP Annals, 66*(1), 547-550. doi:https://doi.org/10.1016/j.cirp.2017.04.074

Verneuil, A. (1860). *De la création d'une fausse articulation par section ou résection partielle de l'os maxillaire inférieur, comme moyen de remédier à l'ankylose vraie ou fausse de la machoire inférieure*. Paris: Rignoux.

Vicars, R., Fisher, J., & Hall, R. M. (2009). The accuracy and precision of a micro computer tomography volumetric measurement technique for the analysis of in-vitro tested total disc replacements. *Proceedings of the Institution of Mechanical Engineers, Part H: Journal of Engineering in Medicine, 223*(3), 383-388. doi:10.1243/09544119JEIM515

Vickerstaff, J. A., Miles, A. W., & Cunningham, J. L. (2007). A brief history of total ankle replacement and a review of the current status. *Medical Engineering & Physics, 29*(10), 1056-1064. doi:https://doi.org/10.1016/j.medengphy.2006.11.009

Walker, P. S., Ranawat, C., & Insall, J. (1976). Fixation of the tibial components of condylar replacement knee prostheses. *J Biomech, 9*(4), 269-275.

Wallbridge, N., & Dowson, D. (1982). The walking activity of patients with articficial hip joints *Eng Med 11*.

Walldius, B. (1957). Arthroplasty of the knee joint using an endoprosthesis. *Acta Orthopaedica Scandinavica 19*.

Wimmer, M. (2002). Joint motion and daily activity profile of total knee patients in comparison with the ISO knee wear simulator. *48th ORS Meeting*, 0159.

Wimmer, M. A., Laurent, M. P., Haman, J. D., Jacobs, J. J., & Galante, J. O. (2012). Surface damage versus tibial polyethylene insert conformity: a retrieval study. *Clin Orthop Relat Res, 470*(7), 1814-1825. doi:10.1007/s11999-012-2274-y

Wünschel, M., Leasure, J. M., Dalheimer, P., Kraft, N., Wülker, N., & Müller, O. (2013). Differences in knee joint kinematics and forces after posterior cruciate retaining and stabilized total knee arthroplasty. *Knee, 20*(6), 416-421. doi:10.1016/j.knee.2013.03.005

Zanini, F., Pagani, L., Savio, E., & Carmignato, S. (2019). Characterisation of additively manufactured metal surfaces by means of X-ray computed tomography and generalised surface texture parameters. *CIRP Annals, 68*(1), 515-518. doi:https://doi.org/10.1016/j.cirp.2019.04.074

Appendix A – Data attained as part of Surface Topographical Parameter Study

The following tables display the raw results taken as part of the study into Surface Topographical Variation between worn and unworn areas detailed in Chapter 4. The information below is also available in Surface Topography: Metrology and Properties Volume 6 Number 3.

	Amplitude parameters						Spacing parameters				Sk family					Other	
FILENAME:	Sq (μm)	Ssk	Sku	Sp (μm)	Sv (μm)	Sz (μm)	Sds(1/mm^2)	Sdq	Ssc (1/μm)	Sdr(%)	Spk (μm)	Sk (μm)	Svk (μm)	Smr1(%)	Smr2(%)	S5z (μm)	Sa (μm)
LCS1-1	0.455	−0.139	3.243	1.833	2.505	4.338	3.81×10^3	0.122	0.047	0.75	0.428	1.173	0.508	8.8	89.8	3.684	0.36
LCS1-10	0.522	−0.125	3.679	2.95	4.185	7.135	4.43×10^3	0.156	0.063	1.204	0.542	1.302	0.627	9.5	89.6	4.523	0.408
LCS1-2	0.693	−0.315	11.334	6.627	23.274	29.901	5.52×10^3	0.267	0.116	3.326	0.777	1.748	1.233	9.6	90	6.659	0.542
LCS1-3	0.472	−0.105	3.898	3.677	4.554	8.231	4.46×10^3	0.144	0.061	1.033	0.509	1.174	0.593	9.7	89.8	4.237	0.368
LCS1-4	0.374	−0.15	3.781	2.207	2.418	4.625	4.07×10^3	0.102	0.041	0.521	0.403	0.908	0.462	9.3	88.9	3.411	0.29
LCS1-5	0.595	0.109	3.36	3.1	2.367	5.467	3.61×10^3	0.156	0.059	1.205	0.661	1.491	0.581	10.1	89.9	4.762	0.467
LCS1-6	0.467	0.17	3.335	2.168	2.686	4.854	4.04×10^3	0.125	0.05	0.782	0.542	1.165	0.464	11.1	90.9	3.601	0.367
LCS1-7	0.77	−0.057	3.906	4.54	7.428	11.969	5.15×10^3	0.275	0.117	3.679	0.856	1.883	0.946	10.3	89.8	7.74	0.598
LCS1-8	0.561	−0.123	3.212	3.49	2.782	6.272	3.85×10^3	0.148	0.054	1.094	0.56	1.438	0.612	8.6	89.1	4.443	0.445
LCS1-9	0.475	0.187	4.638	2.269	5.374	7.643	3.57×10^3	0.108	0.041	0.595	0.627	1.116	0.557	11.3	90.2	4.17	0.363
LCS2-1	0.582	−0.085	3.542	3.688	3.833	7.522	3.65×10^3	0.146	0.054	1.059	0.622	1.431	0.703	10.4	89.9	4.752	0.454
LCS2-10	0.441	0.244	5.987	4.825	2.903	7.728	4.30×10^3	0.135	0.053	0.898	0.572	1.045	0.52	10.1	89.9	5.162	0.335
LCS2-2	0.346	−0.356	6.053	2.3	2.579	4.879	4.31×10^3	0.098	0.032	0.486	0.438	0.69	0.576	9.6	86.7	3.818	0.249
LCS2-3	0.601	0.632	19.932	16.185	4.303	20.488	3.60×10^3	0.176	0.066	1.452	1.008	1.411	0.732	9.8	89.4	6.029	0.454
LCS2-4	0.509	−0.089	3.611	2.368	3.219	5.588	4.16×10^3	0.136	0.059	0.934	0.55	1.234	0.614	9.3	88.6	4.462	0.395
LCS2-5	0.642	−1.017	7.938	4.587	5.075	9.662	4.18×10^3	0.166	0.059	1.34	0.571	1.433	1.011	8.1	87.9	7.45	0.474
LCS2-6	0.281	0.179	4.184	2.258	1.661	3.92	4.38×10^3	0.08	0.034	0.326	0.345	0.682	0.301	10.6	90.1	2.721	0.217
LCS2-7	0.682	−0.119	6.021	5.784	6.663	12.448	5.00×10^3	0.229	0.09	2.543	0.786	1.52	0.961	9.3	87.2	8.078	0.511
LCS2-8	0.543	−0.415	3.955	2.614	3.147	5.761	4.38×10^3	0.16	0.058	1.256	0.511	1.283	0.742	8.8	87.7	5.086	0.419
LCS2-9	0.394	−0.322	4.425	2.776	2.489	5.265	3.83×10^3	0.11	0.041	0.603	0.444	0.893	0.54	9.6	87.4	3.839	0.299
LCS3-1	1.066	−0.336	5.429	5.451	5.746	11.198	3.38×10^3	0.162	0.055	1.269	1.465	2.102	1.474	12.1	86.7	9.305	0.773
LCS3-10	0.528	0.084	3.895	4	3.059	7.059	3.97×10^3	0.16	0.061	1.263	0.67	1.254	0.591	10.5	89.1	5.111	0.407
LCS3-2	0.324	−0.007	5.578	2.177	4.331	6.508	4.82×10^3	0.099	0.039	0.483	0.433	0.72	0.485	10.9	89.7	3.413	0.241
LCS3-3	0.468	0.067	4.186	4.36	3.445	7.805	4.13×10^3	0.127	0.051	0.799	0.598	1.114	0.559	10.5	89.5	4.081	0.36
LCS3-4	1.002	−0.31	2.65	4.314	3.352	7.666	3.23×10^3	0.122	0.047	0.748	0.66	2.526	1.063	8.4	85.8	5.811	0.807
LCS3-5	0.538	−0.569	3.91	2.041	2.512	4.552	3.83×10^3	0.126	0.043	0.793	0.46	1.241	0.762	8.8	86.7	4.082	0.414
LCS3-6	0.523	−0.398	4.519	4.668	6.152	10.819	3.88×10^3	0.134	0.048	0.885	0.538	1.288	0.709	9.1	88.8	3.976	0.407
LCS3-7	0.487	−0.818	7.116	2.738	5.234	7.971	4.71×10^3	0.153	0.059	1.147	0.536	1.003	0.808	10.9	87.5	6.294	0.354

LCS3-8	0.552	−0.428	4.079	3.506	4.66	8.166	3.78×10^3	0.135	0.051	0.911	0.515	1.34	0.753	8.9	88.3	4.841	0.429
LCS3-9	0.501	−10.308	264.411	2.185	14.754	16.94	4.03×10^3	0.135	0.04	0.732	0.47	0.898	0.781	10.4	89.6	8.937	0.3
LCS4-1	0.658	0.371	4.027	3.34	2.694	6.034	3.49×10^3	0.122	0.044	0.748	1.05	1.439	0.701	11.3	88.4	5.106	0.494
LCS4-10	0.499	−0.032	3.801	2.764	2.906	5.671	4.23×10^3	0.131	0.054	0.862	0.561	1.234	0.564	9.6	89.9	4.487	0.388
LCS4-2	0.454	0.01	4.288	2.949	3.32	6.269	4.89×10^3	0.144	0.063	1.037	0.565	1.079	0.568	10.1	89.8	4.391	0.347
LCS4-3	0.374	−0.257	3.475	3.177	2.242	5.419	4.14×10^3	0.099	0.039	0.488	0.375	0.941	0.448	8.8	88.8	3.034	0.294
LCS4-4	0.411	0.255	3.721	2.448	4.18	6.628	3.60×10^3	0.109	0.043	0.601	0.534	0.984	0.471	12.2	91.2	3.709	0.319
LCS4-5	0.928	−0.446	4.613	3.721	4.079	7.8	3.36×10^3	0.139	0.05	0.961	1.087	1.856	1.601	11.3	87.3	7.438	0.676
LCS4-6	0.376	−0.163	7.357	4.394	3.643	8.037	4.27×10^3	0.099	0.037	0.49	0.427	0.864	0.542	9	88.1	4.054	0.283
LCS4-7	0.957	−0.227	6.961	6.102	16.626	22.728	5.27×10^3	0.354	0.142	5.51	1.267	2.021	1.583	11.2	88.9	12.036	0.697
LCS4-8	0.508	−0.549	4.759	4.594	2.781	7.375	3.86×10^3	0.129	0.041	0.829	0.565	1.123	0.765	7.6	86	4.938	0.384
LCS4-9	0.396	0.329	15.943	10.803	3.56	14.363	4.14×10^3	0.103	0.039	0.526	0.677	0.859	0.567	9.7	87.9	4.339	0.29
LCS5-1	0.419	−0.583	3.927	2.884	2.385	5.269	4.09×10^3	0.111	0.04	0.627	0.369	0.979	0.604	7.7	86.5	3.373	0.324
LCS5-10	0.508	−0.206	5.009	2.647	11.893	14.54	4.57×10^3	0.16	0.064	1.244	0.509	1.279	0.796	9.1	89.6	4.535	0.398
LCS5-2	0.371	−0.354	4.657	2.489	3.345	5.833	4.93×10^3	0.116	0.046	0.67	0.41	0.854	0.534	10	88.6	3.794	0.281
LCS5-3	0.41	−0.298	4.594	2.393	5.478	7.871	4.04×10^3	0.113	0.044	0.643	0.432	0.981	0.602	9	88.7	3.804	0.315
LCS5-4	0.317	0.051	5.325	2.796	3.4	6.196	4.10×10^3	0.092	0.04	0.421	0.423	0.757	0.404	10.4	90.7	3.232	0.242
LCS5-5	0.61	−0.813	4.574	2.706	3.689	6.395	3.67×10^3	0.135	0.046	0.91	0.45	1.393	0.958	7.9	86.6	5.11	0.466
LCS5-6	0.345	−0.781	5.224	2.113	2.44	4.553	3.99×10^3	0.085	0.029	0.367	0.293	0.817	0.513	7.4	88.1	3.22	0.263
LCS5-7	1.056	11.13	214.701	25.369	4.245	29.614	5.24×10^3	0.408	0.1	6.688	1.475	1.605	0.824	8.9	89.1	27.704	0.543
LCS5-8	0.339	−0.737	4.47	1.751	2.241	3.991	4.12×10^3	0.088	0.032	0.39	0.279	0.759	0.552	8.7	86.9	2.883	0.257
LCS5-9	0.321	−0.225	3.926	2.618	2.967	5.585	3.99×10^3	0.084	0.032	0.362	0.347	0.774	0.427	9.6	88.8	2.69	0.248
PFC1-1	0.562	0.276	2.969	3.661	2.45	6.11	3.77×10^3	0.115	0.047	0.671	0.627	1.425	0.454	13	92.3	3.962	0.45
PFC1-2	0.831	−0.001	3.711	5.606	5.849	11.455	4.40×10^3	0.234	0.093	2.657	0.864	2.116	0.933	9.5	90.2	7.446	0.654
PFC1-4	0.532	−0.119	3.536	3.608	4.499	8.107	3.89×10^3	0.142	0.058	1.005	0.562	1.348	0.633	9.1	89.7	4.457	0.418
PFC1-5	0.475	0.193	3.597	2.755	3.613	6.369	3.92×10^3	0.117	0.047	0.703	0.547	1.195	0.488	10.7	90.9	3.805	0.373
PFC1-6	0.556	0.063	3.284	2.225	5.741	7.966	3.86×10^3	0.145	0.061	1.043	0.575	1.432	0.603	10.4	90.9	4.365	0.441
PFC1-7	0.927	−0.264	4.272	7.908	13.727	21.635	4.96×10^3	0.317	0.129	4.77	1.016	2.262	1.345	9.7	89.5	9.88	0.718
PFC1-8	0.556	0.028	3.503	3.996	6.761	10.758	3.70×10^3	0.125	0.052	0.788	0.608	1.446	0.628	9.1	90.2	4.789	0.441
PFC1-9	0.753	0.308	7.039	7.497	5.638	13.135	3.62×10^3	0.179	0.07	1.575	0.854	1.819	0.894	9.2	89.3	7.364	0.575
PFC2-1	0.61	−0.112	3.146	3.689	2.628	6.317	3.66×10^3	0.143	0.055	1.032	0.586	1.576	0.635	8.6	89.3	4.594	0.484
PFC2-2	0.873	0.46	3.971	4.355	14.175	18.53	3.64×10^3	0.21	0.079	2.115	1.123	2.219	1.031	11.1	92.6	7.321	0.687
PFC2-4	0.54	0.166	3.742	2.569	2.439	5.008	3.53×10^3	0.129	0.052	0.829	0.667	1.312	0.554	10.2	89.8	4.627	0.418

(*Continued*)

	Amplitude parameters						Spacing parameters				Sk family					Other	
FILENAME:	Sq (μm)	Ssk	Sku	Sp (μm)	Sv (μm)	Sz (μm)	Sds(1/mm^2)	Sdq	Ssc (1/μm)	Sdr(%)	Spk (μm)	Sk (μm)	Svk (μm)	Smr1(%)	Smr2(%)	S5z (μm)	Sa (μm)
PFC2-5	0.605	0.344	3.886	4.014	2.976	6.991	3.66×10^3	0.121	0.048	0.74	0.739	1.491	0.562	11.3	90.9	5.12	0.472
PFC2-6	0.75	−0.303	3.95	2.715	5.64	8.356	3.46×10^3	0.148	0.059	1.079	0.721	1.826	0.95	10.2	89.5	5.75	0.582
PFC2-7	0.63	0.29	4.221	4.063	3.849	7.913	4.27×10^3	0.173	0.068	1.477	0.808	1.523	0.636	10.6	90.1	6.094	0.486
PFC2-8	0.496	−0.308	6.381	3.423	4.439	7.861	3.62×10^3	0.1	0.039	0.49	0.573	1.092	0.771	11.9	90.7	5.656	0.367
PFC2-9	0.369	0.183	3.986	2.266	1.891	4.157	3.89×10^3	0.092	0.038	0.425	0.463	0.9	0.397	10.3	90.5	3.467	0.286
PFC3-1	0.581	−0.252	3.109	3.544	2.802	6.345	3.74×10^3	0.146	0.055	1.053	0.505	1.519	0.65	7.8	89.2	4.268	0.464
PFC3-2	0.874	0.009	4.46	5.983	18.607	24.589	3.80×10^3	0.205	0.077	2.002	0.934	2.298	1.23	9	90.9	7.457	0.694
PFC3-4	0.83	−0.171	2.811	3.824	3.711	7.535	4.39×10^3	0.122	0.101	0.759	0.625	2.271	0.799	7.9	90.3	5.832	0.673
PFC3-5	0.475	0.42	3.899	2.83	2.592	5.422	3.73×10^3	0.099	0.041	0.499	0.615	1.204	0.402	10.4	91.7	4.159	0.372
PFC3-6	0.625	−0.067	2.914	2.9	2.846	5.746	3.20×10^3	0.11	0.047	0.605	0.546	1.678	0.606	8.6	90.6	4.579	0.502
PFC3-8	0.383	−0.293	3.379	1.823	2.161	3.984	3.67×10^3	0.074	0.028	0.277	0.32	0.987	0.45	8.2	89.2	3.107	0.303
PFC3-9	0.888	−0.241	4.427	5.497	5.151	10.648	3.58×10^3	0.134	0.054	0.879	1.02	2.033	1.131	8.6	86.5	8.424	0.678
PFC4-1	0.787	0.942	14.693	16.809	4.233	21.043	6.69×10^3	0.242	0.441	2.675	1.143	1.9	0.808	9.6	89.8	12.12	0.598
PFC4-2	0.652	0.088	3.528	5.564	4.76	10.323	6.19×10^3	0.207	0.186	2.111	0.777	1.63	0.713	10.6	90.7	5.669	0.511
PFC4-4	0.615	−0.04	3.271	6.024	3.931	9.954	4.89×10^3	0.153	0.114	1.155	0.64	1.643	0.62	9.1	91.1	4.643	0.492
PFC4-5	0.496	−0.127	5.597	9.148	7.866	17.014	4.91×10^3	0.13	0.097	0.831	0.651	1.223	0.682	9.1	88.9	4.556	0.385
PFC4-6	0.716	0.264	3.679	5.882	2.98	8.861	5.13×10^3	0.164	0.181	1.324	0.929	1.788	0.665	10.8	91.3	5.881	0.56
PFC4-7	0.886	−0.205	3.701	5.613	9.391	15.004	8.23×10^3	0.298	0.259	4.275	0.894	2.209	1.159	9.7	89.7	8.48	0.693
PFC4-8	0.591	0.073	3.224	3.812	2.967	6.779	4.71×10^3	0.135	0.111	0.903	0.617	1.551	0.577	9.6	91.1	4.876	0.47
PFC4-9	0.654	0.056	3.433	5.526	3.574	9.099	4.72×10^3	0.17	0.155	1.425	0.754	1.631	0.685	10.5	89.8	5.28	0.514
PFC5-1	0.61	−0.077	3.486	4.81	3.87	8.68	5.43×10^3	0.161	0.147	1.283	0.652	1.556	0.693	8.9	89.7	5.599	0.481
PFC5-2	1.28	2.852	27.639	19.253	6.953	26.206	5.80×10^3	0.39	0.335	6.118	2.231	2.6	1.131	9.8	89.9	20.657	0.862
PFC5-4	0.713	−0.303	3.188	4.537	5.465	10.002	4.46×10^3	0.158	0.122	1.228	0.623	1.858	0.851	7.6	88.8	5.131	0.569
PFC5-5	0.551	0.072	3.384	3.096	4.369	7.465	5.09×10^3	0.143	0.122	1.009	0.601	1.418	0.586	9.7	90.7	4.589	0.435
PFC5-6	0.649	0.042	3.415	4.165	4.807	8.972	5.95×10^3	0.178	0.245	1.547	0.713	1.643	0.693	10.2	90.3	5.164	0.511
PFC5-7	0.804	−0.194	3.967	4.881	5.389	10.27	6.30×10^3	0.243	0.203	2.835	0.86	1.982	0.972	9.7	89.8	8.812	0.624
PFC5-8	0.532	−0.067	3.695	4.631	4.096	8.727	4.87×10^3	0.14	0.116	0.974	0.584	1.326	0.626	9.8	89.5	4.314	0.417
PFC5-9	0.674	0.136	3.028	4.773	3.795	8.568	4.37×10^3	0.146	0.126	1.06	0.735	1.813	0.601	9.5	92	5.059	0.541
PFC6-1	0.714	0.161	3.094	4.044	3.039	7.084	5.46×10^3	0.146	0.156	1.054	0.786	1.873	0.595	9.5	90.7	5.258	0.569

PFC6-2	0.747	−0.068	3.775	6.582	19.075	25.657	6.18×10^3	0.24	0.202	2.76	0.808	1.935	1.191	9.7	90.8	6.75	0.592
PFC6-4	0.53	0.261	3.374	5.296	3.025	8.321	4.30×10^3	0.114	0.096	0.64	0.646	1.373	0.49	11	92.2	3.912	0.421
PFC6-5	0.359	0.079	3.662	1.998	2.99	4.989	5.41×10^3	0.102	0.085	0.516	0.403	0.91	0.389	10.1	90.8	3.329	0.282
PFC6-6	0.572	−0.161	3.343	3.065	2.903	5.968	5.57×10^3	0.142	0.155	0.997	0.537	1.458	0.629	9.2	89.5	5.052	0.452
PFC6-7	0.972	−0.183	3.597	5.943	6.407	12.35	7.43×10^3	0.313	0.284	4.695	1.023	2.409	1.169	9.3	89.2	9.982	0.76
PFC6-8	0.646	−0.673	3.811	3.355	3.719	7.074	4.66×10^3	0.126	0.082	0.794	0.453	1.508	0.947	6.9	85.5	5.388	0.504
PFC6-9	0.641	0.081	3.428	5.157	5.619	10.776	5.52×10^3	0.151	0.184	1.123	0.726	1.633	0.69	10.2	90.4	5.571	0.506
PFC7-1	1.491	−0.233	2.963	4.342	4.275	8.617	3.52×10^3	0.113	0.088	0.646	1.278	3.438	2.085	12.5	88.1	8.248	1.163
PFC7-2	0.582	−0.16	3.151	2.342	3.197	5.539	5.22×10^3	0.126	0.104	0.81	0.522	1.49	0.665	9.3	89.6	4.549	0.461
PFC7-4	0.752	0.336	3.175	3.89	3.175	7.065	4.34×10^3	0.137	0.113	0.931	0.823	2.018	0.566	10.5	93.1	6.008	0.604
PFC7-5	0.48	0.156	4.252	5.794	4.302	10.097	5.47×10^3	0.123	0.101	0.754	0.634	1.183	0.555	10.7	91.2	4.89	0.373
PFC7-6	0.571	0.654	12.156	10.7	2.66	13.36	4.79×10^3	0.145	0.11	0.99	0.785	1.408	0.591	9.6	89.9	8.23	0.439
PFC7-7	1.039	0.834	5.056	7.321	4.283	11.605	4.16×10^3	0.169	0.132	1.444	1.908	2.173	0.98	12.9	90.6	8.703	0.764
PFC7-8	0.496	−0.172	3.447	2.617	2.428	5.045	4.66×10^3	0.107	0.08	0.576	0.48	1.25	0.567	9.6	89.8	4.118	0.389
PFC7-9	0.928	−0.266	2.857	3.1	3.88	6.98	4.24×10^3	0.124	0.096	0.774	0.682	2.446	1.04	7.9	89.1	5.867	0.746
POLY031-1	1.349	−0.113	2.593	4.502	5.163	9.665	2.32×10^3	0.113	0.039	0.637	0.961	3.772	1.228	7.2	90.3	8.003	1.099
POLY031-2	0.699	−1.524	16.33	3.452	9.922	13.374	4.84×10^3	0.189	0.078	1.744	0.66	1.527	1.096	9.8	88.5	8.968	0.508
POLY031-4	0.689	0.122	3.314	3.53	4.261	7.792	3.26×10^3	0.144	0.051	1.03	0.78	1.734	0.714	10.9	91	5.202	0.543
POLY031-5	0.667	−9.701	145.949	2.058	14.298	16.356	4.32×10^3	0.121	0.039	0.671	0.432	0.876	1.195	10.7	90.5	7.143	0.313
POLY031-6	1.344	0.767	3.105	5.211	4.013	9.224	2.34×10^3	0.123	0.055	0.75	2.448	2.344	0.934	22.3	90	7.877	1.047
POLY031-7	0.867	−0.074	10.699	17.151	6.128	23.279	4.81×10^3	0.254	0.102	3.096	1.194	1.95	1.283	9.9	88.5	9.023	0.647
POLY031-8	0.525	−0.349	4.791	2.879	3.34	6.219	3.49×10^3	0.112	0.038	0.618	0.546	1.199	0.751	11.1	89.6	5.422	0.397
POLY031-9	0.777	0.926	4.272	3.687	3.441	7.128	2.81×10^3	0.126	0.052	0.791	1.381	1.48	0.64	18.3	92	5.999	0.588
POLY040-1	0.653	−0.439	3.798	2.877	3.523	6.4	3.63×10^3	0.134	0.048	0.894	0.567	1.608	0.874	8.3	88.7	5.189	0.508
POLY040-2	0.498	0.009	4.372	4.013	2.854	6.867	3.98×10^3	0.132	0.052	0.885	0.588	1.186	0.595	10.3	89.5	4.992	0.383
POLY040-3	1.273	−0.935	4.963	4.932	6.26	11.192	3.35×10^3	0.15	0.052	1.105	1.272	2.118	2.689	15	85.4	9.196	0.895
POLY040-4	0.653	−0.257	3.335	3.286	4.494	7.78	3.85×10^3	0.168	0.066	1.405	0.588	1.657	0.804	7.8	88.5	5.441	0.516
POLY040-5	0.571	−0.504	3.76	2.565	3.694	6.259	3.95×10^3	0.152	0.053	1.144	0.456	1.39	0.774	7.1	87	5.139	0.447
POLY040-6	0.433	−0.469	4.544	2.854	2.715	5.568	4.06×10^3	0.113	0.039	0.637	0.435	0.999	0.628	9.1	88.1	4.259	0.329
POLY040-7	0.432	−0.065	4.038	2.507	2.628	5.135	4.30×10^3	0.12	0.05	0.728	0.485	1.048	0.515	10.5	90.2	4.395	0.334
POLY040-8	0.636	−0.439	4.251	5.706	4.892	10.598	3.99×10^3	0.156	0.071	1.211	0.61	1.597	0.837	8.3	89.3	5.762	0.497
POLY040-9	0.496	−0.048	4.372	4.613	3.052	7.665	3.81×10^3	0.126	0.046	0.787	0.532	1.245	0.56	8.1	88.4	4.648	0.39

	Amplitude parameters						Spacing parameters				Sk family					Other	
FILENAME:	Sq (μm)	Ssk	Sku	Sp (μm)	Sv (μm)	Sz (μm)	Sds(1/mm^2)	Sdq	Ssc (1/μm)	Sdr(%)	Spk (μm)	Sk (μm)	Svk (μm)	Smr1(%)	Smr2(%)	S5z (μm)	Sa (μm)
POLY040-10	0.485	−0.133	3.412	2.507	2.695	5.202	4.16×10^3	0.136	0.055	0.914	0.49	1.211	0.551	9.2	89.1	4.104	0.38
Poly041-1	0.757	1.216	10.797	5.89	2.667	8.557	3.37×10^3	0.107	0.042	0.572	1.353	1.381	1.006	10	87	7.895	0.512
Poly041-2	1.697	−0.924	6.35	12.417	10.81	23.226	2.77×10^3	0.221	0.049	2.089	2.225	3.033	2.954	12.4	85.3	12.623	1.203
Poly041-3	0.255	−0.28	7.679	4.082	2.751	6.833	4.77×10^3	0.077	0.034	0.306	0.335	0.602	0.334	10.1	89.5	2.762	0.194
Poly041-4	0.501	−0.137	4.16	3.79	2.694	6.484	3.89×10^3	0.134	0.053	0.89	0.596	1.183	0.644	9.5	88.8	4.582	0.384
Poly041-5	0.581	−0.272	7.135	3.543	5.371	8.914	3.74×10^3	0.126	0.048	0.786	0.751	1.287	0.761	10	88.9	5.972	0.428
Poly041-6	1.032	−0.094	3.468	3.846	5.721	9.567	2.86×10^3	0.114	0.042	0.649	1.035	2.441	1.262	12.1	89.1	7.478	0.801
Poly041-7	1.04	1.474	5.308	4.954	5.982	10.936	2.10×10^3	0.104	0.042	0.535	2.291	1.564	0.664	21.7	94.7	7.981	0.77
Poly041-8	0.924	−1.146	6.29	2.979	6.552	9.531	3.36×10^3	0.137	0.047	0.935	0.72	1.898	1.81	10.1	87.9	7.542	0.668
Poly041-9	0.504	−0.125	4.47	3.933	2.59	6.523	3.95×10^3	0.129	0.05	0.831	0.502	1.224	0.619	8.8	88.3	4.339	0.391
Poly041-10	0.598	−0.42	3.843	2.75	4.971	7.721	4.06×10^3	0.136	0.054	0.929	0.481	1.491	0.765	8	87.9	5.426	0.47
POLY042-2	0.685	−2.336	31.095	2.726	10.715	13.441	3.73×10^3	0.133	0.046	0.841	0.685	1.461	1.026	10.1	89.4	9.551	0.483
POLY042-3	0.521	0.146	3.622	3.878	4.227	8.105	3.93×10^3	0.106	0.048	0.555	0.617	1.337	0.561	10	91.3	4.696	0.41
POLY042-4	0.334	−1.327	7.736	1.789	2.889	4.677	3.92×10^3	0.083	0.026	0.344	0.267	0.689	0.602	8.3	86.4	3.651	0.242
POLY042-5	0.507	−0.836	9.329	5.361	8.664	14.025	3.71×10^3	0.118	0.039	0.682	0.654	1.023	0.888	9.4	86.8	5.981	0.362
POLY042-6	0.625	−0.709	12.274	3.68	7.582	11.262	3.94×10^3	0.156	0.071	1.182	0.781	1.401	0.783	12.1	90.9	8.886	0.463
POLY042-7	0.556	−0.005	4.304	7.003	3.543	10.546	3.63×10^3	0.12	0.043	0.709	0.697	1.393	0.641	9.4	90.3	5.62	0.433
POLY042-8	0.7	−0.167	3.356	3.018	7.544	10.561	3.90×10^3	0.172	0.063	1.461	0.59	1.875	0.8	8.6	90.7	5.855	0.561
POLY042-9	0.637	−0.298	2.807	3.079	4.311	7.391	3.59×10^3	0.156	0.051	1.206	0.421	1.745	0.69	6.7	89.5	4.243	0.516
POLY042-10	1.254	0.42	3.706	7.136	10.563	17.699	2.85×10^3	0.123	0.04	0.638	1.658	2.949	1.1	12.1	88.6	7.937	0.973
POLY049-1	0.641	−0.425	3.138	3.122	2.847	5.969	3.98×10^3	0.158	0.055	1.239	0.47	1.675	0.759	6.3	88.3	4.661	0.515
POLY049-2	0.277	−0.019	4.616	1.878	2.205	4.083	4.31×10^3	0.077	0.03	0.296	0.321	0.66	0.351	9.2	88.8	2.875	0.212
POLY049-3	0.438	−0.148	5.218	3.71	4.598	8.308	4.51×10^3	0.122	0.052	0.762	0.532	1.013	0.641	10.4	90.1	4.225	0.33
POLY049-4	0.558	−0.382	4.226	2.466	3.344	5.81	4.12×10^3	0.149	0.053	1.099	0.549	1.338	0.727	8.3	88.1	5.357	0.431
POLY049-5	0.543	−0.554	4.605	4.696	4.375	9.071	3.78×10^3	0.129	0.046	0.827	0.546	1.26	0.801	9.5	87.9	6.013	0.415
POLY049-6	0.357	−0.384	4.791	2.213	3.009	5.223	4.28×10^3	0.099	0.039	0.497	0.386	0.796	0.53	9.6	87.5	3.666	0.268
POLY049-7	0.518	−0.057	4.578	4.337	3.38	7.718	4.84×10^3	0.16	0.075	1.269	0.619	1.198	0.654	10.1	88.3	6.213	0.395
POLY049-8	0.634	-8.27×10^{-4}	3.717	3.93	4.058	7.988	3.93×10^3	0.167	0.071	1.385	0.708	1.563	0.711	9.8	89.4	5.809	0.494
POLY049-9	0.451	−0.772	5.66	2.335	3.088	5.422	4.02×10^3	0.112	0.043	0.62	0.431	0.983	0.727	9.2	87.5	4.717	0.334
POLY049-10	0.509	−0.349	3.588	2.725	2.697	5.422	4.58×10^3	0.151	0.062	1.127	0.455	1.243	0.647	8.5	87.9	4.543	0.398